DOCTOR OF PHILOSOPHY

Kinetochore-derived Microtubules
from Molecular Regulation to their Role in Mitosis

Vasileva, Vanya

Award date:
2015

Kinetochore-derived Microtubules: from Molecular Regulation to their Role in Mitosis

By

Vanya Vasileva

Supervisor: Professor Tomoyuki Tanaka

Centre for Gene Regulation and Expression

College of Life Sciences

University of Dundee, Dundee

Thesis submitted for the degree of

Doctor of Philosophy at the University of Dundee,

September 2015

Table of Contents

Dedicated to the Reader:

Did you know your cells divide every 24 hours when actual cell division lasts only about an hour?

During cell division, microtubule 'threads' must first find and capture each chromosome kinetochore before chromosomes can be equally distributed to daughter cells. We can liken kinetochore capture to a fisherman's mission, in which he needs to catch 46 fishes within an hour to feed two daughters. Our aim is to understand how every day the fisherman captures 46 fishes/hour without a failure. What must he optimise? – Number of fishing lines, their extension and rotation, or the use of sophisticated baits. Our study provides direct evidence that use of 'sophisticated baits' or microtubules' originating from kinetochores increases the chance that microtubule 'fishing' lines will hook chromosomes on time. If microtubules are not generated on chromosome kinetochores, their capture will be delayed and a chromosome may be lost, which would lead to cell death or cell anomalies associated with cancers and congenital disorders.

Vanya Vasileva

September 2015, Dundee

List of Abbreviations

S. cerevisiae	*Saccharomyces sereivisae*
S .pombe	*Schizosaccharomyces pombe*
D. melanogaster	*Drosophila melanogaster*
X. laevis	*Xenopus laevis*
C. elegans	*Caenorhabditis elegans*
H. sapiens	*Homo sapiens*
KT(s)	Kinetochore(s)
MT(s)	Microtubule(s)
+TIP(s)	Plus end tracking protein(s)
MTOC(s)	Microtubule organising centre(s)
NLS	Nuclear localisation signal
Kb	Kilobase pair
bp	base pair
MAP(s)	Microtubule-associated protein(s)
SPB	Spindle pole body
γ-TuRC	Gamma-tubulin containing ring complex

List of Figures

List of Tables

Acknowledgments

First and foremost, I would like to thank my supervisor, Prof Tomo Tanaka. I owe my deepest gratitude to him for believing in me and for taking me under his supervision for my Ph.D. studies. Tomo thought me how to question thoughts and express ideas in a story-oriented research. His critical thinking and enforcing validations for each result hold me on high research standard, and thus teaching me how to do research. His patience, support and continuous guidance helped me to overcome my difficult moments during the Ph.D. and finalise this dissertation.

Next, I would like to thank my postdoctoral supervisor in the lab, Dr Etsushi Kitamura. I am very fortunate to have had a supervisor like him during the first year of my Ph.D. Throughout the following years, Etsushi has been always there for me to listen and give advice. I am deeply thankful to him for the long discussions and for helping me to design experiments and sort out technical details.

I am extremely grateful to Dr Marek Gierlinski from Data Analysis Group for his great contribution to this study by developing mathematical model to validate our experimental data and for numerous discussions that helped me improve my knowledge in this area.

I am also very thankful to my dear colleague Dr Nori Kobayashi for his expertise in yeast and for carrying out yeast two-hybrid screens.

I would like to acknowledge past and present members of Tanaka Lab for their help, support and for making time spent in the lab more enjoyable.

I am thankful to Dr Lesley Clayton from Trivalent Editing for proofreading and editing introduction and discussion of the manuscript.

I am deeply grateful to my thesis committee, Dr Mike Stark and Dr Sarah Coulthurst, for their continuous support throughout my studies.

I would like to thank everyone involved in Light Microscopy Facility and in the maintenance of LMF server for their help with the microscopy and for safe data storage. Special thanks to Dr Graeme Ball for his invaluable suggestions on image data processing and analysis.

Many thanks to the media kitchen, washing service and guys from stores for their great efforts in preparing the media, for providing clean plastic and glassware all the time, and for carrying our parcels to the lab.

I am very thankful to Wellcome Trust, ERC and HFSP for funding my Ph.D. studies and this project.

Beyond the realm of science, I would like to thank my friends who have helped me to go forward in the journey of Ph.D. I need to give a special mention of my friends who brought joy and laughter into the hours of solitude during the thesis writing up.

Finally, I would like to thank my family, my mother, father and brother, for encouraging me to follow my dreams and for their endless love and tireless support

along the way. Words cannot express my gratitude for everything you have done for me!!

These last two rows, I would like to dedicate to my better half, Antti. Without your unlimited faith, love and support, none of this would have been possible!!

Thank you!!

Vanya Vasileva

September 2015, Dundee

Abstract

To maintain genetic integrity in cell division, replicated chromosomes must be segregated accurately into newly formed daughter cells. The faithful segregation of sister chromatids is a crucial event in cell proliferation since it ensures maintenance of a stable set of chromosomes that is critical for the genetic integrity of the daughter cells. Mistakes in sister chromatid segregation have been related to chromosome instability and aneuploidy characteristic of a variety of human diseases, such as cancers and congenital anomalies.

During cell division, spindle-pole microtubules (MTs) must capture kinetochores (KTs) so that the chromosomes can be loaded on the mitotic spindle. However, it remains a mystery how spindle-pole MTs can locate KTs with high efficiency, within realistic capture times (Wollman et al. 2005). The appearance of MTs at KTs is correlated with their capture, which is consistent with KT-derived MTs facilitating the initial encounter of KTs by spindle-pole MTs (Kitamura et al. 2010). However, so far it has been difficult to establish a causal relationship between the appearance of KT-derived MTs and efficient KT capture. It has also been unclear how much contribution KT-derived MTs make to efficient KT capture by spindle-pole MTs.

Here we show that a MT-associated protein Stu1^{CLASP} is a good molecular tool to study the role of KT-derived MTs. Depletion of Stu1 protein abolished both localisation of the microtubule polymerase Stu2^{XMAP215} from KTs, and MT/tubulin nucleation at KTs, without affecting KT assembly (i.e. the ability of KTs to interact with spindle-pole MTs) or generation of spindle-pole MTs. Abolishing these KT-derived MTs in Stu1-depleted cells led to a delay in KT capture with an increase in the average capture time.

To test whether KT-derived MTs were solely responsible for this delay in KT capture, we developed a mathematical model to recapitulate the roles of KT-derived MTs in Stu1-depleted cells. The model suggested that Stu1-depletion indeed delays KT capture due to a lack of KT-derived MTs. Our results also revealed the extent to which KT-derived MTs contribute to a rapid KT capture by spindle-pole MTs.

Furthermore we showed that, after initial KT capture, KT-associated $Stu1^{CLASP}$ and $Stu2^{XMAP215}$ are required to regulate dynamics of their associated spindle-pole MTs. Removal of $Stu1^{CLASP}$ and $Stu2^{XMAP215}$ from KTs lead to defects in KT-dependent switch from MT depolymerisation to polymerisation (rescue). Interfering with KT-dependent MT rescue would compromise the maintenance of the KT–MT interaction.

Our study reveals that KT-derived MTs facilitate efficient KT capture by spindle-pole MTs. $Stu1^{CLASP}$ promotes MT generation at KTs by recruiting a MT polymerase $Stu2^{XMAP215}$. Afterwards, $Stu2^{XMAP215}$ recruitment by $Stu1^{CLASP}$ to KTs is also important for MT rescue and sustained KT–MT interaction. Thus, we reveal crucial regulatory mechanisms of KT–MT interaction in early stages of mitosis.

Declaration

I hereby declare that this thesis is based on the results of work conducted by myself, and that the thesis is of my own composition. Wherever contribution of others were involved, every effort is made to indicate this clearly, with due reference to the relevant researcher or to the literature. The experiments presented here, are to my knowledge, have never been presented for a higher degree or publication excluding where clearly stated and referenced.

Vanya Vasileva……Date…….

I certify that Vanya Vasileva has spent 3.5 years in research in the Centre for Gene Regulation and Expression, University of Dundee and that she has fulfilled the conditions of Ordinance General No. 39 of the University of Dundee and she is qualified to submit the accompanying thesis for the degree of Doctor of Philosophy.

Prof Tomo Tanaka……. Date……..

Professor of Cell and Molecular Biology

University of Dundee

INTRODUCTION

I. Every living cell today is derived from a cell by cell division

Omnis cellula e cellula ("All cells arise from (pre-existing) cells") as François-Vincent Raspall first recognised nearly two centuries ago (1825). The process by which new cells (called daughter cells) are formed from a pre-existing one (mother cell) is called cell division. Cell division consists of two parts – nuclear division (mitosis or meiosis) followed by division of the cytoplasm in cytokinesis. Mitosis is a form of nuclear division that results into two daughter cells each having the same number of chromosomes as the mother cell, while meiosis results in four daughter cells each with half the number of chromosomes of the mother cell. The time cells spend in cell division varies in different organisms. For example mitosis of proliferating human cells generally lasts for about 5% of the cell cycle (about 1 hr). The remaining 95% of the cell cycle (about 23 hrs) is occupied by preparation for cell division. In cell division, genetic information is transferred from mother to daughter cells via chromosomes – the carriers of the genetic material. Chromosomes are duplicated in a discrete preparatory phase called the synthetic phase, or S-phase, so they can be equally segregated to the daughter cells in mitosis (M-phase). Usually chromosome duplication (S-phase) and chromosome segregation (M-phase) are separated by two other preparatory gap phases, G1 and G2, which provide additional time for cell growth and serve as important regulatory transitions via G1/S and G2/M checkpoints. The G1/S transition is called Start, which checks that conditions are ideal for chromosome duplication, while the G2/M phase ensures that cells enter mitosis only if chromosomes have been duplicated once and only once. There exists also a third checkpoint, which occurs in M-phase – the spindle-assembly checkpoint (SAC), that ensures that chromosomes are equally distributed to the daughter cells, and satisfaction of this checkpoint leads to completion of cell division; for review (Morgan 2007). It is crucial for each daughter cell to inherit the full set of chromosomes. Chromosome loss could lead to chromosome instability

and aneuploidy, which is characteristic of variety of human diseases such as cancers and congenital disorders (Chandhok and Pellman 2009; Holland and Cleveland 2009; Thompson et al. 2010).

II. Chromosome segregation relies on kinetochore–microtubule attachment

The central role of mitosis is to ensure that duplicated chromosomes are equally segregated to the daughter cells in a process called chromosome segregation. Chromosome segregation relies on chromosome interaction and attachment to sophisticated "threads", called microtubules (MTs). Microtubules are polarized polymers organised in a complex network, called the mitotic spindle, in which their minus ends are organized at the spindle poles, while their plus ends point outward from the poles. To form a bipolar spindle, MTs from one pole overlap with MTs from the other to form a bipolar antiparallel array of MTs. This bipolar spindle contains three types of MTs: (1) interpolar MTs (iMTs), which overlap in the mid-zone of the spindle, thus linking two spindle poles and maintaining spindle bipolarity; (2) astral MTs (aMTs), which extend away form the spindle – typically involved in anchoring and positioning the spindle in the cell; and (3) kinetochore MTs (kMTs, called *K-fibers* in higher eukaryotes), which connect spindle poles to chromosomes; for review (Morgan 2007; Winey and Bloom 2012).

Kinetochore MTs attach to kinetochores (KTs) on chromosomes. Kinetochores are large multi-protein complexes assembled at chromosome centromeres; for review (Maiato et al. 2004a; Cheeseman and Desai 2008; DeLuca and Musacchio 2012). Centromeres are divided into two broad categories: 1) diffused (in holocentric chromosomes), where centromere runs along the entire length of the chromosome (for example in arthropods, plants, *C. elegans*) and 2) localised (in monocentric chromosomes), where centromere

represent a constricted region of the chromosome (Pluta et al. 1995). Localised centromeres are subdivided into two classes: 1) regional, which span megabases of DNA and are controlled epigenetically (typical for most eukaryotes); and 2) point, which are genetically specified by DNA sequence (Biggins 2013). Centromeres of *S. cerevisiae* are point centromeres that reside within a compact chromatin structure of ~250 bp that binds a single microtubule (Pluta et al. 1995). This "point" centromeric region is ~125-bp long and encloses three unique centromere determining elements (CDEs): CDEI (8-bp palindrome), CDEII (78-86 bp stretch of AT-rich DNA), and CDEIII (a conserved 26-bp element), where CDEIII is absolutely required for centromere function (Biggins 2013).

Like other eukaryotes, *S. cerevisiae* centromeres replicate early in S-phase (McCarroll and Fangman 1988; Natsume et al. 2013). Early centromere replication may ensure enough time for KTs to assemble prior to mitosis (Biggins 2013). This might be important for subsequent KT function especially in budding yeast, which lacks a distinct G2 phase (Biggins 2013).

Kinetochores are large protein complexes assembled at the centromeres of each chromosome. Even the relatively simple KT of *S. cerevisiae* consists of more than 300 proteins (Malvezzi and Westermann 2014). These proteins are organised in a number of subcomplexes, which can be reconstituted from recombinant proteins or purified from cells as individual complexes (Akiyoshi et al. 2010). The inner KT components are closely associated with centromeres and shape the constitutive centromere associated network (CCAN) (Figure 1a) (Biggins 2013; Malvezzi and Westermann 2014). In budding yeast this network recognises 125-bp long point centromere and forms a platform for outer KT complexes that connects the KT to a single MT (Figure 1a)

(Biggins 2013; Malvezzi and Westermann 2014). These outer KT complexes are assembled into a conserved structure, called KMN network (based on the components KNL1/Spc105, Mis12, and Ndc80 complex) (Figure 1a) (Biggins 2013; Malvezzi and Westermann 2014). The KMN network is directly involved in KT–MT interaction via Ndc80 complex and serves as a platform for recruitment of other MT-associated proteins such as Kar3 (a minus-end directed MT motor protein) and Stu2 (a MT polymerase) (Figure 1a) (Malvezzi and Westermann 2014).

During KT–MT interaction, KTs must fulfil both mechanical (provide a robust attachment of chromosomes to spindle MT) and chemical functions (sensing and communicating erroneous attachments to spindle assembly checkpoint (SAC)) (Figure 1a, proteins involved in SAC are highlighted in red) (Malvezzi and Westermann 2014). This study focuses on mechanical functions of KTs.

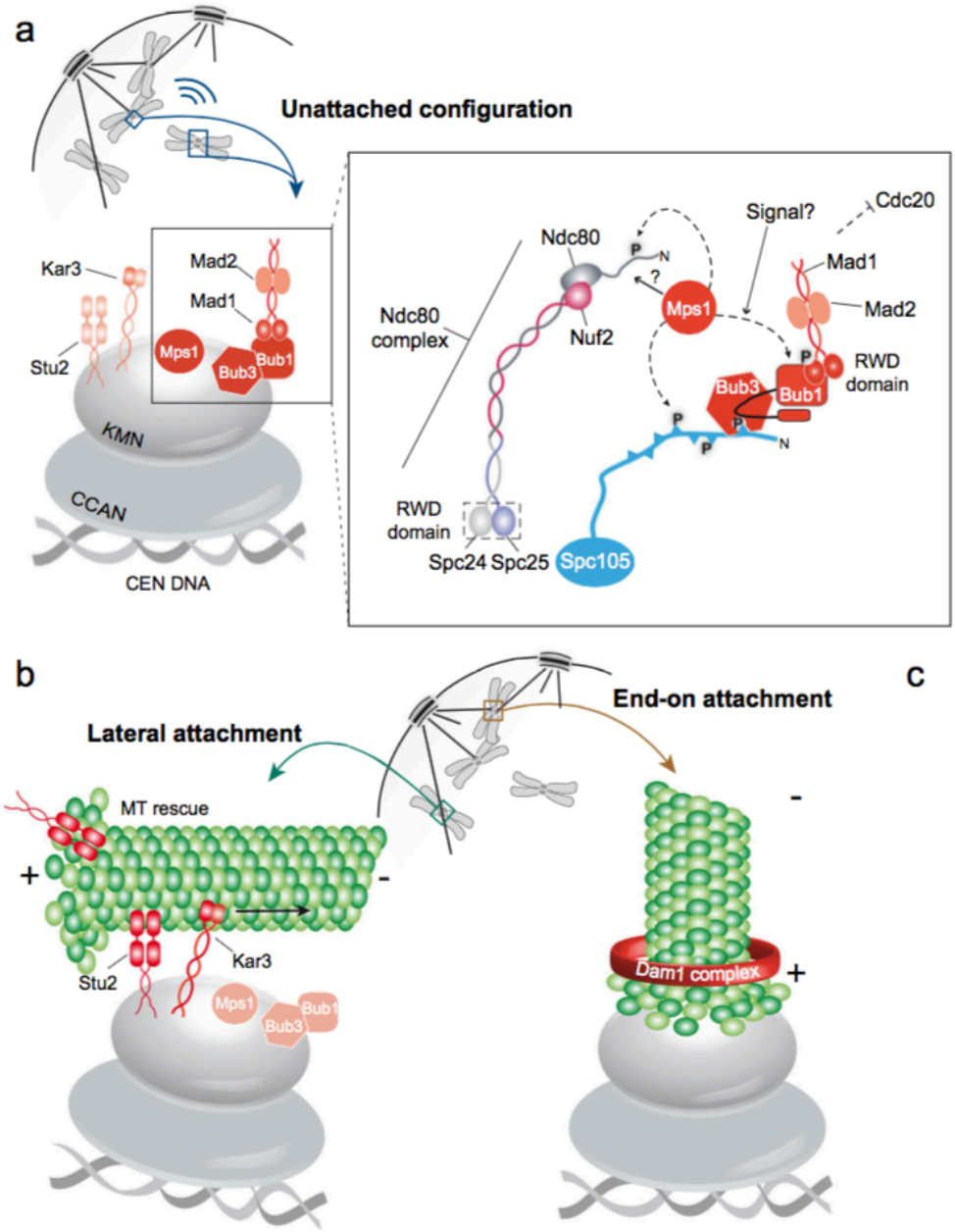

Figure 1. Budding yeast kinetochore structure; figure adapted from (Malvezzi and Westermann 2014). (a) The unattached free KT is shown in light grey, with the subunits of the spindle assembly checkpoint (SAC) highlighted in red (not examined in this study). The kinesin Kar3 and the microtubule associated-protein Stu2 are coloured in light red because they are present at this configuration, but they require microtubules for their function. On the right, Ndc80 and Spc105 complexes, which make part of KMN network. (b) KT attached at MT lateral surface. Kar3 is required for sliding of KT towards the spindle pole while Stu2 translocates to the plus end of MTs where it increases the frequency of MT rescues. (c) KT attached at MT plus end (end-on configuration). Ring-like Dam1 complex encircle MT plus end is attached to KT via Ndc80 complex (part of KMN network).

Kinetochore–microtubule interaction is established in early mitosis in a stepwise manner, as follows: Initially MTs need to "locate" chromosome KTs so that KTs can be first captured and loaded onto the MT lateral surface (Figure 2, Step 1); for review (Tanaka 2010). KTs not only provide MT attachment sites, but also regulate this attachment via various MT-associated proteins (for example Stu2 (Figure 1b), for more info see below) (Tanaka et al. 2005d; Gandhi et al. 2011). On the MT lattice, KTs can be transported actively towards the spindle poles by sliding (Figure 2, Step 2A) – an active transport facilitated by motor proteins (Kar3 in budding yeast (Figure 1b) (Tanaka et al. 2007)(Tanaka 2010). When a dynamic MT plus end reaches the KT, the lateral attachment can be converted to a more stable, end-on attachment of the KT to the MT plus end (Figure 2, Step 2B); for review (Tanaka 2010). This conversion is achieved by interaction between Ndc80 with Dam1 complexes (Figure 1c) (Kalantzaki et al. 2015). This results in a change from lateral sliding of the KT to its transport towards the spindle poles coupled to MT depolymerisation; for review (Tanaka 2010). KTs loaded on the spindle attach to MTs extending from two opposite poles of the spindle (Figure 2, Step 3), which allows bi-orientation (Figure 2, Step 4); for review (Tanaka 2010). After establishment of bi-orientation, sister chromatids will be pulled apart upon removal of sister chromatid cohesion and equally segregated to opposite spindle poles (Figure 2, Step 5); for review (Tanaka 2010). Each one of these steps towards bi-orientation is critical in ensuring that chromosome segregation occurs within characteristic mitotic timescales. Thus, it is very important that spindle-pole MTs "locate" and interact with KTs with high efficiency. How this is achieved in cells remains an enigma.

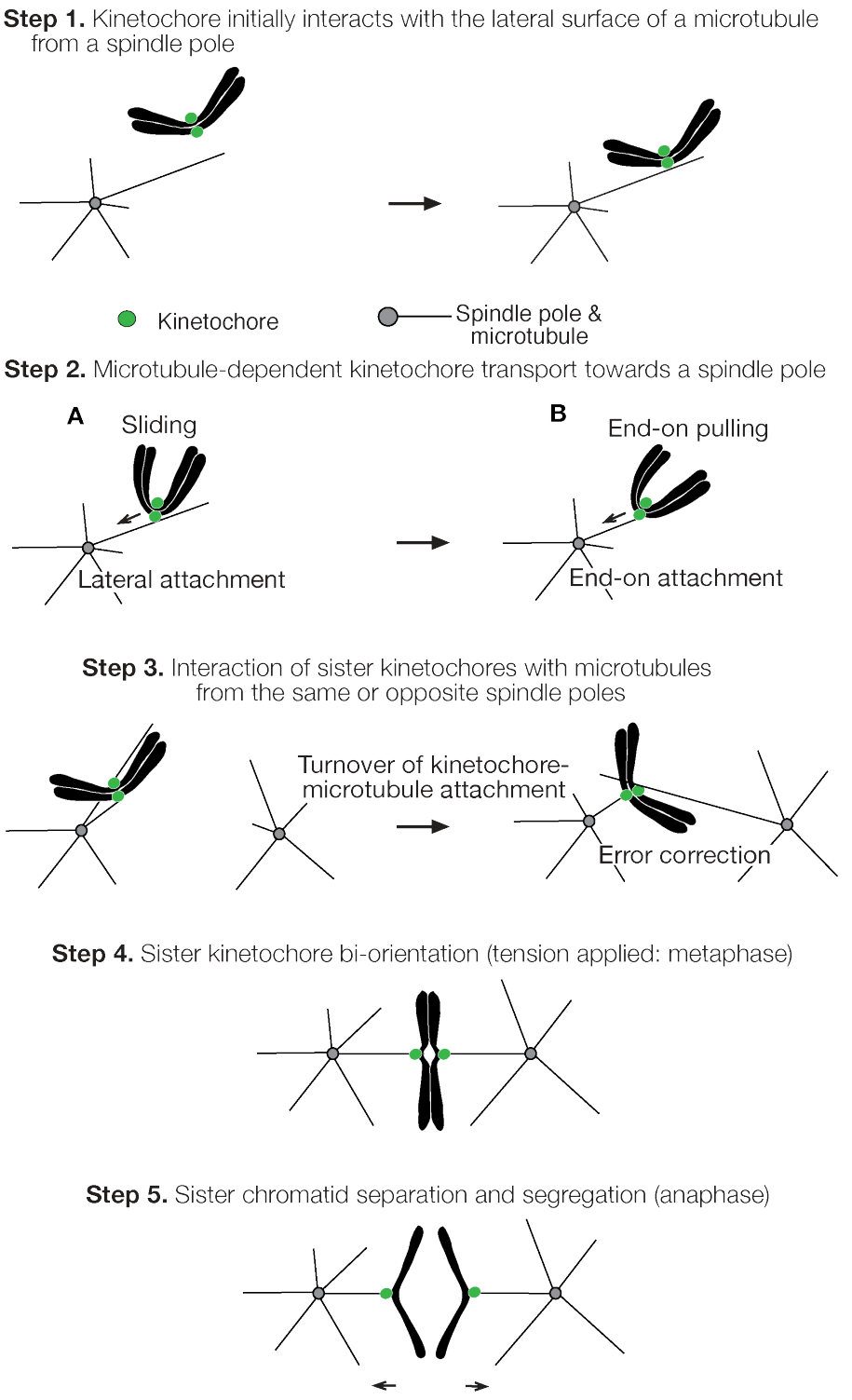

Figure 2. Kinetochore-microtubule interaction is established in early mitosis in a stepwise manner; figure adapted from (Tanaka 2010).

III. How spindle-pole microtubules capture kinetochores within characteristic mitotic timescales?

1. Microtubules exhibit dynamic instability

Spindle-pole MTs extending from spindle poles are not static "threads", but highly dynamic polymers that continuously grow and shrink to explore the cellular space. Understanding their structure, formation and behaviour is key to understanding KT capture. MTs are polarised tubulin polymers of which the basic building unit is a dimer composed of α- and β-tubulin. These are joined head to tail to form linear protofilaments. Generally, 13 protofilaments are then linked together to form a cylinder constituting a MT. The polarity of the MT is based on the orientation of α- and β-tubulin, where the end that has exposed β-tubulin is the plus (or fast-growing) end, and the one with exposed α-tubulin is the minus (or slow-growing) end. The plus and minus ends have different growth and shrinkage properties due to the different rates of binding and dissociation of the tubulin units. One behaviour of MTs recorded *in vitro* is treadmilling – a result of rapid plus end growth and minus end shrinkage – which leads to a net flow of tubulin subunits from the plus end towards the minus end without significant change in the MT length; for review see (Nogales 2001). A similar behaviour of MTs, called microtubule flux, was observed *in vivo*. Microtubule flux is a property of the mitotic spindle in animal cells but, unlike treadmilling, which derives from the intrinsic properties of the MTs, microtubule flux is regulated by microtubule-associated motors and other proteins (Rogers et al. 2005; Buster et al. 2007).

In vivo, MT minus ends are stabilised and generally embedded into the spindle poles, which are organised around centrosomes (in metazoan cells) or a spindle-pole body (SPB, in *S. cerevisiae* and other yeasts). These MT-organising centres (MTOC) serve as templates for MT nucleation, generally via γ-tubulin-containing ring complexes (γ-

TuRC). The γ-TuRC complexes contain at least seven different proteins and γ-tubulin. There are two working models of how γ-tubulin nucleates MTs: 1) The "template model", in which γ-tubulin forms ring-like seeds; and 2) The "protofilament model", in which γ-tubulin forms longitudinal protofilament-like structures. In both models γ-tubulin associates with MT minus ends, allowing the plus end to grow outward; for review (Kollman et al. 2011).

The MT plus end is highly dynamic and exhibits greater dynamic instability, i.e. switching between periods of rapid growth and shrinkage, due to turnover of tubulin subunits and the GTP hydrolysis cycle; reviewed in (Desai and Mitchison 1997a; Desai and Mitchison 1997c; Morgan 2007). This behaviour is because tubulin subunits are not simply building blocks, but are also GTP-ases. Tubulin subunits contain one molecule of non-exchangeable GTP, and one exchangeable GTP that can be hydrolysed to GDP. GDP-tubulin has a changed conformation that favours bending of protofilaments and consequent destabilisation of the MT end. At high tubulin concentrations, MTs grow rapidly, because new GTP-tubulin subunits are added with a greater rate than GTP hydrolysis occurs at the MT end. At low tubulin concentrations, GTP hydrolysis occurs faster than the new addition of tubulin subunits, resulting in loss of the GTP-tubulin cap and destabilisation of the MT plus end. Therefore GDP-bound tubulin subunits will rapidly dissociate, causing MT shrinkage (MT catastrophe). Eventually new GTP-tubulin subunits will be added to the MT plus end, allowing the reformation of a GTP-tubulin cap and MT growth (MT rescue); reviewed in (Desai and Mitchison 1997a; Morgan 2007; Brouhard 2015).

Thus, dynamic instability of MTs allows them to quickly switch between phases of rapid growth and shrinkage as a result of GTP hydrolysis (Kirschner and Mitchison

1986). The dynamic instability of MTs has an important impact on KT capture, because it allows high turnover of MTs, which can then probe large amounts of space, at random, for KTs. Another important consequence of dynamic instability is the potential coexistence of growing and shrinking MTs in the same cell (Kirschner and Mitchison 1986). During KT capture, cells may require that some MTs shrink (for example those transporting a captured KT towards the spindle), while others must keep growing to explore the cell for the remaining uncaptured KTs. Thus, MT dynamic instability has important biological consequences for KT capture. *In vivo* the dynamics of MTs are regulated by a large variety of microtubule-associated proteins (MAPs), which can stabilise or destabilise MTs (see below).

2. Random search and capture model

Spindle-pole MTs exhibit dynamic instability, i.e. they alternate stochastically between phases of rapid growth and shrinkage to probe space for KTs, as described above (Kirschner and Mitchison 1986). Some of these MTs encounter and attach to KTs, but is this process sufficient to "locate" and attach all KTs within characteristic mitotic timescales? According to theoretical estimates random search-and-capture is an efficient way to search cellular space and ensure KT capture within characteristic mitotic timescales (Hill 1985; Holy and Leibler 1994). However, these estimates analyse capture time for a single kinetochore and not for their actual number in cells (Wollman et al. 2005). Random search-and-capture would recapitulate the time it would take for a single KT to get captured (approx. 23 min), but it would be inefficient to explain the capture of multiple KTs (approx. 125 min versus experimentally measured times of 20 min) where the capture time will be determined by the last KT to get captured – the most "unsuccessful" and prolonged search ($T_{capture} \sim \ln N_{k;}$ mean capture time is a logarithmic function of the number of kinetochores) (Wollman et al. 2005). Thus,

efficient KT capture of multiple KTs in cells cannot only be explained by an unbiased random search and capture model, and there must be additional strategies that enable the cell to achieve efficient capture of its entire population of KTs within its characteristic mitotic timescale.

3. Additional strategies to achieve efficient kinetochore capture

The efficiency of random search and capture can be optimised by different strategies such as: bias of MT growth towards KTs[1] (Carazo-Salais et al. 1999; Wollman et al. 2005), pivoting of MTs around the spindle pole[2] (Kalinina et al. 2013), kinetochore movements[3] (Paul et al. 2009), MT nucleation from pre-existing spindle-pole MTs[4] (Burbank et al. 2006; Mahoney et al. 2006) or from KTs[5] (Witt et al. 1980; Kitamura et al. 2010; Paul et al. 2009), or by a combination of any of these[6] (Mogilner and Craig 2010; O'Connell and Khodjakov 2007; Duncan and Wakefield 2011).

A bias of MT growth towards the KT[1] can be generated by a RanGTP gradient, which is formed around chromosomes (Carazo-Salas and Karsenti 2003; Caudron et al. 2005). Such a gradient could guide spindle-pole MTs to KTs by stabilising MTs selectively in the vicinity of chromosomes (Wollman et al. 2005). A RanGTP gradient can be effective over a relatively long range (~ 20 μm) (Athale et al. 2008), for example in vertebrate cells when chromosomes diffuse away from spindle poles after nuclear envelope break down during "open mitosis". Over the short distances (~1 μm) typical for yeast cells that undergo "closed mitosis" i.e. nuclear envelope does not break down, small RanGTP molecules diffuse too rapidly to generate a substantial gradient. Thus, it is unlikely that this mechanism is effective over short ranges.

At short range, a MT pivoting motion[2] (MTs change their orientation with respect to the spindle) (Sagolla et al. 2003) around spindle pole could facilitate KT capture (Kalinina et al. 2013). This pivoting of MTs is a random passive motion (independent of ATP-driven motor activity) that allows spindle-pole MTs to explore space laterally as they search for their target KTs (Kalinina et al. 2013).

So far we have considered only spindle-pole MTs as dynamic structures in KT capture. Nevertheless, they are not unique in undergoing complex random motions; KTs similarly move within the cellular space during prometaphase (Ostergren et al. 1960), often with characteristic random walk movements (Levesque and Compton 2001) (Murata-Hori and Wang 2002; Paul et al. 2009). These random KT displacements[3] accelerate KT capture by exposing each KT to multiple searching MTs (Paul et al. 2009).

Spindle poles (centrosomes in metazoans or SPBs in yeasts) are MTOCs that orchestrate nucleation and extension of spindle-pole MTs. Nevertheless, recent studies show that spindles can be also assembled in the absence of functional centrosomes (Khodjakov et al. 2000; Mahoney et al. 2006). In the absence of functional centrosomes, γ-tubulin is not concentrated at the poles, but dispersed within the cell and can still promote formation of functional spindles by generation of MTs at different sites along the length of the spindle (Mahoney et al. 2006). Thus, it is possible that, in physiological conditions, acentrosomal pathways, probably facilitated by pre-existing (interphase) MTs[4], contribute to spindle assembly (Mahoney et al. 2006; Burbank et al. 2006) and therefore to KT capture. Such natural acentrosomal spindles have been observed in meiotic spindles of oocytes in *Xenopus*, *Drosophila* and mammals (Khodjakov et al. 2000).

A widely studied acentrosomal pathway is kinetochore-driven MT nucleation[5] (Khodjakov et al. 2000; Maiato et al. 2004b). In addition to spindle poles, KTs have the capacity to orchestrate MT nucleation and extension (Telzer et al. 1975; Witt et al. 1980). Moreover, such so-called KT-derived MTs originate at KTs prior to their interaction with spindle-pole MTs, suggesting that they could facilitate KT capture (Kitamura et al. 2010).

Thus KT capture appear to be a complex process, which may be dependent on a combination of any of the above-mentioned mechanisms[6] (Mogilner and Craig 2010; O'Connell and Khodjakov 2007; Duncan and Wakefield 2011). How do these mechanisms contribute separately to efficient KT capture? Mathematical modelling may be able to answer this question when it is hard to experimentally resolve their individual contribution.

IV. Kinetochore-derived microtubules: from their discovery to today

KT-derived MTs were first described in 1975 when Telzer and colleagues observed that KTs of isolated chromosomes from human HeLa cells were able to assemble MTs *in vitro* (Telzer et al. 1975). Five years later, Witt and colleagues confirmed that KTs nucleated and extended MTs *in vivo,* in Chinese hamster ovary cells (Witt et al. 1980). Initially it was thought that these MTs originated at KTs with distal plus ends, similar to those originated from the spindle poles, based on their growth rate (Summers and Kirschner 1979; Bergen et al. 1980). This theory was contested by Euteneuer and colleagues, who proposed that KT-derived-MT plus ends were associated with KTs, rather than their minus ends (Euteneuer and McIntosh 1981; Euteneuer et al. 1983). This dispute was resolved in 1985 when Kirschner and Mitchison, the originators of MT

dynamic instability theory, reported that KTs *in vitro* can generate MTs with both distal plus and minus ends (Mitchison and Kirschner 1985a). Nevertheless, it is still unclear whether KT-associated MT nucleation with mixed polarity is an *in vitro* artefact, and it is widely thought that, in metazoans, KTs nucleate MTs with distal minus ends by incorporating tubulin subunits at KTs (Khodjakov et al. 2003; Maiato et al. 2004b). These KT-derived MTs nucleated with distal minus ends would have the same polarity as that of spindle-pole MTs, and so can be incorporated into the spindle poles (Khodjakov et al. 2003; Maiato et al. 2004b). Nevertheless, it is still difficult to study the polarity of KT-derived MTs in metazoans due to their high density both at KTs and at spindle poles. Moreover, for four decades into experimentation, little is known about what happens when KT-derived MTs encounter a spindle MT. If MT generation from spindle poles is the primarily mechanism for spindle assembly, as was initially suggested (Kirschner and Mitchison 1986; Rieder and Alexander 1990), then what is the role of KT-associated MT formation in KT capture?

V. Why budding yeast *S. cerevisiae* is a good model organism to study the role of kinetochore-derived microtubules in mitosis?

The yeast *S. cerevisiae* is a unicellular organism that divides by budding. Due to its amenable genetics, budding yeast has been a great model system for much of the molecular research into understanding basic cellular mechanisms. Today's awesome power of yeast genetics is a result of the ability to easily manipulate its fully sequenced haploid genome. It is possible to quickly modify multiple genetic loci and thus to study mutants causing particular phenotypes. An understanding of the roles of the genes involved in cellular mechanisms controlling cell division in yeast is applicable to higher eukaryotes (such as metazoans), including humans, because genes and mechanisms are generally highly conserved; for more information see (Schneiter 2004).

From yeast to humans, KTs can nucleate and extend MTs, but despite much research, little is known about their roles in mitosis. In higher eukaryotes MTs are generated with high density both at KTs and at the spindle poles. Due to this dense network of MTs, it is still challenging to study individual spindle-pole MT interactions with KTs or KT-derived MTs, in order to investigate their potential roles in KT capture. However, budding yeast is a very good model organism to study potential roles of KT-derived MTs in KT capture, because the interaction of individual KT with a single MT can be observed in relatively good resolution in physiological conditions (Kitamura et al. 2007). In addition, our laboratory has developed an engineered assay *in vivo* to specifically isolate a single KT from the spindle and investigate its interaction with spindle-pole MTs at higher resolution (Tanaka et al. 2005a). In budding yeast KT-derived MTs are generated with distal plus ends, which suggests that it is unlikely that these are incorporated into the spindle poles and participate in spindle assembly. These KT-derived MTs often appear prior to KT interaction with spindle pole MTs and have a limited lifetime in mitosis (Kitamura et al. 2010). When KT-derived-MTs extended from KTs, in several examples they appeared to interact with spindle-pole MTs (Kitamura et al. 2010). Once the interaction was established, they quickly disappeared as the KT was transported towards the spindle poles (Kitamura et al. 2010).

Altogether these observations suggested that KT-derived MTs might have a role in the capture of the KT by spindle-pole MTs. Moreover, generation of KT-derived MTs is correlated with efficient KT capture, but a causative relationship is still unclear (Kitamura et al. 2010). Investigating KT-derived MTs generated with distal plus ends in budding yeast provides and excellent system to investigate whether generation of MTs

at KTs with distal plus ends may have any physiological relevance in KT capture and mitosis.

VI. MAPs for microtubule nucleation and extension at kinetochores

Microtubules exhibit dynamic instability both *in vitro* and *in vivo*. However, *in vivo* their behaviour is modulated by proteins called microtubule-associated proteins (MAPs). These MAPs can be divided into four categories based on their function: 1) promotion and stabilisation of MT polymerisation; 2) destabilisation or severing of MTs; 3) functioning as linkers between various structures; or 4) motility-related functions e.g. motor proteins. MAPs are essential to coordinate and regulate the dynamic growth and shrinkage of MTs and their interaction with various cellular structures, such as KTs (Maiato et al. 2004e).

For many years it was believed that MAPs either stabilise or destabilise MTs until it was discovered that a MT polymerase from the family of Dis1/TOG MAPs (also known as XMAP215 family) is able to promote both MT polymerisation and depolymerisation, giving rise to more dynamic MTs; reviewed by (McNally 2003). Members of this MAP family are highly conserved from yeast to humans, and are involved in wide variety of MT and spindle functions; reviewed in (Ohkura et al. 2001). All members of this family (*S. cerevisiae* Stu2 (identified as a suppressor of tubulin mutation in 1997 by (Wang, 1997 #518)); *S. pombe* Dis1, Alp14; *C. elegans* ZYG-9; *D. melanogaster* Msps; *X. laevis* XMAP215; *H. sapiens ch*-TOG) localised at MT minus ends, at SPB/centrosomes, where they are required for nucleation of astral spindle-pole MTs (Ohkura et al. 2001). In addition, Dis1/TOG MAPs have a high affinity for MT plus ends, and are thought to promote MT extension by acting as MT polymerases; reviewed in (Al-Bassam and Chang 2011). Dis1/TOG MAPs interact with free tubulin dimers via conserved TOG domains, and promote MT polymerisation or depolymerisation by

antagonising MT pauses – a temporary state, in which MTs undergo neither growth nor shrinkage; reviewed in (Al-Bassam and Chang 2011).

Intriguingly, some Dis1/TOG members such as Dis1, Alp14, and Stu2p localise also to the kinetochores (Nakaseko et al. 2001; Garcia et al. 2001; He et al. 2001). In *S. cerevisiae,* Stu2 localisation at KTs is required for nucleation and extension of KT-derived MTs (Kitamura et al. 2010). Stu2 localised at KTs prior to first signs of MT generation and, upon their extension, stayed closely associated with both their nucleating minus ends and tracked their growing plus ends (Kitamura et al. 2010). Moreover, Stu2 was able to generate MTs when tethered at an engineered site, suggesting that Stu2 is sufficient *per se* to promote KT-associated MT formation (Kitamura et al. 2010). Although Stu2 homologues such as Msps and TOG have not been detected at KTs, based on recent reports they appear to be important for KT-driven MT formation (Bucciarelli et al. 2009) and MT nucleation in vicinity of chromosomes (Cassimeris et al. 2009).

Intriguingly, KT-associated MT formation in *S. cerevisiae* is not dependent on the canonical MTOC-generated pathway, which includes γ-tubulin (Kitamura et al. 2010) (Erlemann et al. 2012). In mammalian cells, γ-tubulin signals were faintly detected around the KT-associated MT centres, but they were never as prominent as those at centrosomes (Tulu et al. 2006). Biochemical studies suggest that γ-TuRC localises at KTs and is required for nucleation of KT-derived MTs (Mishra et al. 2010). This result creates a problem for the polarity of KT-derived MTs, which if nucleated via the standard template mechanism, will have their minus ends at KTs (Mishra et al. 2010). Thus it remains unclear whether γ-tubulin is required for generation of MTs at KTs that are initially un-anchored and subsequently interact with KTs via their plus ends, or

whether γ-tubulin is anchored during the nucleation and is subsequently released with the distal MT minus ends. Alternatively, as suggested by Kirschner and Mitchison, MTs at KTs may be nucleated with mixed polarity (Mitchison and Kirschner 1985a) as an assembly intermediate to facilitate KT capture by spindle-pole MTs, via antiparallel and parallel MT–MT interactions.

To summarise, investigating the mechanism for Stu2 recruitment and MT generation at KTs in *S. cerevisiae* may give an insight into a non-canonical γ-tubulin independent pathway operating at KTs. Such a KT-driven, Stu2-dependent pathway may facilitate initial KT capture by spindle-pole MTs. Furthermore, as a MAP that modulates the dynamics of MTs, KT-associated Stu2 may also play an important role after KT capture, to sustain KT-MT interaction by promoting MT rescue and preventing KT detachment (Gandhi et al. 2011).

Aim of This Study

The objective of this study was to understand the roles of KT-derived MTs in mitosis, more specifically in KT capture. To do this, one must first understand the molecular mechanisms promoting MT generation at KTs, and find a molecular tool to abolish MT nucleation specifically at KTs without compromising their extension from the spindle poles. Stu2^{XMAP215} is a MAP from the Dis1/TOG family, required for KT-associated MT formation (Kitamura et al. 2010). Nevertheless, reduction of Stu2 function in a *stu2-10* temperature-sensitive mutant led not only to the reduction of KT-derived MTs, but also of those at the spindle poles, because Stu2 is a MT polymerase required for the extension of both types of MTs (Kitamura et al. 2010). Therefore, to study the roles of KT-derived MTs in KT capture, it is necessary to specifically target the mechanism for Stu2 recruitment and MT-generation at KTs.

MATERIALS AND METHODS

I. Plasmids and yeast strains used in this study

All yeast strains used in this study and plasmids for their construction are listed in Table 1 and Table 2, respectively. All strains are derived from K699 or K700 (*MATa* or *MATα ade2-1, trp1-1, can1-100, leu2-3,112, his3-11,15, ura3, Gal+, Psi+* ; Nasmyth lab). For mating type checks, K216 (*MATa his1*; Nasmyth lab) and K217 (*MATα his1*; Nasmyth lab) strains were used. For viability checks, diploid K842 (*MATa*/*MATα ade2-1, trp1-1, can1-100, leu2-3,112, his3-11,15, ura3, Gal+, Psi+*) or K842 derived strain, in which original gene locus was deleted, were transformed with a mutant construct of interest and then dissected. The strain containing *Oryza sativa* TIR1 E3 ubiquitin ligase (T7179 *MATa ura3::*P_{ADH1}*-OsTIR1-2-9Myc::URA3 ade2-1, his3-11,15, trp1-1, leu2-3,112, can1-100*) and *IAA17::NatNT2* tagging cassette for the *aid* system (Nishimura et al. 2009) were kindly provided by Dr Masato Kanemaki. The strain containing *tor1-1 fpr1*Δ and *RPL13A-2xFKBP12* (T9421 *MATα tor1-1 fpr1*Δ*::NAT1 RPL13A-2xFKB12::TRP1 SCC1-FRB::kanMX6 ade2-1, trp1-1, leu2-3,112, his3-11,15, can1-100, ura3, Gal+, Psi+*) for the anchor-away technique (Haruki et al. 2008) was supplied by EUROSCARF (Y40356). The L40 strain (T8765 *LYS::lexA-HIS3 URA3::lexA-lacZ*) for lexA two-hybrid system was a gift from Prof Yoshiyuki Watanabe (Yamagishi et al. 2008). Plasmid construct used for labelling of α-tubulin with GFP fluorescent protein (pT341 *pAFS125-GFP-TUB1 (URA3)*) was supplied by E. Sciebel's lab (originally constructed by Dr A. Murray's lab). *TetR-GFP* and P_{MET3}*-CDC20* constructs were donated by Nasmyth's lab (Michaelis et al. 1997; Uhlmann et al. 2000). *TetR-3ECFP* construct at *ade1* locus (pDB075) was a gift from J Haber's lab (Bressan et al. 2004). Plasmid construct for amplification of *3GFP-KanMx6* cassette (pT404 ref. pSM1023) for labelling proteins at their endogenous loci were kindly provided by Dr H Maekawa and Dr E Schiebel (Maekawa et al. 2003). *CFP-TUB1* construct at *trp1* locus (pT342) was a gift by Schiebel's lab (Janke et al. 2002). *REC102::lacOs* construct used for

ectopic tethering of Stu1 and Stu2 proteins on the chromosome arm was kindly provided by Dr Frank Uhlmann (Sullivan et al. 2004). Basic *VN173-HIS3MX6* (pT940) and *VC155-HIS3MX6* (pT941) constructs used for studying protein-protein interaction *in vivo* were gift from Dr Won-Ki Huh (Sung and Huh 2007).

Table 1. Yeast strains used in this study

Figure	Strain	Genotype	Source
Figure 5	T11537	*MATa/MATalpha* *ndc80Δ::HPH1* *his3::P_{NDC80}-ndc80Δ444-459::HIS3*	This study
	BP13489	*MATa/alpha* *ndc80Δ::HPH1* *his3::P_{NDC80}-ndc80ΔL462-482::HIS3*	This study
	T11570	*MATa/alpha* *ndc80Δ::HPH1* *his3::P_{NDC80}-ndc80(L449-P)::HIS3*	This study
	T11572	*MATa/alpha* *ndc80Δ::HPH1* *his3::P_{NDC80}-ndc80(Y465-S)::HIS3*	This study
	BP13491	*MATa/alpha* *ndc80Δ::HPH1* *his3::P_{NDC80}-ndc80(L479-S)::HIS3*	This study
	T11484	*MATa* *cen3::P_{GAL}-CEN3-tetO$_{2x112}$::URA3* *ade1::TetR-3ECFP::HPH1* *ura3::P_{TUB1}-GFP-TUB1::URA3* *stu2::STU2-4mCherry::clonNat1* *cdc20::P_{MET3}-CDC20::TRP1* *ndc80::P_{NDC80}-HIS3- ndc80(L449-P)::HIS3*	This study
	T11485	*MATa* *cen3::P_{GAL}-CEN3-tetO2x112::URA3* *ade1::TetR-3ECFP::HPH1* *ura3::P_{TUB1}-GFP-TUB1::URA3* *stu2::STU2-4mCherry::clonNat1* *cdc20::P_{MET3}-CDC20::TRP1* *ndc80::P_{NDC80}-HIS3- ndc80(Y465-S)::HIS3*	This study
	T11486	*MATa* *cen3::P_{GAL}-CEN3-tetO2x112::URA3* *ade1::TetR-3ECFP::HPH1* *ura3::P_{TUB1}-GFP-TUB1::URA3* *stu2::STU2-4mCherry::clonNat1* *cdc20::P_{MET3}-CDC20::TRP1* *ndc80::P_{NDC80}-HIS3- NDC80(w.t.)::HIS3*	This study

	T11590	*MATa* *cen3::P_{GAL}-CEN3-tetO2x112::URA3* *ade1::TetR-3ECFP::HPH1* *ura3::P_{TUB1}-GFP-TUB1::URA3* *stu2::STU2-4mCherry::clonNat1* *cdc20::P_{MET3}-CDC20::TRP1* *ndc80::P_{NDC80}-HIS3-ndc80(L479-S)::HIS3*	This study
Figure 6	T9778	*MATa* *stu1::STU1-4mCherry::NatMX6* *cen15::PGAL-CEN3-tetO2x112::URA3* *ura3::P_{ADH1}-OSTIR1-2-9Myc::URA3* *his3::P_{TUB1}-GFP-TUB1::HIS3* *ade1::tetR-3CFP::HPH1* *cdc20::P_{MET3}-CDC20::TRP1*	Tanaka lab
	T3734	*MATa* *cen3::P_{GAL}-CEN3-tetO2x112::URA3* *ade1::tetR-3ECFP::HPH1* *ura3::CFP-TUB1::URA3* *cdc20::P_{MET3}-CDC20::TRP1* *stu1::STU1-3GFP::kanMX6*	Tanaka lab
	T10794	*MATalpha* *slk19::SLK19-4mCherry::natMX6* *cen15::PGAL-CEN3-tetO2x112::URA3* *ura3::P_{ADH1}-OSTIR1-2-9Myc::URA3* *his3::P_{TUB1}-GFP-TUB1::HIS3* *ade1::tetR-3CFP::HPH1* *cdc20::P_{MET3}-CDC20::TRP1*	Tanaka lab
Figure 7	T10501	*MATa* *ura3::P_{ADH1}-OSTIR1-2-9::URA3* *stu1::STU1-IAA17::ClonNat* *cen3::P_{GAL}-CEN3-tetO2x112::URA3* *ade1::tetR-3ECFP::HPH1* *cdc20::P_{MET}-CDC20::TRP1* *his3::P_{TUB1}-GFP-TUB1::HIS3*	This study
	T10594	*MATa* *ura3::P_{ADH1}-OSTIR1-2-9::URA3* *cen3::P_{GAL}-CEN3-tetO2x112::URA3* *ade1::tetR-3ECFP::HPH1* *cdc20::P_{MET3}-CDC20::TRP1* *his3::P_{TUB1}-GFP-TUB1::HIS3*	This study
Figure 8	T10823	*MATa/MATalpha* *stu1::stu1ΔC1174-1513::Nat1 (stu1ΔC339)*	This study
	T10888	*MATa/MATalpha* *stu1::stu1ΔC1174-1513-SV40::NatMx6 (stu1ΔC339-NLS)*	This study
	T10889	*MATa/MATalpha* *stu1::stu1ΔC1263-1513::NatMx6 (stu1ΔC250)*	This study
	T10890	*MATa/MATalpha* *stu1::stu1ΔC1263-1513-SV40::NatMx6 (stu1ΔC250-NLS)*	This study
	T10891	*MATa/MATalpha* *stu1::stu1ΔC1343-1513::NatMx6 (stu1ΔC170)*	This study
	T10892	*MATa/MATalpha* *stu1::stu1ΔC1343-1513-SV40::NatMx6 (stu1ΔC170-NLS)*	This study
	T11058	*MATa/MATalpha* *stu1::stu1ΔC1200-1513::Nat1 (Stu1dC313)*	This study
	T11059	*MATa/MATalpha* *stu1::stu1dC1453-1513::Nat1 (Stu1dC60)*	This study
	T10779	*MATa* *stu1Δ::KanMx4* *leu2::5UTR-stu1ΔC1175-1513-SV40-3GFP::LEU2*	This study

		trp1::P_{ADH1}-mCherry-TUB1::TRP1 *cen3::P_{GAL}-CEN3-tetO2x112::URA3* *ade1::tetR-3ECFP::HPH1* *cdc20::P_{MET3}-CDC20::TRP1*	
	T10960	*MATalpha* *cen15::P_{GAL}-CEN3-tetO2x112::URA3* *his3::P_{TUB1}-GFP-TUB1::HIS3* *ade1::tetR-3CFP::HPH1* *cdc20::P_{MET3}-CDC20::TRP1* *stu1::stu1ΔC1175-1513-SV40::NatMx6* *stu2::STU2-4xmCherry::Nat1Mx6*	This study
Figure 9	T9778	*MATa* *stu1::STU1-4mCherry::NatMX6* *cen15::P_{GAL}-CEN3-tetO2x112::URA3* *ura3::P_{ADH1}-OSTIR1-2-9Myc::URA3* *his3::P_{TUB1}-GFP-TUB1::HIS3* *ade1::tetR-3CFP::HPH1* *cdc20::P_{MET3}-CDC20::TRP1*	Tanaka lab
	T10822	*MATa* *stu1::STU1-4mCherry::NatMX6* *cen15::P_{GAL}-CEN3-tetO2x112::URA3* *ura3::P_{ADH1}-OSTIR1-2-9Myc::URA3* *his3::P_{TUB1}-GFP-TUB1::HIS3* *ade1::tetR-3CFP::HPH1* *cdc20::P_{MET3}-CDC20::TRP1* *slk19Δ::klLEU2*	This study
	T10660	*MATa* *cen15::P_{GAL}-CEN3-tetO2x112::URA3* *stu2::STU2-4mCherry::kanMX4* *ura3::P_{ADH1}-OSTIR1-2-9Myc::URA3* *his3::P_{TUB1}-GFP-TUB1::HIS3* *ade1::tetR-3CFP::HPH1* *cdc20::P_{MET3}-CDC20::TRP1* *slk19Δ::natNT2*	Tanaka lab
	T9407	*MATa* *cen15::P_{GAL}-CEN3-tetO2x112::URA3* *stu2::STU2-4mCherry::kanMX4* *ura3::P_{ADH1}-OSTIR1-2-9Myc::URA3* *his3::P_{TUB1}-GFP-TUB1::HIS3* *ade1::tetR-3CFP::HPH1* *cdc20::P_{MET3}-CDC20::TRP1*	Tanaka lab
Figure 10	BP12161	*MATa* *ura3::P_{ADH1}-OSTIR1-2-9Myc::URA3* *stu1::STU1-IAA17::ClonNat* *trp1::P_{ADH1}-mCherry-TUB1::TRP1* *cen3::P_{GAL}-CEN3-tetO2x112::URA3* *ade1::tetR-3ECFP::HPH1* *cdc20::P_{MET3}-CDC20::TRP1* *stu2::STU2-3GFP::KanMx6*	This study
	T10699	*MATalpha* *ura3::P_{ADH1}-OSTIR1-2-9Myc::URA3* *trp1::P_{ADH1}-mCherry-TUB1::TRP1* *cen3::P_{GAL}-CEN3-tetO2x112::URA3* *ade1::tetR-3ECFP::HPH1* *cdc20::P_{MET3}-CDC20::TRP1* *stu2::STU2-3GFP::KanMx6*	This study
	T10833	*MATa* *trp1::P_{ADH1}-mCherry-TUB1::TRP1* *cen3::P_{GAL}-CEN3-tetO2x112::URA3* *ade1::tetR-3ECFP::HPH1* *cdc20::P_{MET3}-CDC20::TRP1*	This study

		stu1::STU1-2GFP::KanMX6 *ura3::P_{ADH1}-OSTIR1-2-9Myc::URA3*	
	T10834	*MATa* *trp1::P_{ADH1}-mCherry-TUB1::TRP1* *cen3::P_{GAL}-CEN3-tetO2x112::URA3* *ade1::tetR-3ECFP::HPH1* *cdc20::P_{MET3}-CDC20::TRP1* *stu1::STU1-2GFP::KanMX6* *ura3::P_{ADH1}-OSTIR1-2-9Myc::URA3* *stu2::STU2-IAA17::NatNT2*	This study
Figure 11	T11037	*MATalpha* *REC102::lacOs::URA3* *his3::P_{GALS}-STU2-GFP-LacI::HIS3* *trp1::CFP-TUB1::TRP1* *cdc20::P_{MET3}-CDC20::TRP1* *stu1::STU1-4xmCherry::NatMx6*	This study
	T11686	*MATa* *ura3::P_{ADH1}-OSTIR1-2-9Myc::URA3* *stu1::STU1-IAA17::natNT2* *REC102::lacOs::URA3* *his3::P_{GALS}-STU2-GFP-LacI::HIS3* *trp1::CFP-TUB1::TRP1* *cdc20::P_{MET3}-CDC20::TRP1*	This study
	T5477	*MATa* *cen3::P_{GAL}-CEN3-tetO2x112::URA3* *ade1::TetR-3ECFP::HPH1* *cdc20::P_{MET3}-CDC20::TRP1* *STU2-GFP::URA3*	Tanaka lab
	T11722	*MATalpha* *ura3::P_{ADH1}-OSTIR1-2-9Myc::URA3* *REC102::lacOs::URA3* *his3::P_{GALS}-STU2-GFP-LacI::HIS3* *trp1::CFP-TUB1::TRP1* *cdc20::P_{MET3}-CDC20::TRP1*	This study
Figure 12	T11106	*MATalpha* *REC102::lacOs::URA3* *trp1::CFP-TUB1::TRP1* *cdc20::P_{MET3}-CDC20::TRP1* *his3::p_{GALS}-STU1-GFP-lacI::HIS3*	This study
	T11263	*MATalpha* *cen15::P_{GAL}-CEN3-tetO2x112::URA3* *ade1::tetR-3CFP::HPH1* *trp1::P_{TEF1}-mcherry-TUB1::TRP1* *REC102::lacOs::URA3* *cdc20::P_{MET3}-CDC20::TRP1* *his3::P_{GALS}-STU1-GFP-LacI::HIS3*	This study
	T11339	*MATa* *ura3:::P_{ADH1}-OSTIR1-2-9::URA3* *stu1::STU1-IAA17::NatMx6* *cen3::P_{GAL}-CEN3-tetO2x112::URA3* *ade1::tetR-CFP::HPH1* *trp1::P_{TEF1}-mcherry-TUB1::TRP1* *REC102::lacOs::URA3* *his3::P_{GALS}-STU1-GFP-LacI::HIS3* *cdc20::pMET-CDC20::TRP1*	This study
Figure 13	T10912	*L40* *MATa* *trp1 leu2 his3 LYS::lexA-HIS3 URA3::lexA-lacZ* *pBTM-Stu1* *pGAD-Stu1*	Tanaka lab

BP12459	*L40* *MATa* *trp1 leu2 his3 LYS::lexA-HIS3 URA3::lexA-lacZ* *pBTM-Stu1* *pGAD-Stu1N*	Tanaka lab
BP12460	*L40* *MATa* *trp1 leu2 his3 LYS::lexA-HIS3 URA3::lexA-lacZ* *pBTM-Stu1* *pGAD-Stu1M*	Tanaka lab
BP12461	*L40* *MATa* *trp1 leu2 his3 LYS::lexA-HIS3 URA3::lexA-lacZ* *pBTM-Stu1* *pGAD-Stu1C*	Tanaka lab
BP12306	*L40* *MATa* *trp1 leu2 his3 LYS::lexA-HIS3 URA3::lexA-lacZ* *pBTM-Stu1* *Stu2-ORF-27-37-pGAD-C1*	Tanaka lab
BP12307	*L40* *MATa* *trp1 leu2 his3 LYS::lexA-HIS3 URA3::lexA-lacZ* *pBTM-Stu1* *Stu2-(1-658)-40-41-pGAD-C1*	Tanaka lab
BP12308	*L40* *MATa* *trp1 leu2 his3 LYS::lexA-HIS3 URA3::lexA-lacZ* *pBTM-Stu1* *Stu2-(550-888)-46-45-pGAD-C1*	Tanaka lab
BP12462	*L40* *MATa* *trp1 leu2 his3 LYS::lexA-HIS3 URA3::lexA-lacZ* *pBTM-Stu1N* *pGAD-Stu1*	Tanaka lab
BP12463	*L40* *MATa* *trp1 leu2 his3 LYS::lexA-HIS3 URA3::lexA-lacZ* *pBTM-Stu1N* *pGAD-Stu1N*	Tanaka lab
BP12464	*L40* *MATa* *trp1 leu2 his3 LYS::lexA-HIS3 URA3::lexA-lacZ* *pBTM-Stu1N* *pGAD-Stu1M*	Tanaka lab
BP12465	*L40* *MATa* *trp1 leu2 his3 LYS::lexA-HIS3 URA3::lexA-lacZ* *pBTM-Stu1N* *pGAD-Stu1C*	Tanaka lab
BP12466	*L40* *MATa* *trp1 leu2 his3 LYS::lexA-HIS3 URA3::lexA-lacZ* *pBTM-Stu1N* *Stu2-ORF-27-37-pGAD-C1*	Tanaka lab
BP12467	*L40* *MATa* *trp1 leu2 his3 LYS::lexA-HIS3 URA3::lexA-lacZ* *pBTM-Stu1N* *Stu2-(1-658)-40-41-pGAD-C1*	Tanaka lab

BP12468	*L40* *MATa* *trp1 leu2 his3 LYS::lexA-HIS3 URA3::lexA-lacZ* *pBTM-Stu1N* *Stu2-(550-888)-46-45-pGAD-C1*	Tanaka lab
T10893	*L40* *MATa* *trp1 leu2 his3 LYS::lexA-HIS3 URA3::lexA-lacZ* *pBTM-Stu1M* *pGAD-Stu1*	Tanaka lab
BP12413	*L40* *MATa* *trp1 leu2 his3 LYS::lexA-HIS3 URA3::lexA-lacZ* *pBTM-Stu1M* *pGAD-Stu1N*	Tanaka lab
BP12414	*L40* *MATa* *trp1 leu2 his3 LYS::lexA-HIS3 URA3::lexA-lacZ* *pBTM-Stu1M* *pGAD-Stu1M*	Tanaka lab
BP12415	*L40* *MATa* *trp1 leu2 his3 LYS::lexA-HIS3 URA3::lexA-lacZ* *pBTM-Stu1M* *pGAD-Stu1C*	Tanaka lab
BP12416	*L40* *MATa* *trp1 leu2 his3 LYS::lexA-HIS3 URA3::lexA-lacZ* *pBTM-Stu1M* *Stu2-ORF-27-37-pGAD-C1*	Tanaka lab
BP12417	*L40* *MATa* *trp1 leu2 his3 LYS::lexA-HIS3 URA3::lexA-lacZ* *pBTM-Stu1M* *Stu2-(1-658)-40-41-pGAD-C1*	Tanaka lab
BP12418	*L40* *MATa* *trp1 leu2 his3 LYS::lexA-HIS3 URA3::lexA-lacZ* *pBTM-Stu1M* *Stu2-(550-888)-46-45-pGAD-C1*	Tanaka lab
BP12423	*L40* *MATa* *trp1 leu2 his3 LYS::lexA-HIS3 URA3::lexA-lacZ* *pBTM-Stu1C* *pGAD-Stu1*	Tanaka lab
BP12424	*L40* *MATa* *trp1 leu2 his3 LYS::lexA-HIS3 URA3::lexA-lacZ* *pBTM-Stu1C* *pGAD-Stu1N*	Tanaka lab
BP12425	*L40* *MATa* *trp1 leu2 his3 LYS::lexA-HIS3 URA3::lexA-lacZ* *pBTM-Stu1C* *pGAD-Stu1M*	Tanaka lab
BP12426	*L40* *MATa* *trp1 leu2 his3 LYS::lexA-HIS3 URA3::lexA-lacZ* *pBTM-Stu1C* *pGAD-Stu1C*	Tanaka lab

	BP12427	*L40* *MATa* *trp1 leu2 his3 LYS::lexA-HIS3 URA3::lexA-lacZ* *pBTM-Stu1C* *Stu2-ORF-27-37-pGAD-C1*	Tanaka lab
	BP12428	*L40* *MATa* *trp1 leu2 his3 LYS::lexA-HIS3 URA3::lexA-lacZ* *pBTM-Stu1C* *Stu2-(1-658)-40-41-pGAD-C1*	Tanaka lab
	BP12429	*L40* *MATa* *trp1 leu2 his3 LYS::lexA-HIS3 URA3::lexA-lacZ* *pBTM-Stu1C* *Stu2-(550-888)-46-45-pGAD-C1*	Tanaka lab
Figure 14	T6453	*MATa* *stu2::Stu2-VC155:TRP1*	Tanaka lab
	T6586	*MATa* *stu2::Stu2-VN173:TRP1*	Tanaka lab
	T11335	*MATa* *stu2::Stu2-VN173::TRP1* *stu1::Stu1-VC155::HIS3Mx6*	This study
	T11336	*MAT a* *stu2::Stu2-VC155:TRP1* *stu1::Stu1-VN173::HISMx6*	This study
	T11516	*MATalpha* *ura3::P_{ADH1}-OSTIR1-2-9::URA3* *trp1::P_{ADH1}-mCherry-TUB1::TRP1* *cen3::P_{GAL}-CEN3-tetO2x112::URA3* *ade1::tetR-3ECFP::HPH1* *cdc20::P_{MET3}-CDC20::TRP1* *stu1::STU1-VC155::HISMx6* *stu2::STU2-VN173::TRP1*	This study
	T11379	*MATalpha* *trp1::P_{ADH1}-mCherry-TUB1::TRP1* *cen3::P_{GAL}-CEN3-tetO2x112::URA3* *ade1::tetR-3ECFP::HPH1* *cdc20::P_{MET3}-CDC20::TRP1* *stu1::Stu1-VN173::HisMx6* *stu2::Stu2-VC155::TRP1*	This study
Figure 16, Figure 17, Figure 18, Figure 20, Figure 21, Figure 22	T11242	*MATalpha* *1.4Kb from CEN5::tetO2x112::HIS3* *ade1::tetR-3CFP::HPH1* *trp1::P_{TUB1}-YFP-TUB1::TRP1* *tor1-1* *fpr1Δ::NAT* *rpl13a::RPL13A-2xFKBP12::TRP1* *mtw1::MTW1-4mCherry::Nat1* *ndc80::Ndc80-4mCherry::Nat1*	This study
	T11230	*MATalpha* *1.4Kb from CEN5::tetO2x112::HIS3* *ade1::tetR-3CFP::HPH1* *trp1::pTUB1-YFP-TUB1::TRP1* *tor1-1* *fpr1Δ::NAT* *rpl13a::RPL13A-2xFKBP12::TRP1* *stu1::STU1-FRB::Nat1* *mtw1::MTW1-4mCherry::Nat1* *ndc80::Ndc80-4mCherry::Nat1*	This study

Figure 19	T11766	*MATa* *1.4Kb from CEN5::tetO2x112::HIS3* *ade1::tetR-3CFP::HPH1* *his3::GFP-TUB1::HIS3* *tor1-1* *fpr1Δ::NAT* *rpl13a::RPL13A-2xFKBP12::TRP1* *stu1::STU1-FRB::Nat1* *nic96::NIC96-4mCherry::KanMx4*	This study
	T11802	*MATa* *1.4Kb from CEN5::tetO2x112::HIS3* *ade1::tetR-3CFP::HPH1* *his3::GFP-TUB1::HIS3* *tor1-1* *fpr1Δ::NAT* *rpl13a::RPL13A-2xFKBP12::TRP1* *nic96::NIC96-4mCherry::KanMx4*	This study
Figure 23	T11965	*MATalpha* *cen15::P_{GAL}-CEN3-tetO2x112::URA3* *leu2::tetR-GFP::LEU2* *tor1-1* *fpr1Δ::NAT* *rpl13a::RPL13A-2xFKBP12::TRP1* *stu1::STU1-FRB::Nat1* *cdc20::P_{MET3}-CDC20::TRP1* *his3::GFP-TUB1::HIS3*	This study
	T11966	*MATalpha* *cen15::P_{GAL}-CEN3-tetO2x112::URA3* *leu2::tetR-GFP::LEU2* *tor1-1* *fpr1Δ::NAT* *rpl13a::RPL13A-2xFKBP12::TRP1* *cdc20::P_{MET3}-CDC20::TRP1* *his3::GFP-TUB1::HIS3*	This study
Figure 24	T10836	*MATa* *cen15::P_{GAL}-CEN3-tetO2x112::URA3* *ade1::tetR-3CFP::HPH1* *his3::GFP-TUB1::HIS3* *tor1-1* *fpr1Δ::NAT* *rpl13a::RPL13A-2xFKBP12::TRP1* *cdc20::P_{MET3}-CDC20::TRP1* *stu1::STU1-FRB::Nat1*	This study
	T10546	*MATa* *cen15::P_{GAL}-CEN3-tetO2x112::URA3* *ade1::tetR-3CFP::HPH1* *his3::GFP-TUB1::HIS3* *TOR1-1* *fpr1Δ::NAT* *rpl13a::RPL13A-2xFKBP12::TRP1* *cdc20::P_{MET3}-CDC20::TRP1*	This study
Figure 25	T12067	*MATa* *cen15::P_{GAL}-CEN3-tetO2x112::URA3* *ade1::tetR-3CFP::HPH1* *his3::GFP-TUB1::HIS3* *TOR1-1* *fpr1Δ::NAT* *rpl13a::RPL13A-2xFKBP12::TRP1* *cdc20::P_{MET3}-CDC20::TRP1* *ndc80::P_{NDC80}-ndc80Δ490-510::LEU2*	This study
	T12068	*MATa* *cen15::P_{GAL}-CEN3-tetO2x112::URA3*	This study

	ade1::tetR-3CFP::HPH1 *his3::GFP-TUB1::HIS3* *tor1-1* *fpr1Δ::NAT* *rpl13a::RPL13A-2xFKBP12::TRP1* *cdc20::P_{MET3}-CDC20::TRP1* *stu1::STU1-FRB::Nat1* *ndc80::pNDC80-ndc80Δ490-510::LEU2*

Table 2. Plasmids used for the construction of yeast strains used in this study

Plasmid	Description	Source
pT2361	*5UTR-ndc80ΔL444-459-3UTR-5UTR/pRS303 (HIS3)*	This study
pT2357	*5UTR-ndc80ΔL462-482-3UTR-5UTR/pRS303 (HIS3)*	This study
pT2358	*5UTR-ndc80(L449-P)-3UTR-5UTR/pRS303 (HIS3)*	This study
pT2360	*5UTR-ndc80(Y465-S)-3UTR-5UTR/pRS303 (HIS3)*	This study
pT2359	*5UTR-ndc80(L479-S)-3UTR-5UTR/pRS303 (HIS3)*	This study
pT1903	*5UTR-NDC80-3UTR-5UTR/pRS303 (HIS3)*	Tanaka lab
pT909	*pFA6a-4mCherry-natMX6*	Tanaka lab
pT1219	*P_{TUB1}-GFP-TUB1/pRS403 (HIS3)*	Tanaka lab
pT389	*P_{GAL}-CEN3-CYC1-tetO_{2x112}/YIplac211* for integration at *CEN3*	Tanaka lab
pT623	*P_{GAL}-CEN3-CYC1-tetO_{2x112}/*YIplac211 for integration at *CEN15*	Tanaka lab
pT1955	*5UTR-stu1dC1175-1513-NLS-3GFP-TADH1/pRS405 (LEU2)*	This study
pT1711	*pFA-4mCherry-kanMX4*	Tanaka lab
pT1244	*P_{ADH1}-mCherry-Tub1/pRS304 (TRP1)*	Tanaka lab
pT779	*P_{GALS}-STU2-GFP-LacI/pRS303 (HIS3)*	Tanaka lab
pT2160	*P_{GALS}-STU1-GFP-LacI/ pRS303 (HIS3)*	This study
pT1243	*P_{TEF1}-mCherry-Tub1/pRS304 (TRP1)*	Tanaka lab
pT2083	*pBTM-Stu1-ORF-(1-1513)*	Tanaka lab
pT2087	*pGAD-Stu1-(1-1513)*	Tanaka lab
pT2094	*pGAD-Stu1N-(1-510)*	Tanaka lab
pT2095	*pGAD-Stu1M (500-1010)*	Tanaka lab
pT2096	*pGAD-Stu1C-(1000-1513)*	Tanaka lab
pT1583	*Stu2-ORF-27-37-pGAD-C1*	Tanaka lab
pT1585	*Stu2-(1-658)-40-41-pGAD-C1*	Tanaka lab
pT1587	*Stu2-(550-888)-46-45-pGAD-C1*	Tanaka lab
pT2098	*pBTM-Stu1M-(500-1010)*	Tanaka lab
pT2099	*pBTM-Stu1C-(1000-1513)*	Tanaka lab
pT943	*pFA6A-VC155-TRP1*	Tanaka lab
pT942	*pFA6A-VN173-TRP1*	Tanaka lab
pT371	*P_{TUB1}-YFP-TUB1/ pRS304 (TRP1)*	Tanaka lab
pT2266	*5UTR-ndc80ΔL490-510-3UTR-5UTR /pRS405 (LEU2)*	Tanaka lab

II. Materials

1. Chemicals and solutions

All chemicals used in this study were purchased from Sigma, Roche Molecular Biologicals, British Drug House (BDH) and Amersham International, unless otherwise indicated. Water was filtrated and deionized with MilliQ (Millipore) water filtration stations.

50X TAE (2M Tris-acetate, 50mM EDTA) and 50X PBS (Phosphate-buffered saline) stock solutions were prepared by College of Life Sciences Media Kitchen, University of Dundee, following a standard formula (Sambrook and Russell 2001).

2. Enzymes and other molecular biology reagents

All restriction enzymes used in this study with their respective buffers and bovine serum albumin (BSA) supplements were supplied by New England Biolabs and Roche. The Biotaq DNA polymerase (Bioline) was used for diagnostic PCRs, while high fidelity PrimeStar DNA polymerase (Takara) was used for amplification of DNA fragments used for cloning and transformation.

3. Growth media

All liquid and solid growth media used in this study were made by College of Life Sciences Media Kitchen, University of Dundee (see below). For all solid media 1.5–2% (w/v) Bacto Agar (Difco) was added.

3.1. *S. cerevisiae* growth media

Yeast growth media was prepared following a standard recipe as described by (Amberg et al. 2005).

Yeast-Peptone-Adenine (YPA) media was used whenever it was possible. YPA media contains 1% (w/v) yeast extract (Difco), 2% (w/v) Bacto-peptone (Difco), 0.004% (w/v) adenine (Sigma). For different purposes the YPA media was supplemented with 2% (w/v) glucose (YPAD) or 2% raffinose plus 2% galactose (YPARG).

Synthetic dextrose (SD) minimal medium was used to check the mating type of strains contains (0.67 % (w/v)) yeast nitrogen base without amino acids (Sigma) supplemented with 2% glucose. Synthetic complete (SC) medium used for the microscopy experiments was prepared with SD minimal medium and 0.2% Drop out mix containing all amino acids and other synthetic growth factors and then supplemented with 2% glucose (SCD) or 2% raffinose plus 2% galactose (SCRG). To test for specific auxotrophic deficiencies of the yeast strains or to grow particular strains (e.g. P_{MET3}-*CDC20*), relevant amino acids were omitted from the medium to apply specific selection or to allow their growth (e.g. drop-out medium Do-met contains drop out mix with all amino acids except methionine).

Sporulation medium (VB medium) used to sporulate diploid strains contains 0.82% (w/v) sodium acetate (BDH), 0.19% (w/v) KCl (BDH), 0.12% (w/v) NaCl (BDH) and 1.5% (w/v) Bacto agar (Difco).

YPAD medium and various SD-derived drop-out mediums (e.g. Do-met) were supplemented with different antibiotics: 100 µg/mL ClonNAT (Werner Bioreagents), 200 µg/mL G-418 (Melford Labs) and 300 µg/mL Hygromycin B (Roche) to apply specific selection for antibiotic resistance genes *NAT*, *KAN* and *HPH*, respectively. For drop-out media supplemented with antibiotics, monosodium glutamate (MSG) (Sigma)

was used as nitrogen source, because ammonium sulfate interferes with the function of G-418 and Hygromycin B antibiotics in minimal medium (Webster and Dickson 1983).

3.2. *E. coli* growth media

Bacterial growth media was prepared as described by (Sambrook and Russell 2001). Luria-Bertani (LB) medium broth, which contains 1% Bacto peptone (Difco), 0.5% Bacto yeast extract (Difco), 1% NaCl (BDH) pH 7.0, was supplemented with 100 µg/mL ampicillin (Formedium) to use for growth and selection of *E. coli* strains containing plasmids of interest with ampicillin resistance gene.

SOC medium (2% (w/v) bacto tryptone, 0.5% (w/v) bacto yeast extract, 0.01 M NaCl, 0.02 M glucose) was used during bacterial transformation for recovery of *E. coli* cells after heat shock and to allow the expression of ampicillin resistance genes.

III. Methods

All experiments were carried out at room temperature unless otherwise indicated. Yeast cells were grown at 25 °C, while bacterial cells were grown at 37 °C.

1. DNA manipulation methods

1.1. Polymerase chain reaction (PCR) to amplify DNA

Diagnostic PCR reactions were carried out with BIOTAQ DNA polymerase (Bioline) to evaluate integration of DNA constructs at specific gene loci on genome. PCR reactions typically included 10X NH_4 reaction buffer (Bioline), 1.5 mM $MgCl_2$ solution and 250 µM dNTPs (dATP, dCTP, dGTP and dTTP) (Invitrogen), oligonucleotide primers designed to flank the area to amplify at 500 nM each, 0.5 unit of BIOTAQ DNA polymerase (Bioline) and 0.5 µl of yeast colony prep DNA as a template in a total PCR

reaction mixture of 10 µl. PCR reactions were then heated to 94 °C for 3 min, then 29 cycles at 94 °C for 1 min, 55 °C for 1 min, 72 °C for 1 min per kb of DNA amplification.

PCR reactions for amplification of DNA fragments, which were used for cloning or transformation, were carried out with PrimeStar HS DNA polymerase (Takara) following manufacturer's instructions: the reactions included 5X PrimeStar buffer (includes $MgCl_2$) and 200 µM dNTPs mix (dATP, dCTP, dGTP and dTTP), oligonucleotide primers designed to flank the area to amplify at 300 nM each, 2.5 units of PrimeStar HS DNA polymerase and 2 µl (50-times diluted after the Miniprep) plasmid or genomic DNA (high purity, see below) in a total PCR reaction mixture of 100 µl. PCR reactions were then heated to 98 °C for 3 min, then 29 cycles at 98 °C for 10 sec, 55 °C for 5 sec, 72 °C for 1 min per kb of DNA amplification.

1.2. Agarose gel electrophoresis to resolve DNA fragments

0.8–1% (w/v) agarose (Invitrogen) / TAE 1X gels supplemented with 0.15 µg/mL ethidium bromide (VWR) were used to separate DNA fragments for applications such as analysis of PCR products, separation of DNA fragments, and plasmid backbone DNA, digested by restriction enzymes prior to cloning and for estimation of the size of DNA molecule after diagnostic enzyme digestion. The DNA samples were loaded with 6X blue/orange loading dye, run at the constant voltage of 100 V and then visualised using GeneFlash (Syngene) UV illumination.

1.3. Purification of DNA from agarose gel

DNA bands were cut out of the agarose gel under UV light and then purified using QIAquick (MinElute) Gel extraction Kit (Qiagen) following manufacturer's instructions.

1.4. Purification of DNA from PCR reaction

DNA molecules were purified from PCR reaction mixture using MinElute PCR Purification Kit (Qiagen) following manufacturer's instructions.

1.5. Digestion of DNA by restriction enzyme

For all restriction enzyme digestions 0.5–2 U/µl of restriction enzymes per 25 µl of reaction were used to digest 2 µg of plasmid DNA (when required 0.1 mg/mL BSA was added). The reactions were then incubated usually for 2.5 hrs at 37 °C unless otherwise required for the activity of the restriction enzyme.

1.6. DNA ligation

All ligation reactions of DNA plasmid backbones and inserts were carried out with Rapid DNA ligation kit (Roche) following manufacturer instructions. The plasmid backbone and the insert were typically added at the molar ratio of 1:3 in the total reaction mixture of 10 µl. The ligation was then incubated usually at 25 °C for 30 min or overnight at 16 °C. For ligation of blunt ends, the plasmid backbone was dephosphorylated with 0.3 U/µl antarctic phosphatase (NEB) / 10X AP reaction buffer at 37 °C for 30 min followed by inactivation of the enzyme at 65 °C for 10 min. For comparison, a control ligation mixture was set up, which contained only the vector, but not the insert DNA.

1.7. DNA transformation methods

Plasmid constructs were transformed into XL1-Blue competent cells (Stratagene) following manufacturer's instructions. Typically 50 µl cells were transformed with 25 ng of ligation mixture and selected overnight on LB plates supplemented with 100 µg/mL ampicillin at 37 °C. In parallel as a control 50 µl cells were also transformed with the control ligation mixture (see above).

1.8. Isolation of plasmid DNA from *E. coli*

Isolation and purification of plasmid DNA was carried out with QIAprep Spin Miniprep Kit (Qiagen) following manufacturer's instructions.

1.9. DNA synthesis

All primer oligonucleotides used in this study were synthesised by Eurofins. DNA fragments used for the construction of *ndc80Δ444-459*, *ndc80Δ462-482*, *ndc80(L449-P)*, *ndc80(Y465-S)*, *ndc80(L479-S)* were synthesized by DNA 2.0 Gene Synthesis & Bioengineering.

1.10. DNA sequencing

DNA molecules of interest (plasmids and PCR products) were sequenced by the facility of DNA sequencing & services, MRC PPU, University of Dundee using semi-automated Sanger DNA sequencing.

2. Yeast methods

2.1. Isolation of genomic DNA from yeast

Extraction of high purity genomic DNA (e.g. for cloning purposes) was as described by (Amberg et al. 2005) with minor modifications. Yeast cells in exponential growth phase

from overnight culture were collected and suspended in 0.5 mL of 1 M sorbitol, 0.1 M Na_2EDTA (pH7.5) and 0.25 mg/mL Zymolyase 100T and incubated for 1 hr at 37 °C to lyse the cell walls. After 1 hr, cell were collected by brief centrifugation and re-suspended in 0.5 mL 50mM Tris-Cl (pH7.4), 20 mM Na_2EDTA and 1% SDS (Sodium dodecyl sulphate). Cell suspension was then incubated at 65 °C. After 30 min 0.2 mL of 5 M KOAc (Potassium Acetate) was added and the suspension was placed on ice for 1 hr. Then the suspension was centrifuged to separate genomic DNA from proteins and cell debris. Genomic DNA was precipitated from the supernatant after adding 1 volume of 100% Isopropanol, the pellet was air dried and re-suspended in 0.3 mL of Tris-EDTA (TE) (pH7.4) and 0.5 M NaOAc (Sodium Acetate). Finally genomic DNA was precipitated after adding isopropanol for a second time and re-suspended in 0.1 mL Tris-EDTA (pH7.4).

Extraction of genomic DNA for diagnostic PCRs (e.g. check integration of transformed DNA into the yeast genome) was carried out by yeast colony preps. Approximately 10 µl of freshly grown yeast cells on a plate were suspended in 50 µl of 0.01% Sarkosyl 0.02 N NaOH and incubated at 94 °C for 10 min. Cell suspension was centrifugated for 30 sec at 13,000 rpm and supernatant was transferred to a new tube. 0.5 µl of the supernatant was used for diagnostic PCR reactions of 10 µl.

2.2. PCR-based one-step gene tagging on yeast genome

To tag yeast genes with tandem copies of fluorescent proteins (e.g. *3xGFP*, *4xmCherry*, *3xCFP*), a PCR-based method was used as described by (Knop et al. 1999). In this method, a tagging cassette (a fluorescent protein gene and a selection marker gene) was amplified by PCR from a relevant plasmid, using PCR primers with additional 50 bp DNA sequences matching to the 5' end of the yeast gene of interest (excluding the

STOP codon) and 3'UTR. The tagging cassette was then purified from the PCR reaction or the electrophoresis gel.

Yeast genes were disrupted by one-step gene replacement, in which constructs that contain a selection marker gene with homologous 50 bp upstream and downstream of the gene ORF, replaced the endogenous ORF (e.g. *ndc80*Δ*::HPH1*).

Stu1 C-terminus was disrupted at its endogenous locus in diploid K842 strain by introduction of a construct containing a stop codon, ADH1 terminator and a selection marker gene (NatMx6) with homologous 50 bp upstream of the codon encoding the amino acid to follow the disruption and 50 bp downstream of the endogenous stop codon. *SV40* NLS signal was introduced in the forward primer (downstream of the homologous 50 bp) used to amplify the C-terminal disruption cassette.

2.3. Plasmid integration into yeast genome by linear replacement or loop-in

Plasmid integration into yeast genome was carried out as following. For linear replacement of yeast genes with a purpose of introducing mutations at their endogenous loci, a plasmid containing the gene with the mutations of interest, its 3'UTR and two 5'UTR regions was designed so that the selection marker resides between the two 5'UTRs in the following order: 5UTR > ORF of the gene containing the mutation > 3UTR < 5UTR > Selection marker. So when the plasmid was linearized between the 5'UTR and the 3'UTR, it can be integrated in the genome in the following order: 5'UTR > Selection Marker > 5'UTR > ORF of the gene containing the mutation > 3'UTR. Correct integration and presence of mutations of interest were confirmed by diagnostic PCRs and sequencing.

For plasmid integrations by loop-in, the auxotrophic loci were used. Plasmids were linearized with suitable restriction enzymes within the auxotrophic markers and then integrated into the yeast genome by transformation. Single or multiple (tandem) integrations were tested by diagnostic PCRs.

2.4. High-efficiency transformation of yeast cells

Transformations were carried out with purified PCR products or linearized plasmids as described by (Amberg et al. 2005) with minor modifications. Yeast cells in exponential growth phase from overnight culture were collected by centrifugation at 2,500 rpm for 5 min. Cells were washed with water, harvested at 2,500 rpm for 5 min and re-suspended in 4 volumes of 100 mM LiAc (Lithium Acetate) (Sigma). Then 25 µl of the cell suspension was centrifugated and cell pellet was re-suspended into the transformation mixture of 30% (w/v) PEG (Polyethilene glycol), 100 mM LiAc (Lithium Acetate) (Sigma), 0.125 mg/mL carrier ssDNA (single strand salmon sperm DNA) supplemented with 0.5–2 µg of PCR product or plasmid DNA. Cell suspension was then incubated at 30 °C for 30 min and heat-shocked at 42 °C for 20 min. Cells were collected by centrifugation at 7,000 rpm for 30 sec. Cell pellet was washed and re-suspended in water. For auxotrophic selections cell suspension was directly plated on appropriate selection plate, while for antibiotic selections cell suspension was incubated for 3 hrs in liquid YPAD or SD minimal media (whenever required by the strain genotype, e.g. P_{MET3}-*CDC20* strains were incubated on Do-met media) to allow the expression of the antibiotic marker before being plated on the appropriate selection plate.

2.5. Crossing yeast strains

For all cell crosses freshly grown yeast cells of opposite mating types were mixed on YPAD or SD minimal media (whenever required by the strain genotype, e.g. P_{MET3}-

CDC20 strains were incubated on Do-met media) and left to mate for 6–8 hrs. Then zygotes were picked up on the micromanipulator (Singer MSM). For diploid selection, cells were left to mate overnight and diploids were selected on appropriate plates for 3 days (diploid selection instead of zygote pick up was carried out whenever appropriate markers were available on the parental strains). Diploid cells were then sporulated for 4–5 days on VB sporulation plates. Four-spored asci developed from diploid cells were then suspended in 1 M sorbitol 1 mg/mL Zymolyase 20T and incubated at 30 °C for 30 min to lyse walls of the asci and release the spores. The tetrads were then dissected using a micromanipulator (Singer MSM) and each individual spore was positioned on a grid. Spores were then left to grow for 4–5 days. Spores phenotypes (mating type and presence of different markers) were tested on appropriate selective plates.

2.6. Storage of yeast strains

Yeast strains were kept on plates for up to 3 weeks during genotypic and phenotypic testing. For longer storage, freshly grown colonies were suspended in 15% glycerol and stored at –80 °C.

2.7. Yeast growth spot assays

To compare growth speed of yeast cells between different strains and different media, spot assays were carried out. For all spot assays, OD_{660} of cells in exponential growth phase was adjusted to 0.2. The spots in lanes were 1:5 dilution series.

2.8. Auxin-induced degron system to conditionally degrade yeast proteins

To conditionally degrade yeast proteins, auxin-induced degron system was used as described by (Nishimura et al. 2009). In this system, the target protein is tagged with an aid (*IAA17*) degron, which can be specifically recognised by unique E3 ubiquitin ligase

(*OsTIR1*). In the presence of auxin (1-NAA; a synthetic auxin) (Sigma), E3 ubiquitin ligase interacts with the aid degron, which is then polyubiquitylated by E2 conjugating enzyme. Once polyubiquitylated, the target protein tagged with the aid degron is rapidly degraded by the proteasome. For treatment of yeast cells on plates, 0.5 mM NAA (in DMSO) for SD media and 2 mM NAA (in DMSO) for YPA media were used. For treatment of cells in liquid media, a concentration of 0.5 mM NAA was used for both SD and YPA media.

2.9. Anchor-away system to conditionally deplete nuclear yeast proteins

To conditionally deplete nuclear proteins, anchor-away system was used as described by (Haruki et al. 2008). In this system, the target protein is fused to *FRB* (FKBP12-rapamycin binding) domain, which upon addition of 10 μM rapamycin (LC Laboratories) binds a *60S* ribosomal component that is tagged with *FKBP12* anchor. This ternary complex was then exported from the nucleus and incorporated into the ribosome. Since rapamycin is toxic to wild-type yeast, rapamycin-resistant strains containing mutated *TOR1* (*tor1-1*) and deleted *FPR1* (*fpr1*Δ) were used.

2.10. Yeast two-hybrid method

Two-hybrid assay was carried out as described previously (Yamagishi et al. 2008). The constructs of *STU1* (wild-type and chopped fragments) and *STU2* (wild-type and chopped fragments) were amplified by PCR and then cloned into *pBTM116* plasmid and respectively fused with the DNA binding domain or cloned into *pGAD-C2* plasmid and fused with the activation domain for transcription. These plasmids were transformed into the L40 strain of *S. cerevisiae* containing the *LexA*-inducible gene of *HIS3* and *LacZ*. Two-hybrid interaction was evaluated by expression of *HIS3* reporter gene on medium omitted by histidine. Constructs with *RAS* and *RAF* were used as controls.

3. Microscopy methods

3.1. Synchronising yeast cells using α- and a-factor

MATa and MATα haploid strains were synchronised in G1 by addition of α- or a-factor to the growth media, respectively. Yeast cells in exponential growth phase from overnight culture were diluted to OD_{660} = 0.15. MATa cells were arrested in G1 for the total period of 2.5 hrs when 0.75 µg/mL α- factor (CRUK peptide synthesis service) was added to cell culture as follows: 0 min, 60 min, 120min; while MATα cells were arrested with 0.02 µg/mL a-factor (kindly provided by Nicola O'Reilly, CRUK) (O'Reilly et al. 2012) added at 0 min, 60 min; for the total period of 2.5 hrs. *For experiments in physiological conditions cells were synchronised by adding α- or a-factors as follows: 0 min, 50 min, 100 min, 150 min for the total period of 3 hrs. Cells were released from G1 by washing cells three times with water on membrane filter (Mixed cellulose ester ME28, Whatman) using vacuum pump. Cells collected on the membrane filter were then released into fresh medium.

3.2. Live-cell imaging in physiological conditions (S phase)

For live-cell imaging in physiological conditions, I used a method as previously described (Kitamura et al. 2007) (Tanaka et al. 2010). In physiological conditions, KTs stay attach with spindle-pole MTs throughout most of the cell cycle (Figure 3-1) (Winey and O'Toole 2001). Only upon centromere replication in S phase, KTs disassemble and detach from the spindle-pole MTs (Figure 3-2) (Kitamura et al. 2007). After centromere replication, KTs are assembled *de novo* onto the replicated centromeres and can be re-captured by spindle-pole MTs (Figure 3-3). During S-phase, new SPB is formed *de novo* in the vicinity of the old SPB, but still remain immature (Tanaka et al. 2002; Lim et al. 1996). Thus, old SPB – the one inherited from the previous cell cycle – organizes spindle-pole MTs for KT re-capture during S phase (Figure 3-2,3). In this context

during KT capture in physiological conditions, spindle-pole MTs are organised in a mono-polar spindle around the old SPB (Figure 3-3).

For live-cell imaging in physiological conditions, yeast cells were grown overnight in YPAD media. Cells were then synchronized in G1 for the total of 3 hrs as described above. After G1 release, cells were incubated for 20 min into fresh YPAD: SCD media in the ratio of 1:3 prior to imaging and were imaged in the same media.

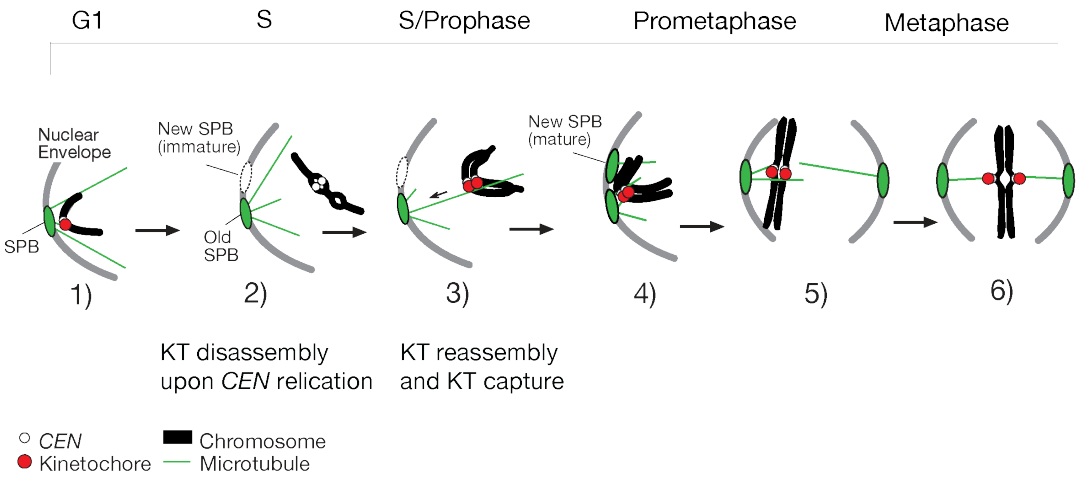

Figure 3. Schematic representation of kinetochore-microtubule interaction in physiological conditions.

3.3. Live-cell imaging at high resolution in the engineered centromere reactivation system

To study the localisation of fluorescent proteins at KTs prior to KT–MT interaction or to dissect the initial KT-MT interaction at high resolution, I used a previously developed assay in our lab called centromere-reactivation system (Tanaka et al. 2005a, 2010). This assay allows us to visualize a single KT–MT interaction by regulating the activity of a centromere via transcription of the short centromere region (~130bp in *S. cerevisiae*) from adjacently inserted *GAL1-10* promoter. In presence of galactose

centromere will be transcribed and therefore inactivated until addition of glucose, when centromere transcription will be shut down and centromere reactivated (Figure 4-1&2). In this way in cells arrested in metaphase (by depletion of P_{MET}-*CDC20*) when multiple kinetochores are captured and bi-oriented on the spindle, a single centromere can be specifically inactivated and therefore isolated from the metaphase spindle (Figure 4-1). Once nuclei are elongated due to forth and back motion of the spindle and centromere is further displaced from the spindle, centromere is reactivated (Figure 4-2) and newly assembled kinetochore can be captured by a spindle pole MT and transported pole-ward along it (Figure 4-3).

$P_{GAL1\text{-}10}$-*CEN3* P_{MET3}-*CDC20* strains were grown overnight in methionine drop-out media (Do-met) supplemented with 2% raffinose and 0.02% glucose as a carbon source. Cells were synchronised in G1 as described above. To repress the expression of *CDC20* gene under *MET3* promoter and to arrest cells in metaphase, 2 mM of methionine was added to the media for the total period of 3–4 hrs.

To express genes under regulation of the *GAL* promoter or to induce transcription of centromere region (centromere inactivation), 2% (w/v) raffinose (Sigma) plus 2% (w/v) galactose (Sigma) was used as a carbon source (e.g. YPARG or SCRG). For transcriptional repression of the *GAL1-10* promoter (centromere reactivation) in live-cell imaging, a synthetic complete media (SC) supplemented with 2% glucose (e.g. SCD) was used.

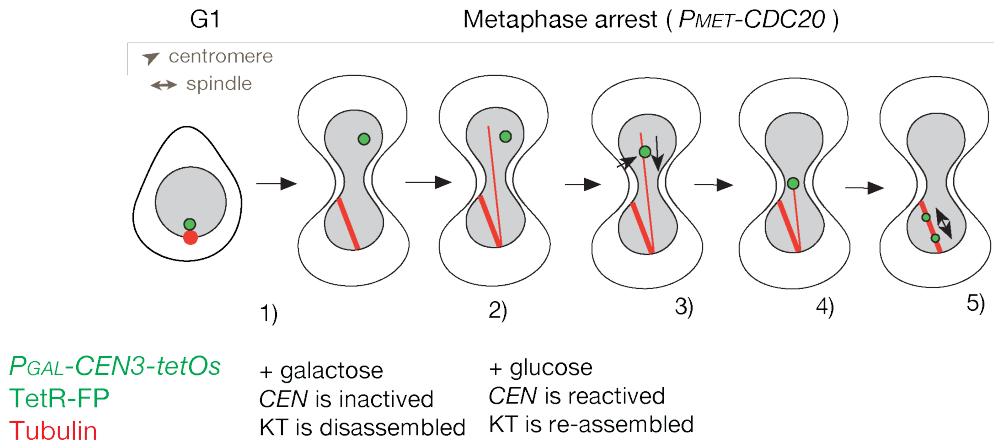

Figure 4. Schematic representation of kinetochore-microtubule interaction in centromere reactivation system.

3.4. Sample preparation for microscopy

From 1.5–3 mL of yeast cells were collected by brief centrifugation at 7,200 rpm for 30 sec. Cells were washed out of the auto-fluorescence YPA* media and then re-suspended in 150 µl low fluorescence SC* media. 100 µl of cells were then loaded onto 35 nm glass-bottom dish (P35G-1.5-10C, MatTek) coated with 0.2 % (w/v) Concanavalin A (X-231, Sigma) and allowed to stand for 4 min. Cells not attached to the glass bottom dish surface were then removed by three washes with 1 mL SC* media. On the stage 3 mL of SC* media was added to the dish for the imaging.

*media supplemented with relevant carbon source; e.g. YPARG, SCRG, SCD

3.5. Fluorescence microscopy (DeltaVision)

Fluorescence images were acquired using DeltaVision RT microscope (Applied Precision) (later upgraded to DeltaVision Core) and DeltaVision Elite (Applied Precision) with UPlanSApo 100^{X} NA 1.40 objective lens (Olympus), a CCD camera (CoolSnapshot HQ^{2}; Photometrics) and SoftWoRx software (Applied Precision). All images were captured with BIN 2x2 mode (pixel size *xy* = 1.32 µm) typically in five to

seven (0.7 μm apart) *z* stacks unless otherwise indicated. For the visualisation of fluorescent proteins in the three channels mCherry, GFP (YFP) and CFP, cells were typically excited with 0.05 sec mCherry at 32%*, 0.05 sec GFP (YFP) 50%* and 0.05-0.08 sec CFP 32%*. Multiple channels images were acquired by imaging first the z-stack followed by a switch to the next channel. The difference in the acquisition between two or more channels was in the range of msec, which is negligible with respect to the motion of our targets. The three channels were discriminated by the 89006 multi-band filter set (Chroma Technology Corp.).

*Transmission of the neutral density (ND) filter

3.6. Image processing

The images were then deconvoluted using Spinlock (deconvolution cluster) run by Microscopy Facility, College of Life Sciences, University of Dundee.

3.7. Image and data analysis

Finally image analysis was carried out using Volocity Software (PerkinElmer) and image data was statistically analysed with PRISM (GraphPad Software), unless stated otherwise. Unpaired t-test was used for the statistical analysis in Figure 7, Figure 10, Figure 11, Figure 19, Figure 20 and Figure 21. Log-rank test for survival curves was used in Figure 17 and Figure 18. Fisher's exact test was used in Figure 23 and Figure 24. Chi-square test was used in Figure 25.

4. Bioinformatic methods

4.1. JPred: A protein secondary structure prediction server

To predict the secondary structure of proteins, a consensus secondary structure prediction internet server (Cuff et al. 1998) was accessed online

(http://www.compbio.dundee.ac.uk/jpred/) in 2012. This server allows the submission of a single sequence or multiple alignments and returns a prediction based on six secondary structures prediction algorithms. The program exploits evolutionary information from multiple sequences and predicts conservation patterns important for the structure and function.

4.2. Jalview: A multiple sequence alignment editor and analysis workbench

The analysis and annotation of multiple sequence alignments was carried out with Jalview Version 2 (Waterhouse et al. 2009). This is a system for interactive WYSIWYG (What you see is what you get) editing, analysis and annotation of multiple sequence alignments. Core features include keyboard and mouse-based editing, multiple views and alignment overviews and linked structure display with Jmol.

5. Mathematical simulation

For the data set of each strain (wild-type *STU1+* and mutant *stu1-frb*) we calculate the cumulative distribution of uncaptured free kinetochores. At each time point a proportion of uncaptured kinetochores is found and its standard error was obtained assuming the binomial distribution:

$$SE_p = \sqrt{\frac{\hat{p}(1-\hat{p})}{n}}$$

where $\hat{p}$ is the proportion of uncaptured kinetochores and n is the total number of kinetochores. This cumulative distribution (with error bars) is then fitted by an exponential function $e^{-k(t-t_0)}$ using Levenberg-Marquardt algorithm (Levenberg 1944; Marquardt 1963). The errors on fit parameters quoted below are 95% confidence

intervals. These errors are only sampling errors and do not reflect the complexity of kinetochore and microtubule distribution. Therefore, we apply a Monte Carlo model to assess these uncertainties better.

Our model is based on a simulation, where KT-derived MTs are randomly applied throughout the mutant *stu1-frb* cell timelines, reducing capture times. We use numbers, durations and outcome (successful capture or not) of KT-derived MTs as observed in the wild-type *STU1+*. To generate a random data set we place these KT-derived MTs in the mutant *stu1-frb* timeline with uniform random distribution across cells and time. The KT-derived MTs are not allowed to overlap and we require a gap of a least 10 s between the two consecutive KT-derived MTs in the same cell. Each successful KT-derived MT truncates the timeline of the given cell (causes KT capture). The KT-derived MTs found after the newly generated capture point are re-distributed with uniform distribution among all cells and times. This way a single simulated mutant *stu1-frb*-based random set of cells is generated. Now we can generate a large number of sets (typically 10,000), find the best-fitting parameter k for each of them and build a simulated distribution of k.

RESULTS

I. Molecular mechanisms guiding microtubule generation at kinetochores

To address the roles of KT-derived MTs in mitosis, we had to first understand what KT components were involved in regulation of KT-derived MTs in order to create a specific mutant defective in MT generation at KTs. It was previously shown that canonical KT components such as Ndc10, Okp1, Dsn1 and Spc24 were required for nucleation and extension of KT-derived MTs (Kitamura et al. 2010). However, neither of these KT components could be used as a molecular tool to investigate the roles of KT-derived MTs, because compromising their function would cause abnormalities in the assembly of key KT complexes such as CBF3, Ctf19, Mtw1 and Ndc80, leading to a general defect in KT–MT interaction. This would not be a specific outcome of a lack of KT-derived MTs. On the other hand, MT-associated proteins localising at KTs may be good targets to create specific mutants defective in KT-associated MT formation. For example, $Stu2^{XMAP215}$ – a MT polymerase and +TIP tracking protein – may be a good candidate for this target.

1. Molecular requirements for Stu2 recruitment to kinetochores

At KTs Stu2 is required for both nucleation and extension of KT-derived MTs (Kitamura et al. 2010) (see Introduction). However, inactivation of Stu2 (with *stu2-10* mutant) led not only to reduction in MT generation at KTs, but also to reduced MT generation at the spindle poles (Kitamura et al. 2010). In the absence of MT generation at the spindle poles, KTs would not be captured, which made it impossible to address the roles of KT-derived MTs in this mutant (Kitamura et al. 2010). Therefore, we tried to find a way to specifically remove Stu2 from KTs by finding and targeting a mechanism for Stu2 recruitment to the KT.

1.1. Ndc80 Loop region is not required for Stu2 recruitment or microtubule generation at kinetochores

From yeast to humans Ndc80 complex situated at the outer KT plays a critical role in KT–MT attachment (DeLuca and Musacchio 2012; Cheeseman et al. 2006). This kinetochore complex is a rod-like heterotetramer composed of Ndc80 (also called Hec1 in mammals), Nuf2, Spc24 and Spc25 (see Figure 1A, left panel) (Ciferri et al. 2008; Wei et al. 2005). Both Ndc80/Hec1 and Nuf2 are located at the KT–MT interface and directly interact with MTs, while Spc24 and Spc25 are oriented towards the inner KT (DeLuca and Musacchio 2012; Ciferri et al. 2008; Malvezzi et al. 2013; Lampert et al. 2013). Globular domains mediate the interaction of Ndc80 complex with MTs and inner KT, while the internal rod-shaped coiled-coil structure is interrupted by ubiquitous loop (Ciferri et al. 2008; Cheeseman et al. 2006). This loop region of the Ndc80 complex is thought to play an important structural role to ensure flexibility of the complex in KT–MT interaction (Wang et al. 2008), but also to recruit various proteins to KTs as it is a protein-protein interaction motif; reviewed in (Tang 2013).

In fission yeast *S. pombe* the Ndc80 Loop region serves as a platform for recruitment of Stu2 orthologues Dis1^{XMAP215} (Hsu and Toda 2011) and Alp14^{XMAP215} (Kakui et al. 2013) via independent functional regions. Dis1 recognises three motifs within the Ndc80 loop (395–408, 431–436 and 473–484) where modification of L405–S compromises Dis1 binding to KTs (Kakui et al. 2013). Meanwhile Alp14 interacts primarily with one motif (473–484), while F420 within a distinct region is required for Alp7^{TACC3}–Alp14^{XMAP215} binding to the loop and respectively to KTs (Kakui et al. 2013).

To test whether Ndc80 loop was also required for Stu2 recruitment to KTs in *S. serevisiae*, we aligned Ndc80 loops across species to design similar *ndc80* point mutations. Although loop region is not well conserved between *S. pombe* and *S. serevisiae*, we divided the loop into two distinct regions (444–459 and 462–482) and designed three point mutations: *ndc80(L449–P)* and *ndc80(L479–S)*, which were likely to correspond to *S. pombe L405–P* and *F420–S* respectively, and an additional *Y465–S* – a well conserved tyrosine within the loop (Figure 5A). Deletions of 15 (*ndc80*Δ*444–459)* and 20 (*ndc80*Δ*462–482)* amino acids out of Ndc80 loop were lethal while cells tolerated better single amino acid substitutions in the three point mutants *ndc80(L449–P)*, *ndc80(L479–S)* and *ndc80(Y465–S),* which were viable (Figure 5A), showing no growth defect both at 25 °C and 37 °C (Figure 5B).

The deletions of Ndc80 loop may compromise folding and flexibility of the molecule, which may cause a general defect (i.e. a defect not specific to Stu2 recruitment) in KT–MT attachment. To avoid such a general defect, we investigated Stu2 localisation at KTs only in the viable point mutants (Figure 5AC). In all three *ndc80* mutants Stu2 was recruited to KTs in similar amounts to that of the wild type *Ndc80+* and able to generate MTs at KTs (Figure 5C). Since point mutations may be more defective at high temperature, we also investigated Stu2 localisation at KTs at 37 °C (data not shown). However, the ndc80 point mutants showed no growth defect (Figure 5B) or defect in Stu2 recruitment to KTs at 37 °C (data not shown).

Altogether these results raise a possibility that in *S. cerevisiae* Ndc80 Loop is not required for Stu2 recruitment or MT generation at KTs. In this regard *S. cerevisiae* and *S. pombe* may use alternative functional domains for recruitment of Stu2 at the KTs.

A

ndc80 mutant	Viability	Stu2 localisation at the kinetochore
ndc80Δ444-459	lethal	NA
ndc80Δ462-482	sick/lethal	NA
ndc80(L449-P)	viable	+ (n=23)
ndc80(Y465-S)	viable	+ (n=26)
ndc80(L479-S)	viable	+ (n=26)

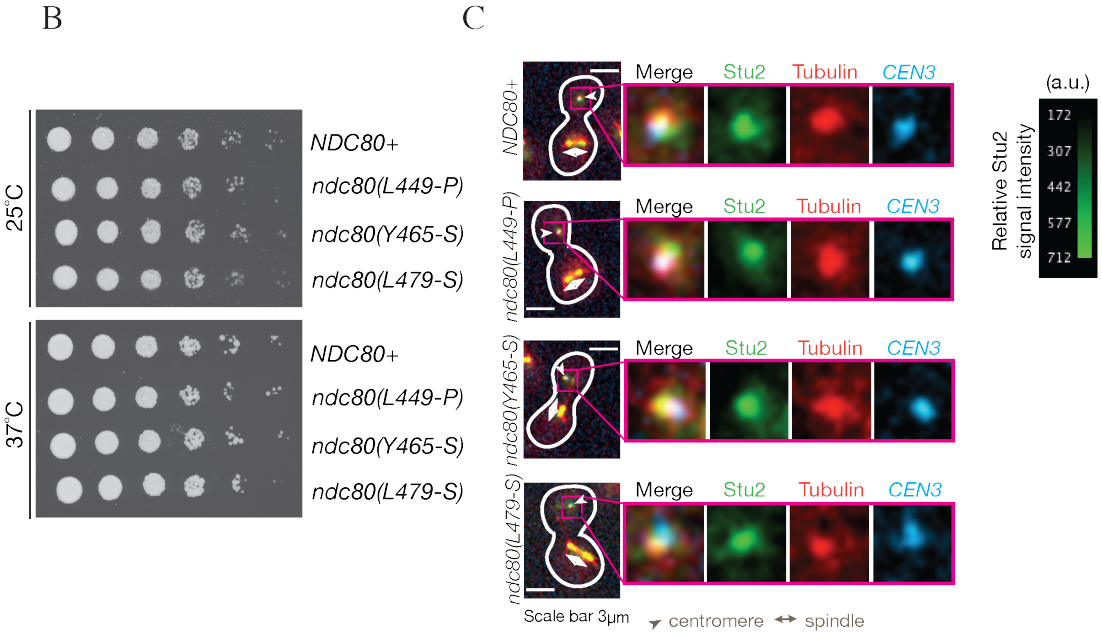

Figure 5. Ndc80 loop region is not required for recruitment of Stu2 and microtubule generation at kinetochores.

(A) Summary of *ndc80* mutant phenotypes. Using the centromere reactivation assay (see Methods), Stu2 signals at KTs were studied in various ndc80 mutant cells. NA, not applicable. (B) Growth analysis at 25 ˚C and 37 ˚C of wild-type *NDC80+ and Ndc80(L449–P), Ndc80(Y465–S), Ndc80(L479–S)* mutants. Growth phenotype was examined by spot assay on methionine drop-out media supplemented with 2% glucose. (C) Localisation of Stu2 at *CEN3* and MT generation at KTs in *ndc80* mutants. Wild-type *NDC80+, Ndc80(L449–P), Ndc80(Y465–S) and Ndc80(L479–S)* cells with P_{GAL}*-CEN3-tetOs TetR-3CFP GFP-TUB1 STU2-4mCherry* P_{MET3}*-CDC20* were treated with α-factor in methionine drop-out medium supplemented with 2% raffinose for 2.5 hrs, and then released into YPA medium containing 2% galactose, 2% raffinose (YPARG) and 2 mM methionine. 3.5 hrs after the release into YPARG medium, cells were suspended in synthetic complete medium containing 2% glucose and 2 mM methionine. Image sequences were acquired in a Z-stack of frames every 1 min for the total of 30 min using three separate channels for mCherry (Stu2 in green), GFP (Tub1 in red) and CFP (*CEN3* in green). Colour reference on the right represents relative signal intensity of Stu2 in arbitrary units (a.u.)

1.2. Microtubule-associated proteins localising at kinetochores: Stu1 and Slk19

After our failure to remove Stu2 specifically from KTs in *ndc80* mutants, we went to target MT-associated proteins localising at KTs such as Stu1 and Slk19.

Stu1 (suppressor of ß-tubulin mutation) was identified in 1994 (Pasqualone and Huffaker 1994) as a microtubule-associated protein that localises to spindle poles and spindle mid-zone where it is required for maintenance of bipolar spindle (Yin et al. 2002). However, Stu1 does not only localise to the spindle, but also to KTs (Ma et al. 2007; Ortiz et al. 2009). At KTs Stu1 is thought to have an important role in KT–MT interaction when KT capture is delayed (Ortiz et al. 2009). Nevertheless, kinetochore function of Stu1 remains unclear.

In our hands we investigated dynamic localisation of Stu1 at KTs (Figure 6A left panel) using the centromere reactivation system (Tanaka et al. 2005a). Upon centromere reactivation, Stu1 was gradually accumulated at uncaptured KTs prior to the first visible signs of MT generation at KTs (Figure 6A left panel). Furthermore in contrast to Stu2, during extension of KT-derived MTs, Stu1 did not track their distal plus ends, but stayed closely associated with MT nucleation sites at their minus ends (Figure 6A left panel). When KTs were captured by MTs extending from spindle poles, Stu1 appeared to diffuse along the length of the MT (Kozo Tanaka, unpublished) when only relatively weak Stu1 signal was retained at the KT (Figure 6A right panel).

Similarly to Stu1, Slk19 (synthetic lethal *KAR3* protein 19) is a microtubule-associated protein that localises to both spindle and KTs (Zeng et al. 1999). At KTs Slk19 has a similar localisation pattern to that of Stu1 (Figure 6B). Slk19 is recruited at KTs prior to first nucleation of KT-derived MTs (Figure 6B left panel). Upon extension of KT-

derived MTs, Slk19 localises close to their nucleation sites and does not track their distal plus ends (Figure 6B left panel). In contrast to Stu1 when spindle MTs capture KTs, Slk19 signal at KT does not seem to be reduced and remains associated with KT during its transport towards the spindle pole (Figure 6B left panel).

Given that Stu1 and Slk19 localize at KTs before their interaction with spindle-pole MTs, we hypothesized that these MT-associated proteins may play a role in KT-associated MT formation. So we further examined their roles at KTs.

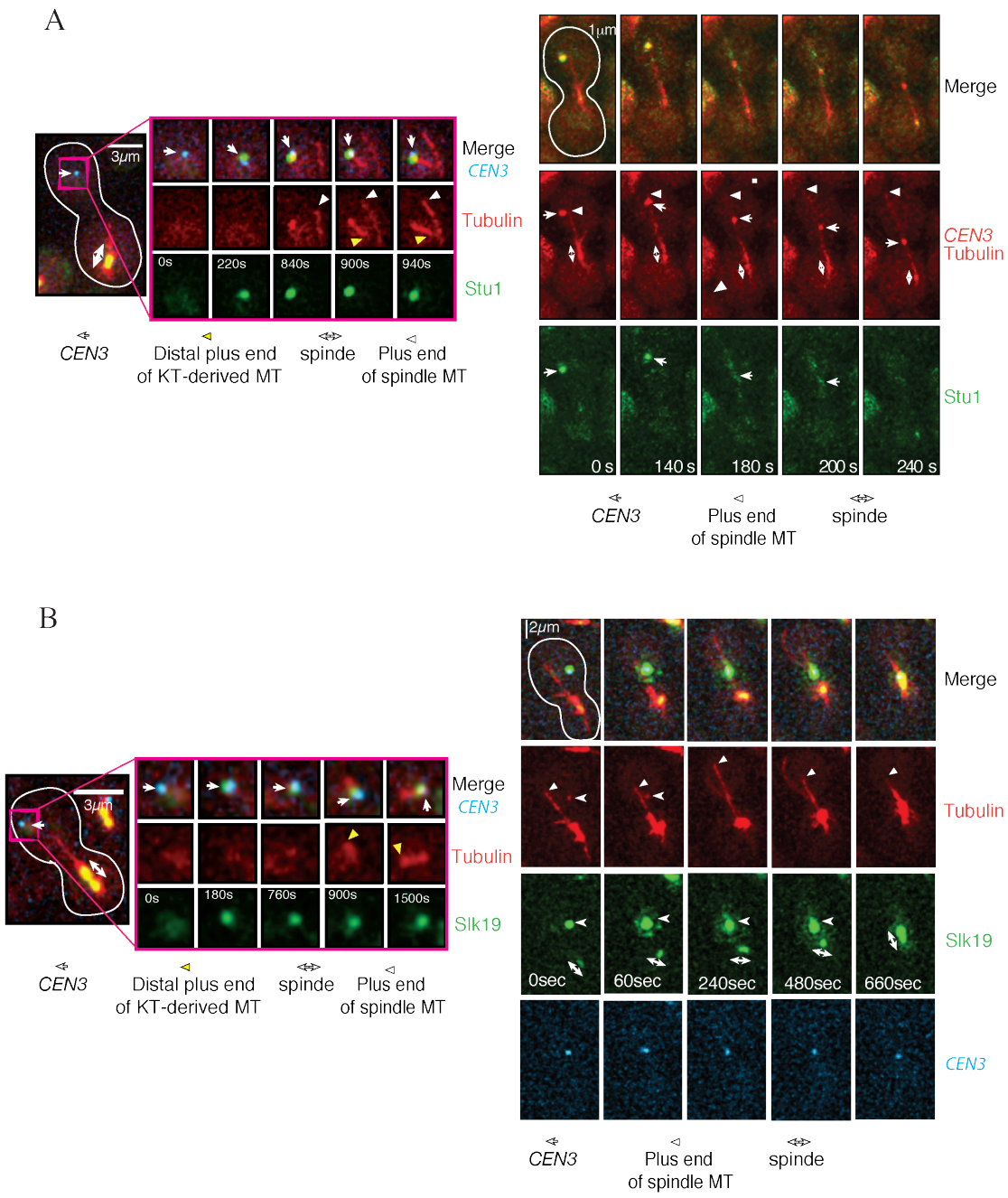

Figure 6. Localisation of Stu1 and Slk19 at kinetochores.

(A) Localisation of Stu1 protein at KTs before (left panel) and after (right panel) interacting with spindle-pole MTs (figure on the left adapted from K.Tanaka, unpublished). *STU1-4mCherry and STU1-3GFP* P_{MET3}*-CDC20* P_{GAL}*-CEN3-tetOs TetR-3CFP GFP/CFP-TUB1* cells were treated as in Figure 5C. (B) Localisation of Slk19 protein at KTs before (left panel) and after (right panel) interacting with spindle-pole MTs. *SLK19-4mCherry* P_{MET3}*-CDC20* P_{GAL}*-CEN3-tetOs TetR-3CFP GFP-TUB1* cells were treated as in Figure 5C.

1.3. Stu1 is required for generation of kinetochore-derived microtubules

Stu1 is an essential protein and therefore to study the outcome of its depletion, we used the auxin-induced degron system (Nishimura et al. 2009) (see Methods) to generate a conditional *stu1-aid* mutant. In this system, upon addition of auxin, Stu1 with the aid tag is polyubiquitinated and degraded by the proteasome (Figure 7A). To test whether Stu1 depletion was efficient, we analysed the growth of *stu1-aid* mutant by serial dilution test (Figure 7B). In presence of auxin, *stu1-aid* mutant showed no growth compared to *STU1* wild-type control strain, which grew normally (Figure 7B). Once we confirmed that Stu1 was efficiently depleted in these growth conditions, we looked into MT nucleation and extension at KTs in the absence of Stu1 (Figure 7C). Interestingly, we observed no accumulation of tubulin signal at KTs in Stu1-depleted cells (Figure 7C). Furthermore we quantified this phenotype in Figure 7D, where we could see that tubulin signal at KTs in *stu1-aid* mutant is significantly reduced compared to *STU1+* control.

Thus our findings indicated that Stu1 plays a crucial role in MT generation at KTs.

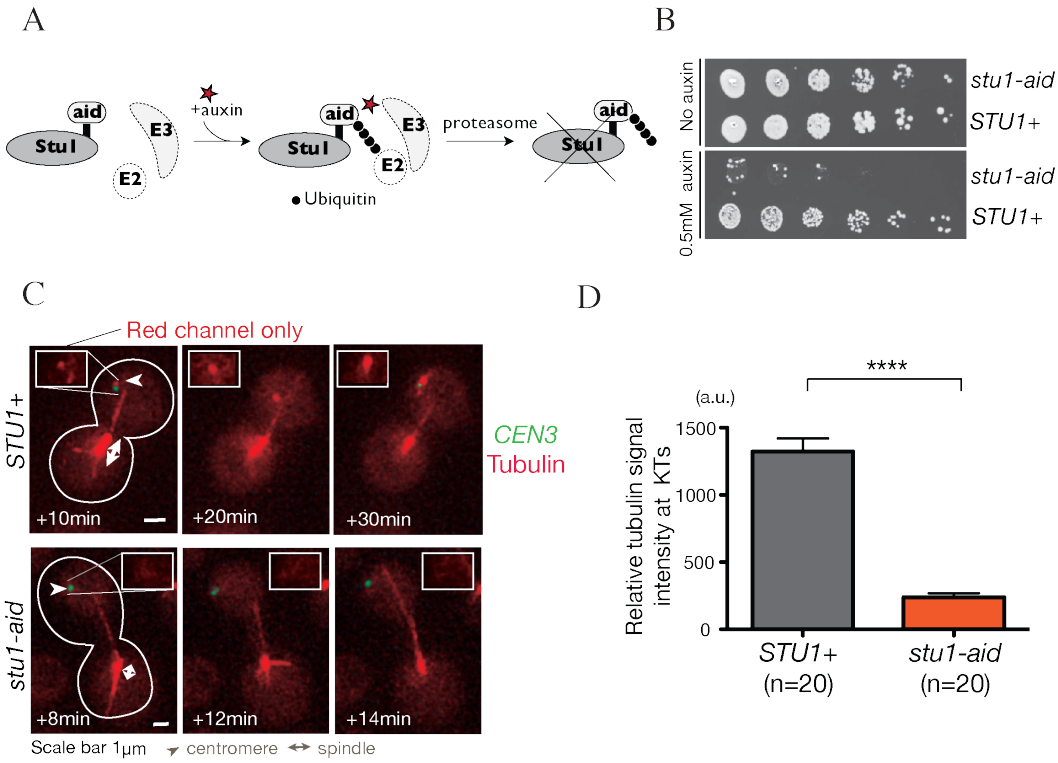

Figure 7. Phenotypic analysis of *stu1-aid* mutant.

(A) Schematic representation of auxin-induced degron system. (B) Growth analysis of *stu1-aid* mutant. Growth of *stu1-aid* mutant was examined by spot assay on methionine drop-out media supplemented with 2% glucose and 0.5 mM synthetic auxin NAA. (C) When Stu1 is depleted, no tubulin is accumulated at uncaptured kinetochores. *stu1-aid OsTIR1* P_{MET3}*-CDC20* P_{GAL}*-CEN3-tetOs TetR-3CFP GFP-TUB1* cells were treated as in Figure 5C. 3 hrs after the release into YPARG medium, 0.5 mM NAA was added to the media and incubated for additional 1 hr. After 4 hrs, cells were re-suspended in synthetic complete medium containing 2% glucose and 2 mM methionine. Image sequences were acquired in a Z-stack of frames every 30 sec for the total of 30 min using two separate channels for GFP (Tub1 in red) and CFP (*CEN3* in green). Time was set after the centromere was reactivated into the synthetic complete medium containing glucose. (D) Intensity of tubulin signal at KTs in *stu1-aid* and *STU1+* cells (unpaired t-test, $p< 0.0001$).

1.4. Stu1 C-terminal tail is not essential for Stu1 recruitment at kinetochores

We have shown above that Stu1 is required for KT-associated MT formation. However in mitosis, Stu1 plays an essential role not only at KTs, but also at the spindle mid-zone, where Stu1 is required for the maintenance of the bipolar spindle after KTs are loaded on the spindle (Pasqualone and Huffaker 1994; Yin et al. 2002; Ortiz et al. 2009; Funk et al. 2014). Thus when Stu1 is depleted during metaphase in the centromere

reactivation system, bipolar spindle collapses causing formation of a larger number of long spindle MTs (see Figure 7C).

In an attempt to remove Stu1 from KTs, we disrupted C-terminal tail of the protein and made *stu1ΔC339-NLS* mutant (Figure 8A), because a previous report suggested that Stu1 C-terminus is required for KT localisation (Ortiz et al. 2009). In addition, we used Jpred (a secondary structure prediction server, see Methods) to design two additional shorter C-terminal truncations chopped out of the predicted coiled-coil areas: *stu1ΔC250* and *stu1ΔC170* with and without *SV40-NLS* (Figure 8B); NLS may be important for the viability and nuclear localisation of these mutants (Ortiz et al. 2009). On the other hand, truncations *stu1ΔC313* and *stu1ΔC60* were reported as viable (Faust 2011). Out of the eight C-terminal truncations, only *stu1ΔC339-NLS* and *stu1ΔC60* supported viability (Figure 8B) and showed an almost normal growth speed (data not shown). On the other hand, *stu1ΔC339* and *stu1ΔC313* mutants were sick and grew very slowly, while *stu1ΔC250(NLS)* and *stu1ΔC170(NLS)* were lethal (Figure 8B).

Next we analysed the localisation of the largest viable truncation stu1ΔC339-NLS in metaphase upon centromere reactivation (Figure 8C). Truncated stu1ΔC339-NLS protein localised at the spindle mid-zone (Figure 8C). When centromere was activated, Stu1 seemed to delocalise from spindle and re-localise to the uncaptured kinetochore (Figure 8C). Localization of Stu1ΔC339-NLS protein at KTs is not consistent with a result in Ortiz and colleagues (Ortiz et al. 2009).

Furthermore we looked into MT generation at KTs in *stu1ΔC339-NLS* mutant (Figure 8D). Although tubulin accumulation at KTs was reduced in a small subset of cells with this mutant (Figure 8C), MTs were still generated at KTs in many cells with

stu1ΔC339-NLS (Figure 8D). In this respect it was also not surprising that in *stu1ΔC339-NLS* mutant Stu2 localised at KTs (Figure 8D).

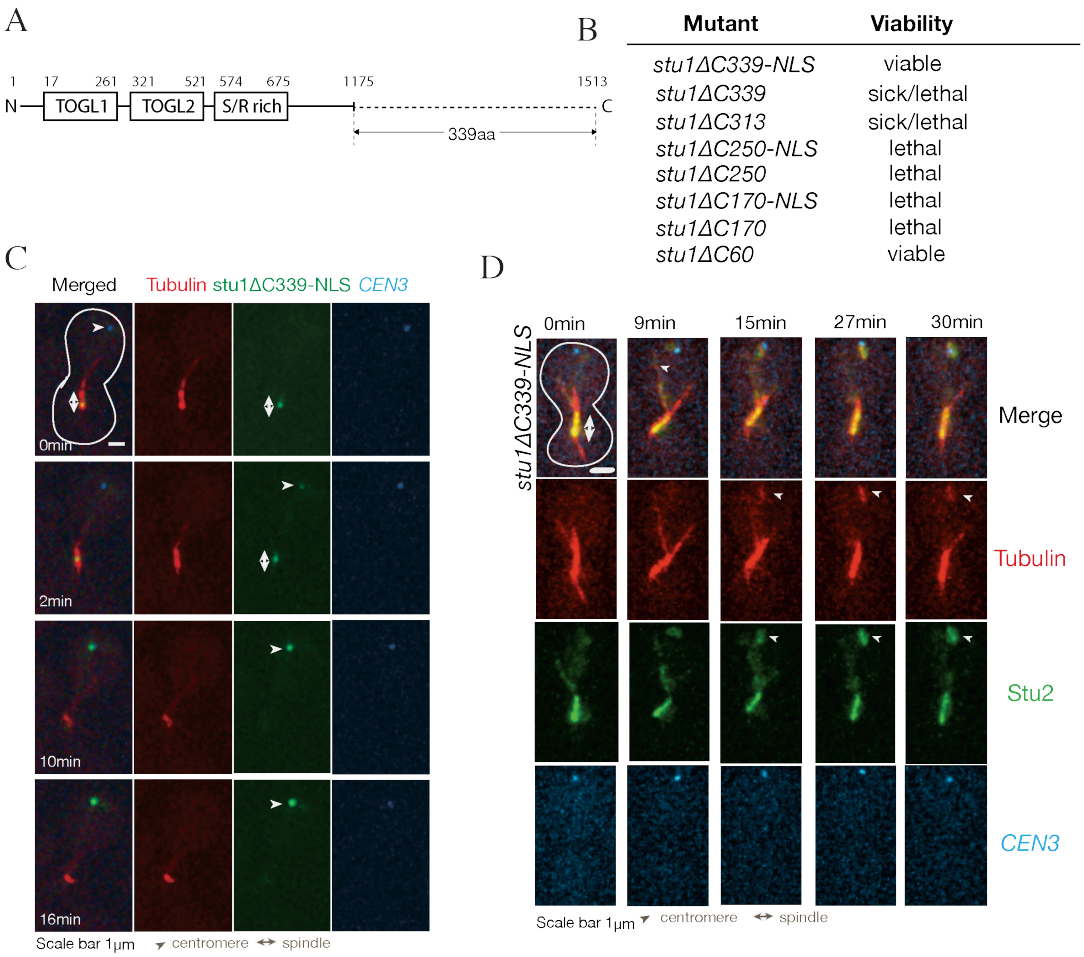

Figure 8. Phenotypic analysis of Stu1 C-terminal truncations.

(A) Schematic representation of stu1 Δ C338-NLS protei . (B) Viability of Stu1 C-terminal truncation mutants. One of the Stu1 alleles was truncated at the C-terminus into the diploid *K842* strain, which were then sporulated and dissected onto YPAD plates. Spores were grown for at 25 ˚C for 5 days. (C) Stu1 Δ C339-NLS localises at uncaptured kinetochore. *stu1 Δ C339-NLS-3GFP* P_{MET3}*-CDC20* P_{GAL}*-CEN3-tetOs TetR-3CFP mCherry-TUB1* cells were treated as in Figure 5C. Time was set in an arbitrary manner. (D) Stu1 Δ C339-NLS recruits Stu2 and generates MTs at the uncaptured KTs. *stu1 Δ C339-NLS STU2-4mCherry* P_{MET3}*- CDC20* P_{GAL}*-CEN3-tetOs TetR-3CFP GFP- TUB1* cells were treated as in Figure 5C.

1.5. Slk19Δ reduces recruitment of Stu1 and Stu2, but does not completely abolish their kinetochore localisation

Slk19 interacts with Stu1 and it was shown that upon Slk19 deletion, Stu1 lacks localisation at the spindle mid-zone in anaphase (Faust 2011). Since Slk19 is not only a spindle mid-zone component, but also a KT-associated protein (see Section 1.2.), we

investigated whether Slk19 was required for the recruitment of Stu1 at the KT. We discovered that in the *slk19*Δ mutant, only a small fraction of Stu1 was recruited at the uncaptured KT, while the majority of Stu1 was retained at the spindle (Figure 9A). Likewise tubulin accumulation at KTs was reduced in *slk19Δ* mutant (Figure 9A), which was very likely due to decreased amount of Stu1 at the KT. This result suggests that Slk19 plays an important role in kinetochore recruitment of Stu1.

When we discovered that Slk19 was involved in Stu1 accumulation at KTs and KT-associated MT formation, we further investigated Stu2 localisation in the absence of Slk19 (Nori Kobayashi, unpublished). Stu2 recruitment at the uncaptured KTs in *slk19Δ* mutant was also reduced (Figure 9B). Thus our findings indicated that Slk19 is important for accumulation of Stu1 and Stu2 at KTs.

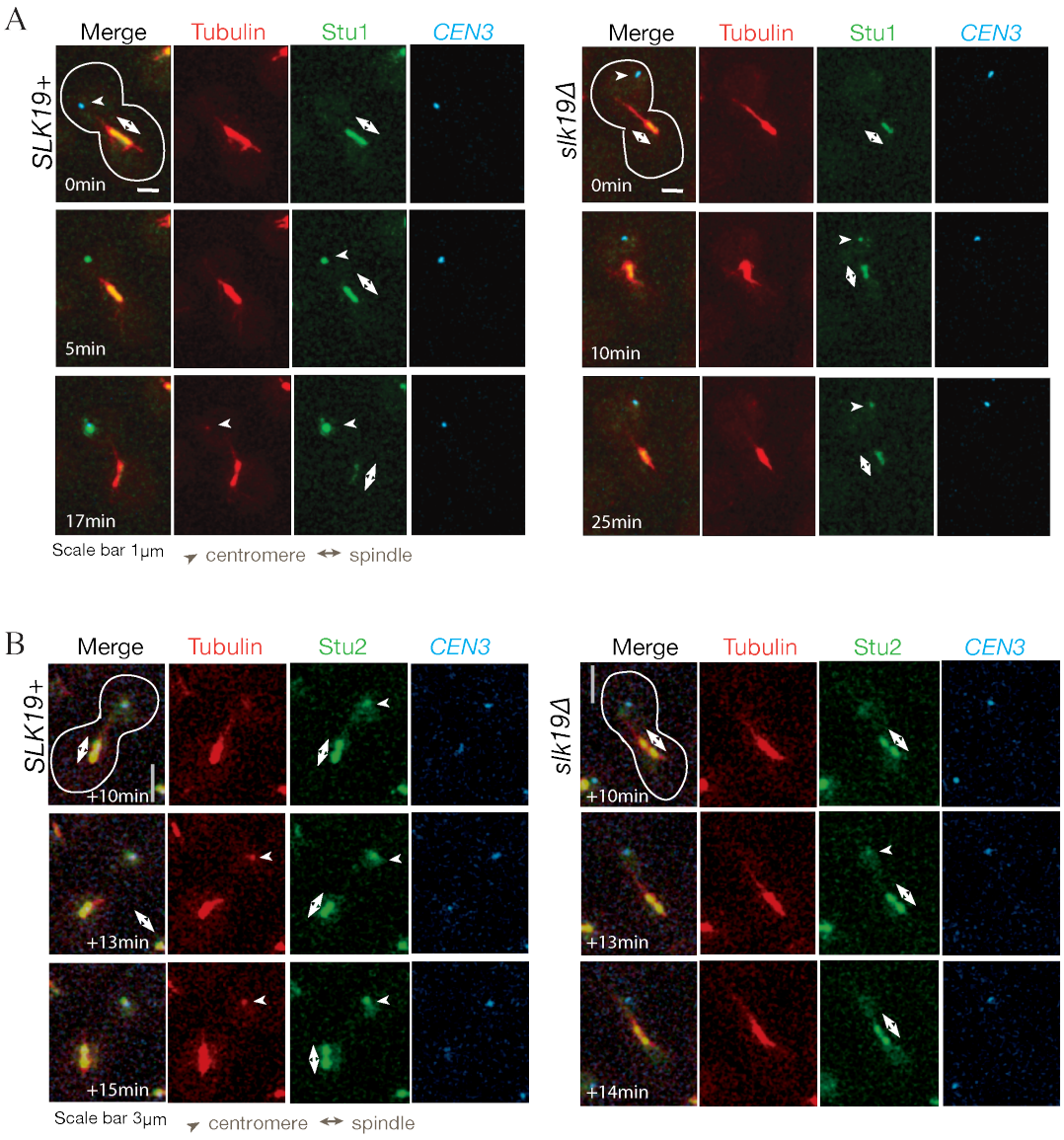

Figure 9. Localisation of Stu1 and Stu2 in *slk19Δ* mutant.

(A) Stu1 accumulation at the uncaptured KT in the *slk19Δ* mutant is impaired. *slk19Δ STU1-4mCherry* P_{MET3}*- CDC20* P_{GAL}*-CEN3-tetOs TetR-3CFP GFP- TUB1* cells were treated as in Figure 5C. mCherry (Stu1; green), GFP (tubulin; red), CFP (CEN3; blue). Time zero was set arbitrarily. (B) Stu2 recruitment at the uncaptured KT in *slk19Δ* mutant is reduced with only weak temporal signals detected.

2. Molecular regulation of kinetochore-derived microtubules: Stu1 and Stu2 interplay at kinetochores

2.1. Stu1 recruits Stu2 to promote microtubule generation at kinetochores

Both Stu1 and Stu2 are required for MT generation at KTs (this study) (Kitamura et al. 2010). Then do Stu1 and Stu2 work in parallel to promote MT generations at KTs or in the same pathway?

To address this question I investigated whether there is any interdependency between Stu1 and Stu2 in their recruitment at KTs. To do this I first visualised Stu2 in the *STU1+* and *stu1-aid* cells and investigated Stu2 localisation in metaphase using the centromere reactivation assay (see Methods). During the metaphase arrest of *STU1+* cells, Stu2 localised along the spindle, at spindle pole bodies and MT plus ends (Figure 10A). In the presence of auxin, Stu1-aid protein was successfully depleted within the interval of 30 min, which caused a collapse of the bipolar spindle leading to unusually long and numerous spindle MTs (Figure 10A bottom); in agreement with previous observations (Pasqualone and Huffaker 1994). Despite the bipolar spindle collapse, with Stu1 depletion Stu2 still localised with spindle poles of the monopolar spindle and MT plus ends, similarly to wild-type cells (Figure 10A). Intriguingly, when centromere was reactivated, Stu2 recruitment at the newly assembled uncaptured KT was significantly lower in Stu1-depleted cells than in *STU1+* cells (Figure 10AB). This suggests that Stu1 is specifically required for the recruitment of Stu2 at KTs, but not at the spindle poles or MT plus ends.

Next I visualised Stu1 in *stu2-aid* cells and investigated Stu1 localisation in the absence of Stu2 in the centromere reactivation assay. Stu2 was successfully depleted by the auxin-induced degron system (Figure 10C), which in metaphase compromised the

extension of spindle MTs (Figure 10D); in agreement with previous observations in the lab (Kitamura et al. 2010). With Stu2 depletion, Stu1 still localised at both spindle poles and the uncaptured KTs (Figure 10DE).

Altogether these results suggest that Stu1 facilitates recruitment of Stu2 to KTs, but not vice versa. Nevertheless, although Stu1 was still recruited at uncaptured KTs in the absence of Stu2, no MT signal was detected at uncaptured KTs (Figure 10D). This is consistent with the central role of Stu2 in nucleation and extension of KT-derived MTs (Kitamura et al. 2010). Thus it is likely that Stu1 and Stu2 operate in the same pathway, in which Stu1 facilitates the recruitment of Stu2 to promote MT generation at KTs.

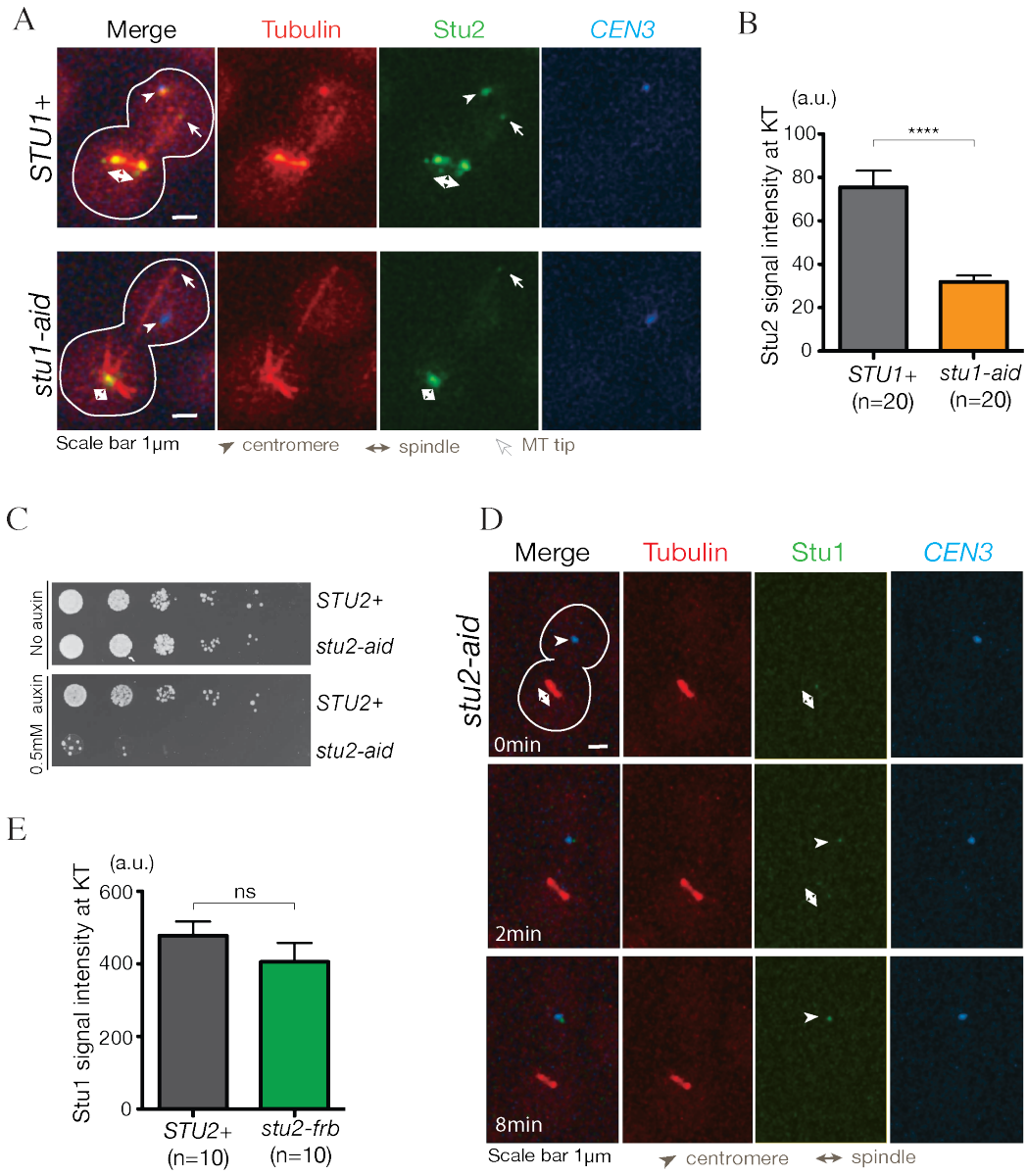

Figure 10. Stu2 recruitment at kinetochore is Stu1-dependent.

(A) Stu2 is not recruited at KT in the *stu1-aid* mutant. *stu1-aid OsTIR1 STU2-3xGFP* P_{MET3}*-CDC20* P_{GAL}*-CEN3-tetOs TetR-3xCFP mCherry-TUB1* were treated as in Figure 7C. mCherry (tubulin; red), GFP (Stu2; green), CFP (*CEN3*, blue) images were acquired. Time was set arbitrarily. (B) Diagram of maximum signal intensity of Stu2, detected at uncaptured KT in the *stu1-aid* mutant and in the control *STU1+* strain. (C) Growth analysis of *stu2-aid* mutant. Growth phenotype of *stu2-aid* mutant was examined by spot assay on Do-met media supplemented with 0.5 mM NAA. (D) Stu2 is not required for Stu1 localisation at uncaptured KT. *stu2-aid OsTIR1 STU1-2xGFP* P_{MET3}*- CDC20* P_{GALs}*-CEN3-tetOs TetR-3xCFP mCherry-TUB1* were treated as in Figure 7C. mCherry (tubulin; red), GFP (Stu1; green), CFP (*CEN3*, blue) images were acquired. (E) Diagram of maximum signal intensity of Stu1, detected at uncaptured KT in the *stu2-aid* mutant and in the control *STU2+* strain.

2.2. Stu2 generates microtubules independently of Stu1 when tethered on the chromosome arm

In the previous section I showed that Stu1 recruits Stu2 to promote nucleation and extension of KT-derived MTs. Stu2 is a MT plus end tracking protein (+TIP), which regulates MT plus end dynamics by acting as a MT polymerase (Wolyniak et al. 2006). In contrast to other +TIPs such as Bim1 and Bik1, which were solely involved in MT extension at KTs, Stu2 was required for both nucleation and extension of KT-derived MTs (Kitamura et al. 2010). Moreover, when artificially tethered at an engineered site on the chromosome arm locus, Stu2 was sufficient to nucleate and extend MTs (Kitamura et al. 2010). Thus it seems that Stu2 promotes both MT nucleation and extension at KTs. Then, given that Stu1 acts upstream of Stu2 to promote MT generation at KTs, is Stu1 only involved in the recruitment of Stu2 or directly participates in the MT nucleation process?

To investigate the role of Stu1 in the mechanism of MT generation, I first examined whether Stu1 was recruited to the Stu2-dependent MT nucleation site, engineered on a chromosome arm (Kitamura et al. 2010). For this purpose I visualised Stu1 in cells where Stu2-LacI fusion protein was tethered at the *lacO* (*lac* operator) array that was inserted on the long arm of chromosome 12 (*REC102:: lacOs* site) (Figure 11A). Thus, in metaphase arrest when all the centromeres were at the metaphase spindle, Stu2 localised with spindles and with the chromosome arm locus (Figure 11B). Although tubulin signals were often found on the Stu2 tethered chromosome locus, no Stu1 signal was detected at these Stu2-dependent nucleation-sites (Figure 11B). This result provided the first evidence that Stu2 may be able, independently of Stu1, to promote MT nucleation at KTs. Nevertheless, one could not rule out the possibility that small undetectable amounts of Stu1 were still recruited and required at the engineered site.

To rule out this possibility, I designed a new experiment; in which Stu2 localisation at the tethered site was monitored in the absence of Stu1 (Figure 11C). When Stu1-aid protein was degraded by the auxin-induced degron system, Stu2-LacI was still recruited at the *REC102::lacOs* site (Figure 11C, top) in comparable amounts to those at centromeres (Figure 11C, bottom). Although the average accumulation level of Stu2 at its tethered site was higher than that at the centromere, several cells showed similar Stu2 signal intensity at the tethered site to that at the centromere; such Stu2 signals were still associated with tubulin signals (Figure 11D). This result suggests that Stu1 is dispensable for Stu2 recruitment and MT generation at the engineered site.

To confirm this more rigorously, I measured tubulin signal intensities at Stu2-LacI / *REC102::lacOs* tethered site in *STU1+* and *stu1-aid* cells as described above (Figure 11E) and I did not detect any statistically significant difference in their distribution (Figure 11F). Therefore Stu1 depletion does not seem to alter MT nucleation at the tethered site. In the absence of Stu1, MT nucleation seemed even slightly enhanced (Figure 11F), which could be due to collapse of a bipolar spindle in this mutant leading to higher concentration of free tubulin available in the nucleus, which can be incorporated into MTs at the tethered site.

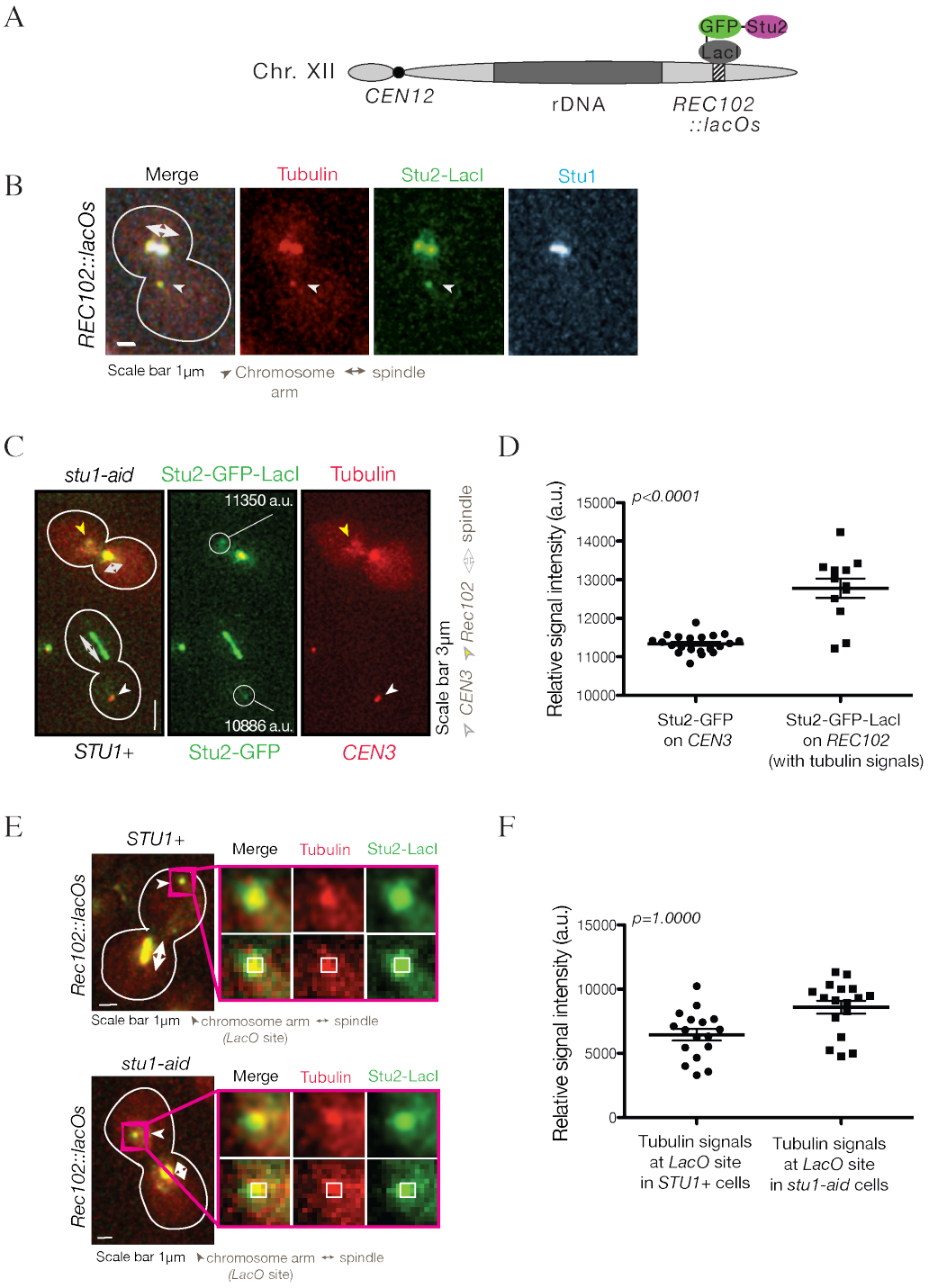

Figure 11. Stu2 is sufficient to generate microtubules, independently of Stu1, when tethered on a chromosome arm locus.

(A) A schematic diagram represents Stu2 tethering on the chromosome arm locus (adapted from (Kitamura et al. 2010); (B) Stu1 is not recruited at Stu2-dependent MT nucleation site. *P_{GALS}-STU2-GFP-LacI REC102::lacOs CFP-TUB1 STU1-4xmCherry P_{MET3}-CDC20* cells were treated as in Figure 5C. After 2.5 hrs in metaphase arrest, 2% galactose was added to the medium for an hour. (C) In the absence of Stu1, Stu2 is recruited at the tethered site in similar amounts to those at KTs. Images of representative of *STU1+ Stu2-GFP* on *CEN3* (bottom) and *stu1-aid Stu2-GFP-LacI* on *REC102::lacOs* (top) cells. Two kinds of cells were distinguished by the presence CFP signals (in red) for *CEN3* or tubulin. *STU2-GFP P_{GAL}-CEN3::tetOs tetR-3xCFP P_{MET3}-CDC20* and *stu1-aid OsTIR1 P_{GALS}-STU2-GFP-LacI REC102::lacOs CFP-TUB1 P_{MET3}-CDC20* cells were treated as in Figure 5C. After 2 hrs, 2%

galactose was added to the medium for 1.5 hrs when *STU2-GFP* P_{GAL}*-CEN3::tetOs terR-3xCFP* P_{MET3}*-CDC20* cells were directly released into galactose-containing medium for the total of 4 hrs. (D) Comparison of the intensity of Stu2-GFP signals at *CEN3* and at the *REC102::lacOs* site (where Stu2-GFP-LacI is tethered) on the chromosome arm. Two types of cells were mixed and imaged for 30 min in time-lapse sequence, in the presence of media containing 2% glucose. (E) Stu2 nucleates and extends MTs, independently of Stu1, when tethered on the chromosome arm. *STU1+* and *stu1-aid OsTIR1 Stu2-LacI REC102::lacOs* cells were treated as in (C). (F) Comparison of the intensity of tubulin signals at *Stu2-LacI/REC102::lacOs* site in two types of *STU1+* and *stu1-aid* cells.

2.3. Stu1 tethered on the chromosome arm is insufficient to generate microtubules

After I discovered that Stu2 was independent of Stu1 in promoting MT nucleation at an engineered site on the chromosome arm (see Section 2.2.), I investigated whether Stu1 was also sufficient to nucleate MTs (Figure 12A). In contrast to Stu2, Stu1-GFP-lacI fusion protein, tethered at the *lacOs* site on the long arm of chromosome 12 (Figure 12A), was insufficient to nucleate and extend MTs (Figure 12B). The fact that Stu1-GFP-lacI was not only localising at the *lacOs* site, but also at the spindle, suggested that this fusion protein was in a correct structural conformation for its function (Figure 12B). Moreover, Stu1-GFP-LacI was also recruited at KTs and still able to nucleate MTs, which provided further evidence that the protein was functional (Figure 12C). However, given that Stu1 forms homodimer *in vivo* (Yin et al. 2002), Stu1/Stu1-GFP-lacI dimer may be functional, but Stu1-GFP-lacI homodimer may not. To rule out this possibility, I also investigated Stu1-GFP-LacI localisation and MT generation at KTs upon depletion of the authentic Stu1 (Figure 12D). In the absence of Stu1 (depletion of Stu1-aid), Stu1-GFP-LacI (probably Stu1-GFP-LacI homodimer) was still recruited at KTs and able to generate MTs, proving that these homodimers were indeed functional (Figure 12D).

Altogether these results suggest that Stu1 may not be directly involved in the MT nucleation at KTs, but rather facilitate the recruitment of Stu2. Once Stu2 is recruited at KTs, it is likely that Stu2 does not require Stu1 for nucleation of KT-derived MTs. In addition, these results imply that Stu1 is not sufficient to recruit Stu2 and there might be additional kinetochore components facilitating its recruitment to KTs.

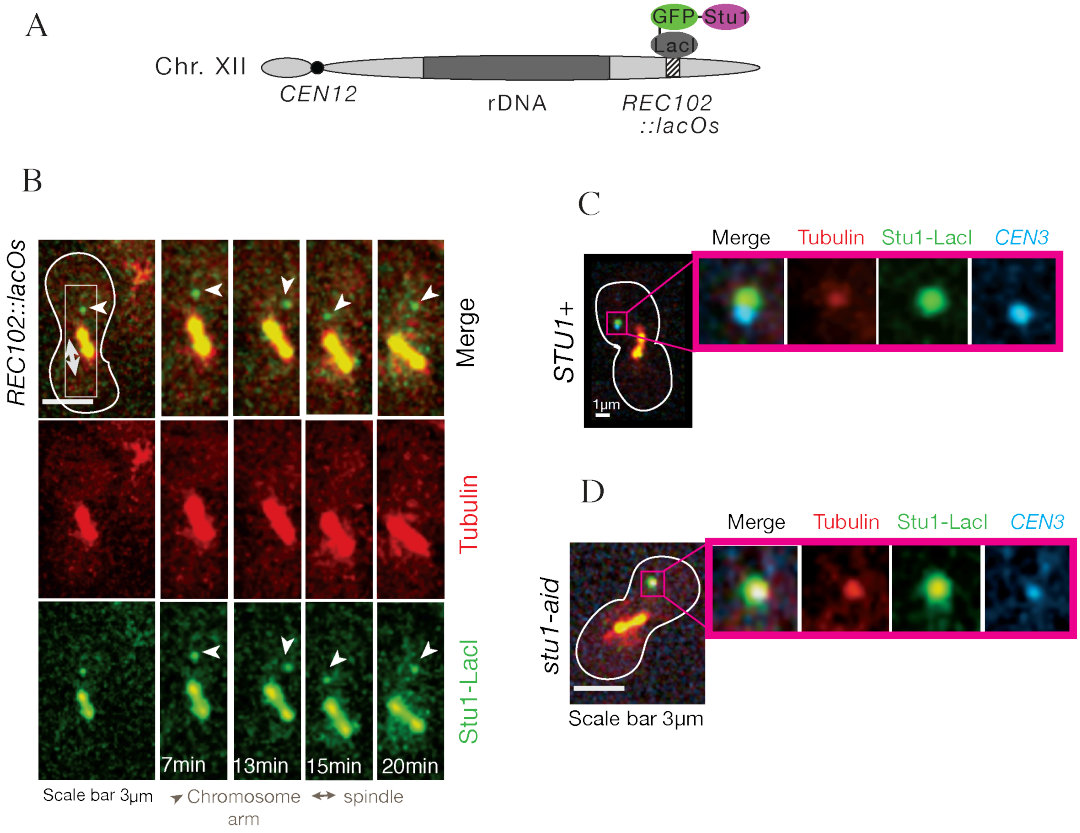

Figure 12. Stu1 is insufficient to nucleate microtubules when tethered on a chromosome arm locus.

(A) Schematic representation of Stu1-GFP-LacI tethering at an engineered *REC102: lacOs* site on the chromosome arm. (B) Stu1 tethered at *lacOs* site does not lead to nucleation of MTs. P_{GALS}-*STU1-GFP-LacI REC102::lacOs CFP-TUB1* P_{MET3}-*CDC20* cells were treated as in Figure 11C. (C) Stu1-GFP-LacI protein is recruited to KTs and leads to MT nucleation at KTs. P_{GALS}-*STU1-GFP-LacI mCherry-TUB1* P_{MET3}-*CDC20* P_{GAL}-*CEN3-tetOs TetR-3xCFP* cells were treated as in Figure 11C. (D) Stu1-GFP-LacI homodimers are functional. P_{GALS}-*STU1-GFP-LacI stu1-aid OsTIR mCherry-TUB1* P_{MET3}-*CDC20* P_{GALs}-*CEN3-tetOs TetR-3xCFP* cells were treated as in Figure 11C.

2.4. Stu1 and Stu2 do not interact in yeast two-hybrid (Y2H), but do show close physical interaction in bimolecular fluorescence complementation (BiFC) assay

2.4.1. No interaction between Stu1 and Stu2 was detected by Y2H screens

As described earlier Stu1 facilitates Stu2 recruitment to KTs, which promotes MT nucleation at KTs. How does Stu1 recruit Stu2 at KTs? Does Stu1 show physical interaction with Stu2? To address this we first used yeast two-hybrid assay (Y2H). In the two-hybrid assay, whole length Stu1 and three parts of N-Stu1 (1–510), M-Stu1 (500–1011) and C-Stu1 (1001–1513) were used as baits against Stu2 prays: Stu2, N-

Stu2 (1–658) and C-Stu2 (550–888), and vice versa (Figure 13A). However, no interaction between Stu1 and Stu2 was detected (Figure 13A) (Nori Kobayashi, unpublished). Nevertheless, we detected an interaction between Stu1 C-terminus and itself (Figure 13AB) (Nori Kobayashi, unpublished), which is very likely responsible for the dimerization of Stu1, which was reported *in vivo* (Yin et al. 2002). In addition, we detected two additional weak interactions between N-Stu1 and M-Stu1 peptides, which accommodate the two TOG-like (TOGL1 and TOGL2) and the S/R-rich domains, respectively (Figure 13AB) (Nori Kobayashi, unpublished).

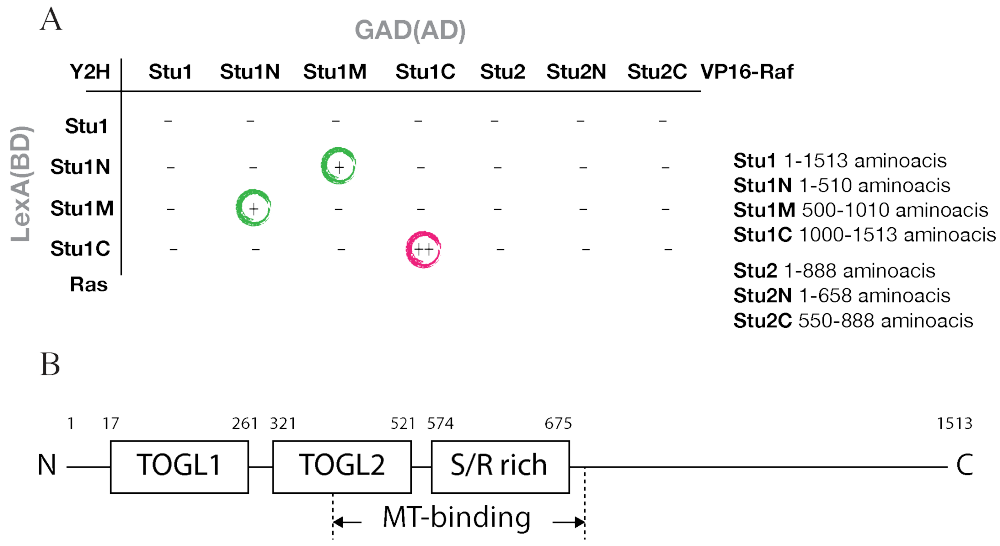

Figure 13. Yeast two-hybrid analysis.

(A) Stu1 does not interact with Stu2, while the Stu1C peptide interacts with itself (Nori Kobayashi, unpublished). BD stands for a DNA-binding domain, while GAD stands for a transcription-activating domain. (B) Schematic representation of Stu1 domains. TOGL1 and TOGL2 domains reside in the N-terminal part of the protein, while S/R rich domain is accommodated into the middle Stu1M region. MT-binding motif encloses significant part of the TOGL2 domain and entire S/R rich domain.

2.4.2. Stu1 and Stu2 show a close physical interaction along the spindle and at spindle pole bodies, but no interaction was detected at kinetochores by BiFC assay

Next I investigated a close physical interaction between Stu1 in Stu2 *in vivo* by bimolecular fluorescence complementation (BiFC) analysis (Sung and Huh 2007;

Gandhi et al. 2011). BiFC analysis enables visualisation of a close physical protein interaction in living cells via the association of two fragments of Venus fluorescent protein – VN173 and VC155 (Figure 14A). Each of Stu2–VN173 and Stu2–VC155 separately does not give fluorescent signals (Figure 14B), but when combined with Stu1–VC155 and Stu1–VN173 respectively, fluorescent Venus signals were observed along the spindle and at spindle pole bodies, indicating that Stu1 and Stu2 come in close proximity (Figure 14C).

Furthermore, I addressed if Stu1 and Stu2 were closely associated also at KTs. Nevertheless, in both combinations Stu2–VN173 Stu1–VC155 and Stu2–VC155 Stu1–VN173, no Venus signals were detected at KTs (Figure 14D). This raises the possibility that Stu1 and Stu2 are not associated closely at the KTs. However we cannot rule out that they are actually associated closely at KTs and, in that case, there are two possible explanations why we cannot detect this association. First, C-terminus tagging of VN and VC may not be suitable for the detection and we plan to use N-terminus tagged VN and VC. Second, according to recent studies Stu1 is the least abundant MAP expressed at very low levels within the cell (Aravamudhan et al. 2014). It may be difficult to detect VN–VC association signals from such a low amount of proteins.

Intriguingly, along with the fact that I could not detect any association between Stu1 and Stu2 at KTs, in both combinations Stu2–VN173 Stu1–VC155 and Stu2–VC155 Stu1–VN173, I could not either detect any tubulin signal associated with KTs (Figure 14D in red). Independent labelling of Stu2 (Figure 5C) or Stu1 (Figure 6A) with fluorescent tags did not interfere with MT generation at KTs. However, when labelled together in both VN–VC and VC–VN combinations, expression levels of Stu1 and Stu2 may be reduced leading to suppression of MT generation at KTs.

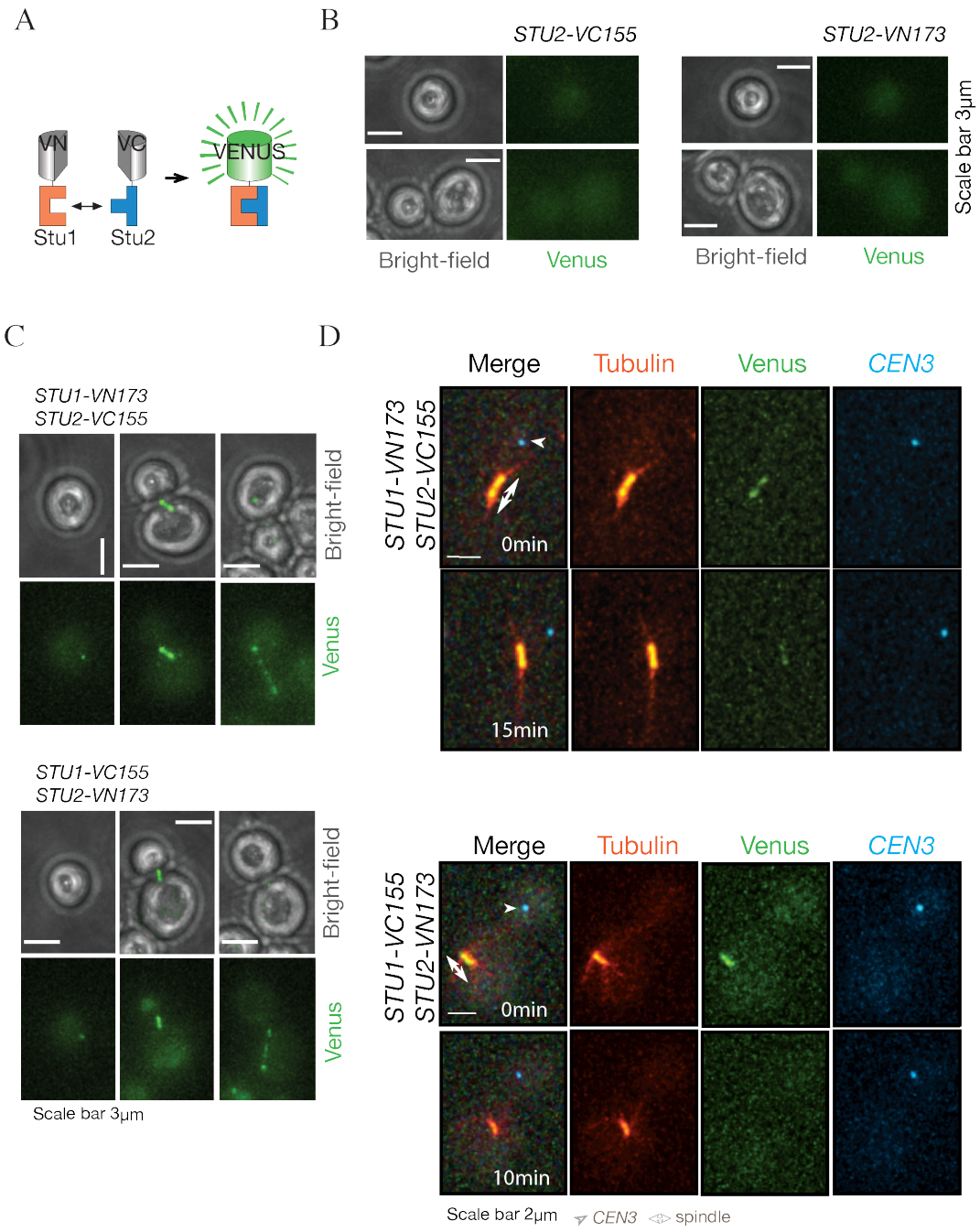

Figure 14. Stu1 interacts Stu2 along the spindle and at spindle pole bodies, but no interaction was detected at the kinetochores (BiFC assay).

(A) Schematic representation of BiFC assay. (B) Separately Stu2–VC155 and Stu2–VN173 does not give fluorescent signals. (C) Stu1 and Stu2 interact along the spindle and at spindle pole bodies. *STU1–VN173 STU2–VC155* and *STU1–VC155 STU1–VN173* cells were grown overnight in synthetic complete media supplemented with 2% glucose. Cells represented in the panels are after 1 sec exposure into the YFP channel. (D) *STU1–VN173 STU2–VC155* and *STU2–VN173 STU1–VC155* P_{GAL}*-CEN3-tetOs tetR-3CFP mCherry-TUB1* P_{MET3}*-CDC20* cells were treated as in Figure 5C.

II. Roles of kinetochore-derived microtubules in kinetochore capture

To investigate the roles of KT-derived MTs, we had to first understand molecular mechanisms facilitating MT nucleation at KTs. Both microtubule-associated proteins Stu1 and Stu2 play crucial roles in MT generation at KTs. Stu2 is also required for the extension of spindle pole MTs (Kitamura et al. 2010). On the other hand, Stu1-depletion compromised MT generation specifically at KTs without suppressing that at the spindle poles (Figure 7). Moreover, in the previous chapter I showed that Stu1 is required for the recruitment of Stu2 at KTs. Once recruited at KTs, Stu2 plays the central role in nucleation and extension of KT-derived MTs independently of Stu1. These results highlight Stu1 as a convenient molecular tool to study the roles of KT-derived MTs, because Stu1 depletion allows us to remove Stu2 from KTs, which abolishes specifically the pathway for MT nucleation at KTs.

1. Live-cell analysis of initial kinetochore-microtubule interaction in physiological conditions

To understand molecular mechanisms facilitating MT generation at KTs, I have been using the engineered centromere reactivation system (Tanaka et al. 2010), which provides a good spatial resolution to observe KTs prior to the interaction with MTs from spindle poles. However, I aim to understand the role of KT-derived MTs in physiological conditions. So, to study it, I first focused on physiological conditions. Another reason for use of physiological conditions is as follows – Stu1 depletion causes collapse of bipolar spindle in the engineered centromere reactivation system, in which cells are arrested in metaphase. The collapse of the bipolar spindle leads to an increase of the number of MTs extending from spindle poles, which makes it tricky to analyse the outcome of loss of KT-derived MTs. This problem can be bypassed in physiological

conditions, in which KTs initially interact with spindle pole MTs prior to formation of a bipolar spindle (Kitamura et al. 2007).

1.1. Live-cell imaging of kinetochore-derived microtubules and kinetochore capture in physiological conditions (S-phase)

Studying KT-derived MTs in physiological conditions has a number of limitations, such as low spatial resolution to visualise the uncaptured free KTs due to their very close proximity to the spindle (Figure 15AB) (Kitamura et al. 2007). In budding yeast, KTs stay attach with spindle MTs throughout most of the cell cycle (Figure 15A) (Kitamura et al. 2007). Only in S-phase upon centromere replication, KTs disassemble and detach from spindle. Once centromeres are replicated, KTs will assemble *de novo* and can nucleate MTs (Kitamura et al. 2010)(Figure 15B). When spindle pole MTs "locate" KTs, KTs will be captured and brought again close to the spindle pole (Kitamura et al. 2007).

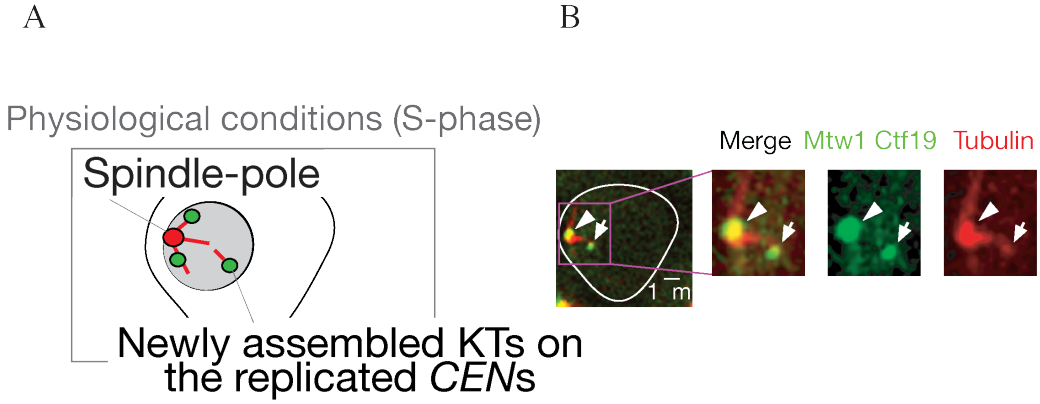

Figure 15. Kinetochore–microtubule interaction in physiological conditions.

(A) Schematic representation of KT–MT interaction in S-phase. (B) Newly assembled KTs onto the replicated centromeres are on average 1 µm away from the spindle pole (Figure (B) adapted from (Kitamura et al. 2010)).

1.2. In physiological conditions microtubule nucleation at kinetochores is suppressed after Stu1 depletion

To analyse initial KT–MT interaction in detail in physiological conditions (S-phase), I acquired live-cell imaging with short time intervals. Short time intervals allowed me to track the period between *de novo* KTs assembled onto the replicated centromeres and their subsequent capture by spindle-pole MTs. To avoid quick photobleaching of fluorescent proteins, I used the anchor-away (AA) system (Haruki et al. 2008), which proved to be significantly better in terms of photobleaching compared to the previously used auxin-induced degron system in Chapter I. The reason for a relatively quick photobleaching with the Aid system is currently unknown.

With the AA technique, I conditionally excluded Stu1 from the nucleus by tethering it to the ribosome in cytoplasm, in the presence of rapamycin (Figure 16A). Nuclear depletion of Stu1 in this system was as efficient as degrading the protein in the Aid system (Figure 16B; see also Figure 7B), but allowed me to observe generation of KT-derived MTs and KT capture in physiological conditions with minimal photobleaching (Figure 16C). In *STU1+* cells, KTs were assembled *de novo* (Figure 16C, in red) and these KTs could nucleate MTs (Figure 16C, indicated as arrows). In most of cells, I observed dot-like MT/tubulin signals at KTs (Figure 16C, *STU1+* left). However, in a few examples I also observed extension of KT-derived MTs, which seemed to interact with spindle-pole MTs prior to KT capture (Figure 16C, *STU1+* right, 90 sec). When Stu1-frb protein was excluded from the nucleus in the presence of rapamycin, MT nucleation at KTs was abolished and KT capture seemed to be delayed (Figure 16C, *stu1-frb*). At several time points spindle MTs extended in close proximity to the KT, but seemingly failed to capture the KT with high efficiency (Figure 16C, *stu1-frb*).

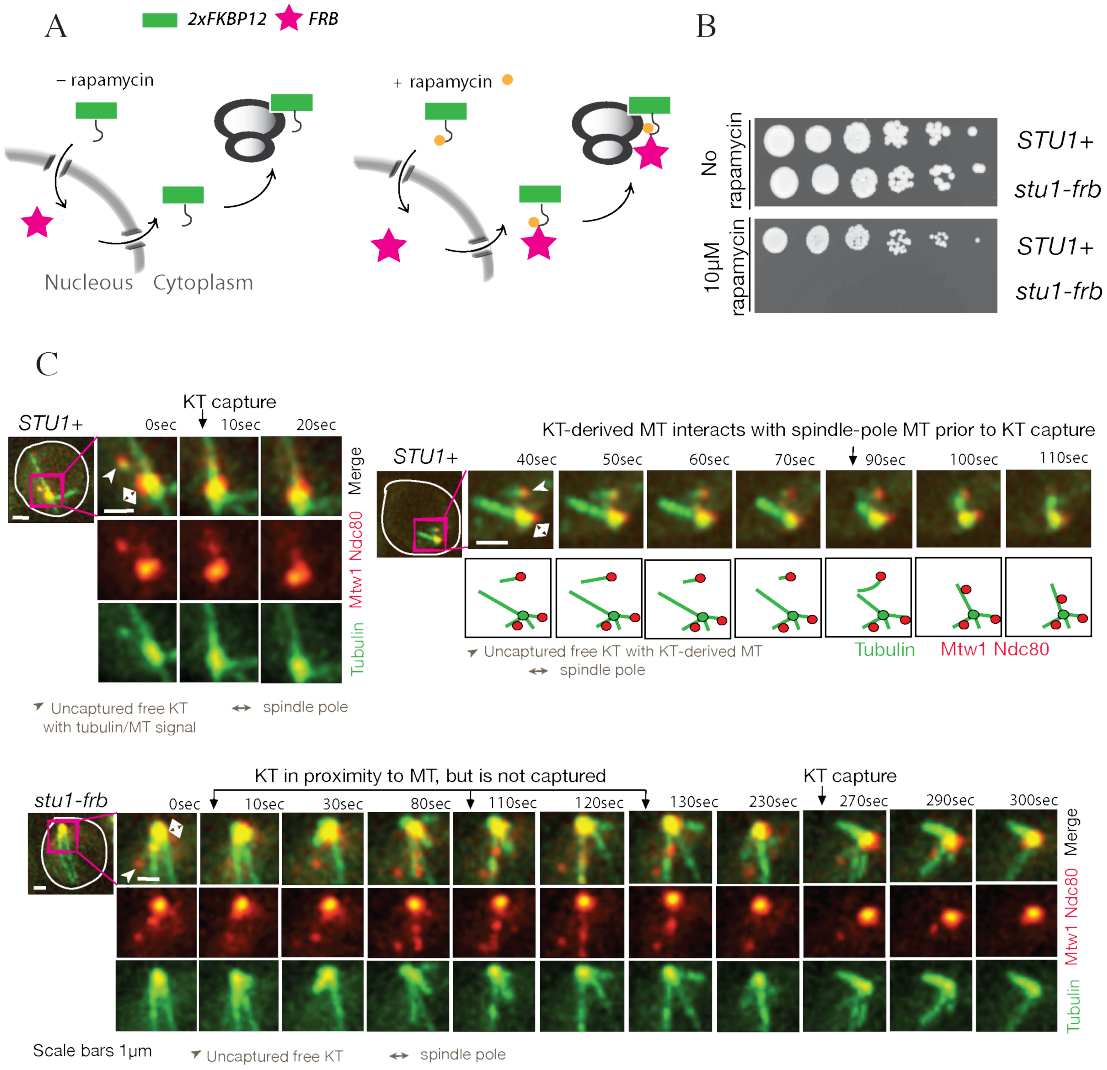

Figure 16. In physiological conditions microtubule nucleation at kinetochores is specifically abolished in *stu1-frb* mutant.

(A) Schematic representation of the anchor-away (AA) technique. (B) Growth analysis of *stu1-frb* mutant. Growth of *stu1-frb* mutant was examined by spot assay on Do-met media supplemented with 10 μM rapamycin. (C) Representative time-lapse images of *STU1+* and *stu1-frb* cells. *STU1+ and stu1-frb RPL13A-2FKBP12 tor1-1 fpr1Δ MTW1-4mCherry Ndc80-4mCherry YFP-TUB1* cells were treated with α-factor in YPA rich medium supplemented with 2% glucose for 2.5 hrs. Then 10 μM rapamycin was added to the media for additional 0.5 hr during α-factor arrest. Subsequently, cells were released into mixed rich YPA: synthetic SC media containing 2% glucose in 1:3 proportions. Image sequences were acquired 20 min after the release in a Z-stack of frames every 10 sec for the total of 8 min using two separate channels for YFP (TUB1 in green) and mCherry (Mtw1 and Ndc80 in red).

2. Statistical analysis of appearance of microtubules at kinetochores and their role in kinetochore capture

2.1. Kinetochore capture is a stochastic process that follows a simple exponential decay curve

To quantify the delay of KT capture in *stu1-frb* mutant caused by depletion of KT-derived MTs, I first tried to understand more about the nature of KT capture by spindle-pole MTs. KT capture is a stochastic process at a level of a single KT (Kirschner 1986), which means it is impossible to predict when a particular KT would be captured. Indeed some of KTs are captured quickly within 10–30 sec following their assembly is discerned (Figure 17A, events on the top), but for others it takes significantly longer time to be "located" and captured by spindle-pole MTs (Figure 17A, events on the bottom). However, if we plot how the entire population of free KTs gets captured in time, we could observe that KT capture is very well fitted by a simple one-phase exponential decay curve (Figure 17B, black curve, R^2= 0.99), characterised with a specific half-life $t_{1/2}$ of 35 sec (Figure 17B); in reasonable agreement with previous observations (Kitamura et al. 2010). Half-life is the time required for free (i.e. uncaptured) KTs to fall to one half of their initial number, which means that in the first 35 sec, 50% of the initially free KTs will be captured, in the next 35 sec – 25% and so forth. Thus the probability for any given KT to get captured within a 35-sec interval never changes, and it is always 50%.

If the KT capture (i.e. reduction of the fraction of uncaptured KTs along time) indeed follows a simple exponential decay curve, the expected time required for a KT capture should still be the same from a randomly selected time point (This is similar to a radioisotope whose expected decay time is always the same as it does not depend on how long time the radioisotope existed). To test this, I randomly picked KTs at random

time point between their first appearances (i.e. 0 sec) and the KT capture from the experimentally recorded time-points. I then redefined the randomly selected time point as zero and recorded the time interval up to KT capture. In this way, I selected 50 time points in one trial, and drew a new KT capture curve based on the redefined zero time points. I made 5 such trials and found that new KT capture curves were similar to the original KT capture curve (Figure 17B, discontinuous lines). For example, half-lives of the 5 new KT capture curves were $t_{1/2}$= 34.56 ± 3.36 sec, which is very similar to the half-life of the original KT capture curve. Therefore, at any given time point, the expected time for any given free KT to be captured by a spindle-pole MT is about 35 sec.

2.2. Appearance of kinetochore-derived microtubules is correlated with advanced kinetochore capture

Utilizing the property of a simple exponential decay curve I studied above, I next addressed if appearance of KT-derived MTs make any change in timing of KT capture. Tubulin/MT signals at KTs (Figure 17A, green squares) appear at random time-points and have different duration in time (Figure 17A). Some of them appear immediately prior to KT capture (example events #1, #20 and #56), others at earlier time-points (example events #11, #40 and #60). To investigate whether the appearance of MT/tubulin signals biases timing of KT captures, I plotted how KTs that nucleated MTs get captured along the time from the first appearance of MTs/tubulin at KTs (Figure 17C, green curve). In the plot of Figure 17C, the curve in green, which represents the kinetics of KT capture after the first appearance of MT/tubulin signal, declines similarly to the black curve of all KTs, but with shorter half-life $t_{1/2}$ of 22 seconds. Thus the time from the appearance of MTs at KTs to their capture (Figure 17C, green line) is clearly shortened, which can be interpreted as an acceleration of KT capture by KT-derived

MTs. This suggests that appearance of MT/tubulin signals at KTs is correlated with advanced KT capture. Moreover, the effect that appearance of MT/tubulin signals at KTs has on reducing the timing of KT captures seemed to be significant (Figure 17D, $p< 0.5$).

If KT-derived MTs had no effect on KT capture, given the fact that they appear randomly, one would have expected them to be captured with the same kinetics of that of randomly picked time-points (Figure 17C, discontinuous lines). This is due to the fact that if there was no bias, the expected time, in which KT should interact with spindle MT will be always the same and equal to 35 sec, no matter how long time KT existed (see Section 2.1). However, this is a simple correlation of the appearance of KT-derived MTs with advanced KT capture. In order to establish a causal relationship between the roles of KT-derived MTs and efficient KT capture, I went to further study KT capture when MT generation at KTs was abolished.

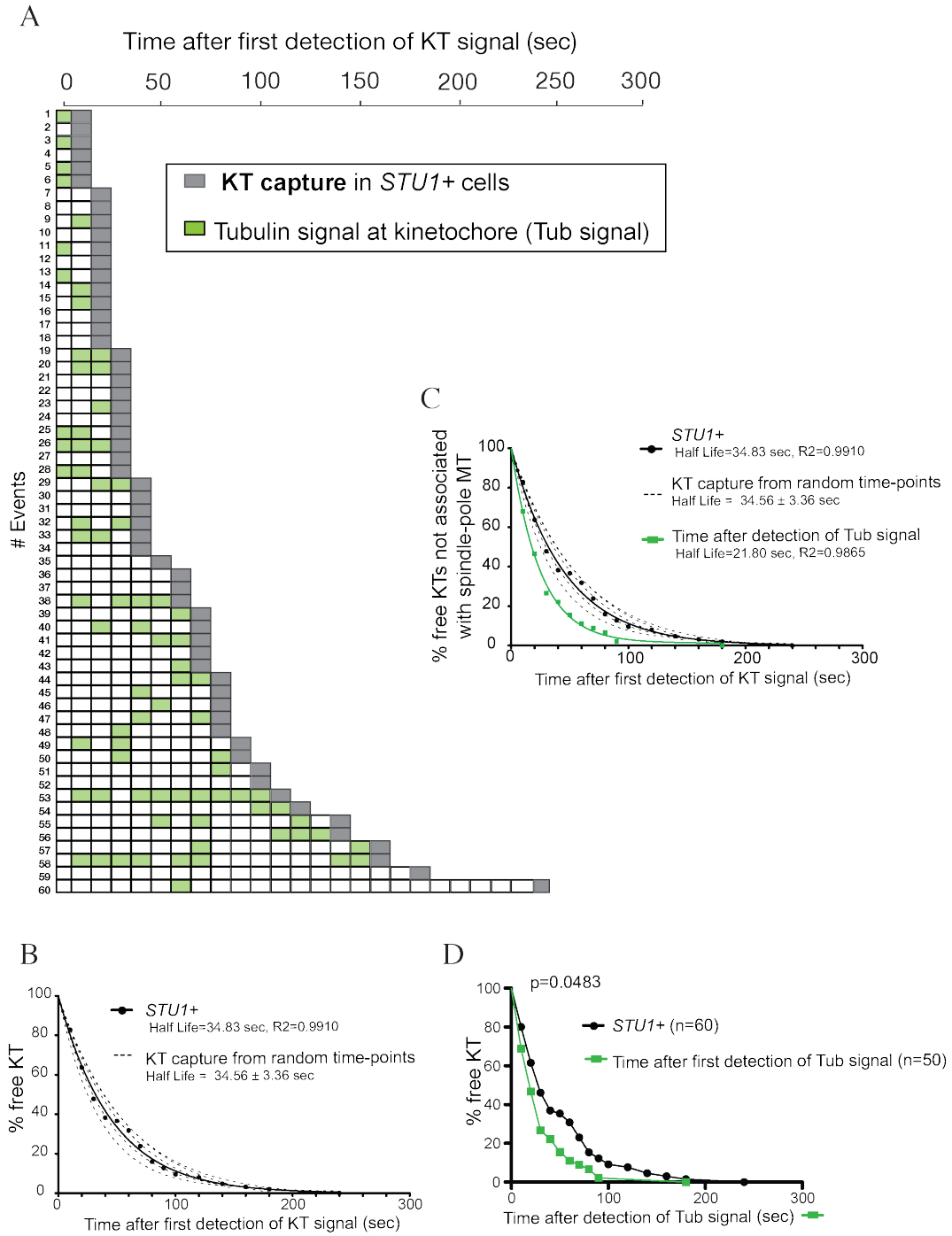

Figure 17. Kinetochore capture is a stochastic process that follows a one-phase exponential decay curve.

(A) Time points in each event (60 events recorded out of 268 cells), in which KT signals were detected (first detection at time 0) away from a spindle pole and subsequently interacted with spindle pole MTs (grey box). Time points showing KT-associated MT/tubulin signals (not connected to spindle pole MTs) indicated by green boxes. (B) Capture kinetics of KTs in wild type *STU1+* cells follows simple exponential decay curve, no matter how long KTs existed. (C) Appearance of tubulin/MT signal at KTs is correlated with advanced KT capture. Appearance of all 50 KT-derived MTs (25 successful, which appear prior to KT capture and 25 unsuccessful, which appear at earlier time-points) was analysed (continuous KT-derived MT was counted as a single MT) in respect to KT capture (D) Regression curves were drawn based on the exponential decay curves. The total number of KTs at time 0 was predicted from these exponential decay curves, including those that escaped my observation due to rapid interaction with spindle pole MTs after KT assembly at 10 sec (4 hypothetical KT capture events were added at 10 sec and 2 hypothetical KT-derived MT for these 4 KTs, based on the frequency of appearance of KT-derived

MTs). The survival curves were compared by log-rank test. (D) KT capture from randomly selected time points (dashed lines, *in silico* result).

2.3. When microtubule generation at kinetochores is abolished with Stu1 depletion, kinetochore capture is delayed

2.3.1. Kinetochore capture is delayed with Stu1 depletion

The above results suggest that appearance of KT-derived MTs is correlated with advanced KT capture by spindle-pole MTs. We next addressed a potential causative relation between the two, i.e. whether KT-derived MTs advance KT capture. With nuclear depletion of Stu1-frb protein, generation of KT-derived MTs was specifically suppressed in physiological conditions (see Section 1.2, Figure 16C). When such MT generation at KTs was compromised, KT capture seemed to be delayed (see Section 1.2, Figure 16C, *stu1-frb* mutant). To quantify the delay in KT capture observed upon nuclear depletion of Stu1-frb protein, I tracked 74 free KTs in the *stu1-frb* mutant from their *de novo* assembly (i.e. their first appearance) until their capture (Figure 18A) and then I plotted how the percentage of these free KTs decreases over time, compared with that in the wild-type *STU1+* (Figure 18B, purple and black curves respectively). Similarly to *STU1+*, *stu1-frb* plot was very well fitted by a simple exponential decay curve (Figure 18B, R^2=0.99), but with longer half-life $t_{1/2(stu1\text{-}frb)}$ of 51 sec, compared with $t_{1/2(STU1+)}$ of 34 sec (*half-life represents the expected time, in which a free KT interacts with spindle MTs, see section 2.1). Therefore at any given time point, a free Stu1-depleted KT, incapable of nucleating MTs, requires on average 16 sec longer, to interact with spindle MTs than does a free $Stu1^+$ KT.

Furthermore, regression curves were drawn based on the exponential decay curves and the difference between these two curves was compared by log-rank test for survival

curves ($p< 0.05$) (Figure 18C). This p-value of < 0.05 suggested that the difference in kinetics of KT capture between *STU1+* and *stu1-frb* cells is significant.

Based on the kinetics of KT capture with a half-life $t_{1/2}$ of 35 sec, we then calculated the fraction of KTs left uncaptured after a certain time, in *STU1+* and *stu1-frb* cells ($D(t_o)=2^{-t_o/t_{1/2}}$, Figure 18D). At 300 sec this fraction is about 7-folds, at 600sec – 50 folds and at 900 sec reaches up to 400 folds higher in *stu1-frb* cells than in *STU1+* cells (Figure 18D).

Altogether these results may provide the first evidence that generation of KT-derived MTs causes efficient KT capture. Nevertheless, one could still argue that the observed delay in KT capture with Stu1 depletion may not be due to a lack of MT/tubulin nucleation at KTs, but rather due to other functions of Stu1 independent of MT generation at KTs. Therefore I further investigated such possibility.

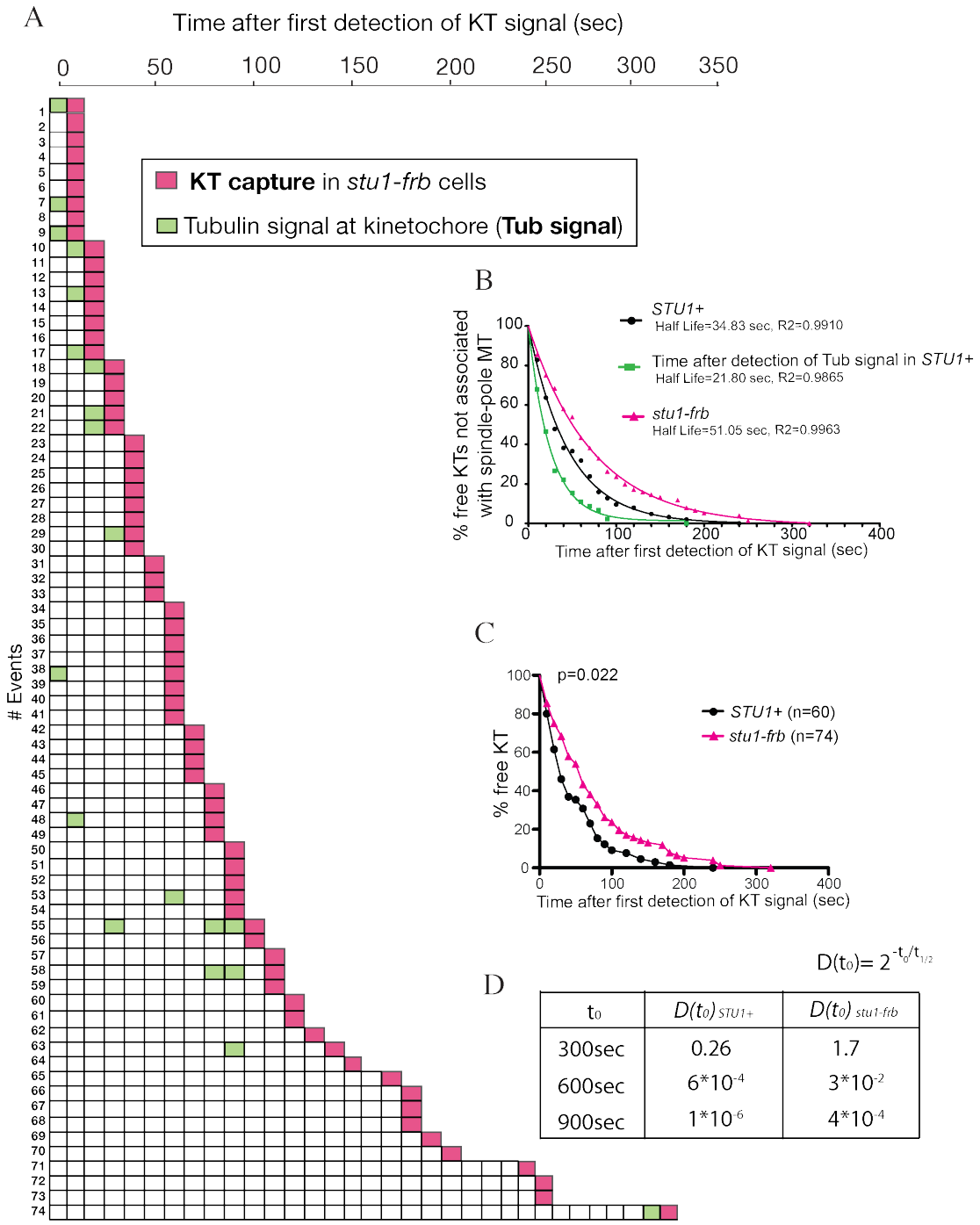

t_0	$D(t_0)_{STU1+}$	$D(t_0)_{stu1\text{-}frb}$
300sec	0.26	1.7
600sec	$6*10^{-4}$	$3*10^{-2}$
900sec	$1*10^{-6}$	$4*10^{-4}$

Figure 18. Kinetochore capture in *stu1-frb* mutant, defective in microtubule nucleation at kinetochores, is delayed.

(A) Time points in each event (74 events recorded out of 177 cells), in which KT signals were detected (first detection at time 0) away from a spindle pole and subsequently interacted with spindle pole MTs (grey box). Time points with KT-associated MT/tubulin signals (not connected to spindle pole MTs) indicated by green boxes. (B) Similarly to wild type *STU1+*, capture kinetics of KTs in *stu1-frb* cells follows simple exponential decay curve, but with longer half-life. (C) Regression curves were drawn based on the exponential decay curves. The total number of KTs at time 0 was predicted from these exponential decay curves, including those that escaped my observation due to rapid interaction with spindle pole MTs after KT assembly at 10 sec (2 hypothetical KT capture events were added). The survival curves were compared by log-rank test. (D) Percentage of KTs left uncaptured at different timing.

2.3.2. Nuclear microtubule dynamics is not compromised after Stu1 depletion

To address if Stu1 has an additional role affecting efficient KT capture, independent of generation of KT-derived MTs, I further evaluated potential defects found in *stu1-frb* mutant. One possibility is that dynamics of nuclear MTs, extending from a spindle pole, changes upon Stu1 depletion, which then affects timing of KT capture. I tested this possibility as follows: to discriminate nuclear and cytoplasmic MTs, I labelled nuclear envelope by visualising nucleopore protein *Nic96-4mCherry* (Figure 19A). With labelled nuclear outlines, I could determine whether a MT lies within, or outside of the nucleus (Figure 19A). The maximum length that nuclear MTs could reach was in the range of 1–3 µm due to the nuclear confinement and was similar between wild-type *STU1+* and *stu1-frb* mutant (Figure 19B, p= 0.30). The numbers of nuclear MTs (longer than 0.5 µm) extending from the spindle-poles in *stu1-frb* and *STU1+* cells were not statistically different (Figure 19C, p= 0.23). These results suggest that Stu1 depletion does not considerably change the dynamics of spindle-pole MTs.

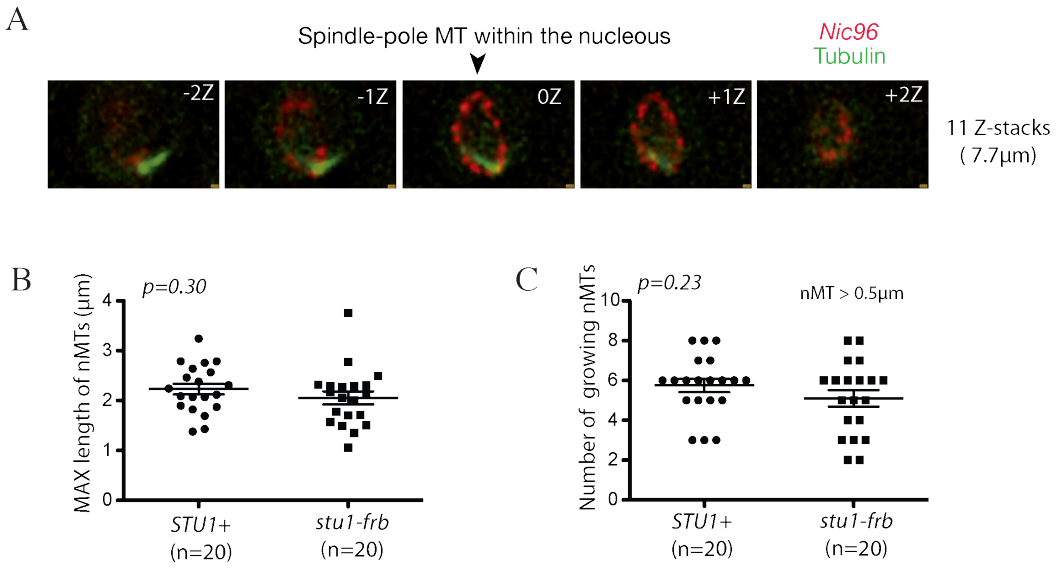

Figure 19. Nuclear microtubule dynamics is not altered in *stu1-frb* mutant.

STU1+ and stu1-frb RPL13A-2FKBP12 tor1-1 fpr1Δ Nic96-4mCherry GFP-TUB1 cells were treated as in Figure 16C. (A) Schematic representation of how nuclear MTs (nMTs) were discerned. (B) Maximum length of nMTs and (C) number of nMTs (> 0.5 µm) extending from the spindle-pole for the period of 300 sec.

2.3.3. Kinetochore assembly is not compromised after Stu1 depletion

Alternatively it is possible that Stu1 is required for assembly of KTs, and therefore Stu1 depletion impairs the KT assembly, delaying KT capture by spindle-pole MTs. To test this possibility, I measured the intensities of KTs in *STU1+* and *stu1-frb* cells at different times after the first appearance of free KT, which reflects the time of *de novo* KT assembly (Figure 20AB). In cell with *Mtw1-4mCherry* and *Ndc80-4mCherry*, the intensity of KT fluorescence signals was quantified in the three dimensional space. The intensities of KTs were in the range of 500–3000 in *STU1+* and *stu1-frb* cells and there was no statistically significant difference between the two cells (Figure 20B), analysed by unpaired T-test). The result suggests that KT assembly is not significantly compromised after Stu1 depletion.

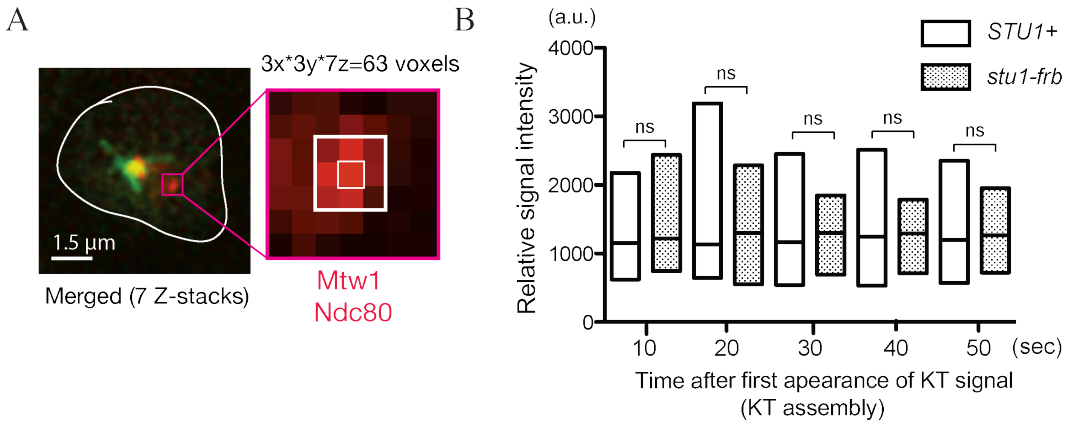

Figure 20. Kinetochore assembly is not compromised in *stu1-frb* mutant.

(A) Schematic representation of how the intensity of KTs was measured. I choose nine pixels (3x3) centred on the brightest one after the 7 z-stacks had been projected into a two-dimensional image at each time point. The signal intensities of the selected area in XYZ (3x3x7=63 voxels) were summed using Volocity, after background subtraction. The background was defined as the most frequently observed pixel intensity in the field of view. (B) Comparison between the intensities of KTs in *STU1+* and *stu1-frb* cells at different time points after their first detection. *STU1+ and stu1-frb RPL13A-2FKBP12 tor1-1 fpr1Δ MTW1-4mCherry Ndc80-4mCherry YFP-TUB1* cells were treated as in Figure 16C.

2.3.4. After Stu1 depletion, kinetochores are assembled and captured within characteristic distances from the spindle pole, similar to *STU1+* cells

By annotating the position of KTs and spindle pole body, I could estimate the distance between them at the moment that KTs appear for the first time (i.e. their detectable *de novo* assembly) or at the moment of KT capture (i.e. their first co-localisation with spindle-pole MTs) in the three-dimensional space. In both *STU1+* and *stu1-frb* cells, free KTs appeared for the first time (i.e. *de novo* KT assembly) within characteristic distances from spindle pole of $D_{free\ (STU1+)}$= 1.53 ± 0.05 μm and $D_{free\ (stu1\text{-}frb)}$= 1.65 ± 0.05 μm, respectively. There is no statistically significant difference between them.

Next I evaluated the distance between captured KTs (i.e. KTs localising for the first time on spindle-pole MTs) and spindle pole. In *STU1+* and *stu1-frb* cells, KTs were captured at similar distances from the spindle pole ($D_{cap(STU1+)}$= 1.29 ± 0.05 μm and $D_{cap(stu1\text{-}frb)}$= 1.30 ± 0.05 μm). Nevertheless these distances were significantly shorter compared to where their uncaptured free KTs appeared for the first time ($D_{free(STU1+)}$= 1.53 ± 0.05 μm and $D_{free(stu1\text{-}frb)}$= 1.65 ± 0.05 μm) with p values of 0.002 and < 0.0001 respectively. This result indicates that KTs get captured closer to spindle pole from where they get initially assembled. In this respect there seemed to be a preferred distance from the spindle pole for KT capture, probably limited by the average length of spindle-pole MTs. It is possible that random KT motions bring KTs within these positions at characteristic distances from spindle pole.

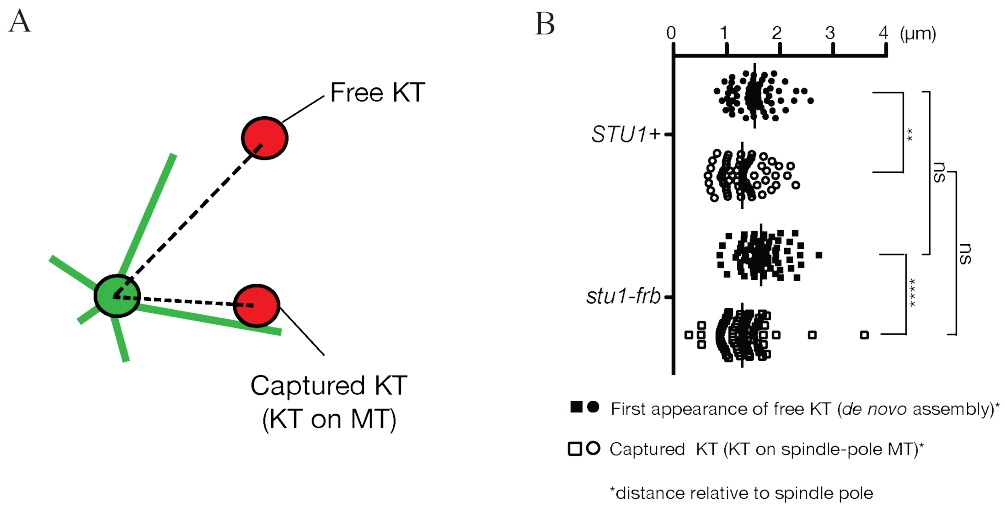

Figure 21. Kinetochores are assembled and captured at characteristic distances from a spindle pole.

(A) Schematic representation of free and captured KTs in respect to their distance from a spindle pole. (B) Distances of free uncaptured and captured KTs from spindle pole in *STU1+* and *stu1-frb* cells. As centres of KTs and spindle pole body, I annotated the brightest pixel in XYZ planes and measured the distance between them in Volocity with pixel size in x and y dx = dy = 0.129 μm and pixel size in z dz = 0.6 μm.

2.4. Mathematical simulation recapitulates the role of kinetochore-derived microtubules in facilitating KT capture

The above results support the notion that after Stu1 depletion a lack of KT-derived MTs causes a delay in KT capture by spindle-pole MTs. If a lack of KT-derived MTs is indeed the sole (or, at least, the major) reason for the observed delay in KT capture with Stu1 depletion, it should be possible to reconstitute mathematically normal kinetics of KT capture by introducing the effect of KT-derived MTs to the capture kinetics with Stu1 depletion. For this, we developed a mathematical model of KT capture in collaboration with Marek Gierlinski, Data Analysis Group. In this model, KT-derived MTs were implemented in *stu1-frb* cells (Figure 22A). To mimic KT-derived MTs in *stu1-frb* cells, we implemented them stochastically but with the same probability of appearance, lifetime and outcome (probability of causing KT capture; as successful were defined KT-derived MTs that appear immediately prior to KT capture, while

unsuccessful are the ones that appear at earlier time points) as observed in wild-type *STU1+* cells (Figure 22C). When KT-derived MTs led to a KT capture, they truncated the timeline of the given cell, i.e. advanced the KT capture. In this way, we obtained a new single data set of simulated events in *stu1-frb* cells with KT-derived MTs implemented mathematically (Figure 22B). We repeated this procedure 10,000 times, finding the best-fitting exponential decay parameter *k* for each run. In this way, we obtained distribution of *k* (Figure 22E). The mean of the simulated distribution of k (0.021 ± 0.003, the error represents 95% of simulation runs; Figure 22G) is very similar to the experimentally measured value of *k* in *STU1+* wild-type cells ($0.020^{+0.002}_{-0.001}$, 95% CI; Figure 22F), but at the same time very different of that in *stu1-frb* cells (0.014 ± 0.001; Figure 22D). This indicates that, by artificially adding the effect of KT-derived MTs in the *stu1-frb* cells, we could recapitulate the advanced KT capture observed in *STU1+* cells (Figure 22ABC). This suggests that KT-derived MTs indeed accelerate the KT capture by spindle-pole MTs. The result implies that a lack of KT-derived MTs is the main reason for the delay in KT captures with Stu1 depletion, thus suggesting the causative relation between the KT-derived MTs and efficient KT capture for the first time.

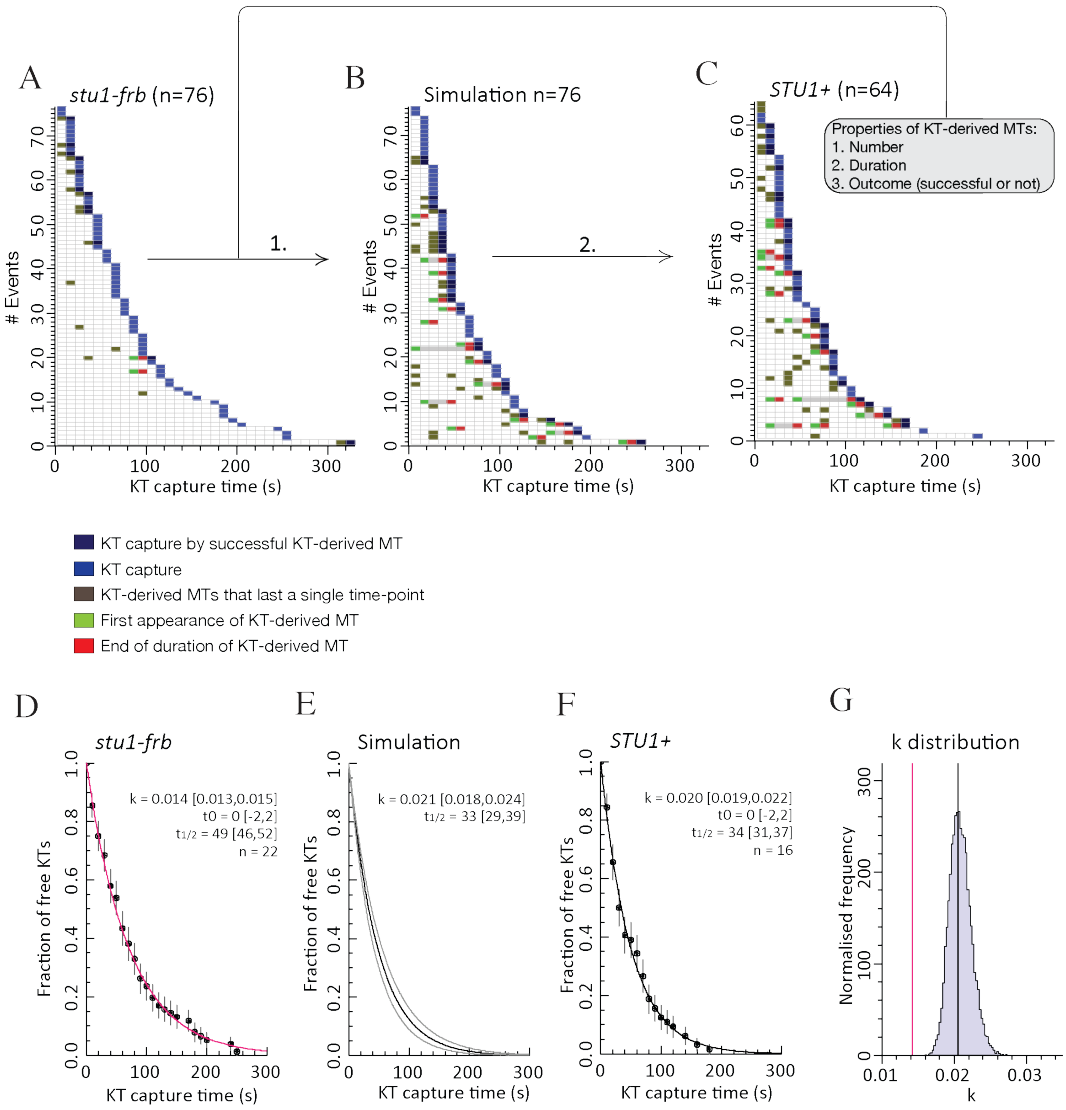

Figure 22. Monte Carlo simulation recapitulates the roles of kinetochore-derived microtubules in *stu1-frb* mutant (Dr Marek Gierlinski, unpublished).

Time points of each event, in which KT signals were detected (first detection at time 0) away from a spindle pole and subsequently captured by spindle-pole MTs (blue box) in (A) *stu1-frb* (B) Simulated *stu1-frb* with KT-derived MTs and (C) *STU1+* cells. Reduction of the fraction of uncaptured KTs in time in (D) *stu1-frb*, (E) Simulated *stu1-frb* with KT-derived MTs and (F) *STU1+* cells. The curve was then fitted by an exponential function $e^{-k(t-t0)}$ using Levenberg-Marquardt algorithm. Error bars in panels (D) and (F) are standard errors of the proportions. Based on the standard errors of the proportions, the uncertainties in best-fitting parameters represented as 95% confidence intervals were calculated from chi-square fitting. The uncertainty in the simulation in panel (E) is represented as 95% confidence interval calculated from random Monte Carlo samples and is shown by grey lines in the figure. (G) The mean of the simulated distribution of *k* in *stu1-frb* cells (with KT-derived MTs) is very similar to the experimentally measured value of *k* in the *STU1+* wild-type cells. The interval of the parameter k in grey contains the central 95% of all parameters k, derived from randomly drawn samples in the Monte Carlo simulation. The corresponding range of exponential decay curves is shown in grey in panel (E).

3. Dissecting initial kinetochore-microtubule interaction at high resolution with the engineered centromere reactivation assay

After Stu1 depletion in physiological conditions, we observed reduction of KT-associated MT formation and a delay in the interaction of KTs with spindle-pole MTs (see Section II/1/1.2.). In these conditions, although at several time-points KTs were in close proximity to MT lattice, they were not captured (see Section II/1/1.2.). This observation suggested that lateral interaction of KTs with spindle-pole MTs was less efficient after removal of KT-derived MTs.

It is not always easy to study initial KT–MT interaction in detail in physiological conditions, because KTs sometimes localize at close proximity to the spindle pole and spindle-pole MTs often overlap. To investigate further the delay in KT capture and potential defect in KT–MT interaction after Stu1 depletion at higher resolution, I went back and used the engineered centromere reactivation assay (see Methods). To investigate initial KT–MT interaction in detail, I analysed *STU1+* and *stu1-frb* cells with *CEN3-GFP*-labelled KTs and *GFP-TUB1*-labelled spindle-pole MTs in a single channel imaging with short intervals of 5 seconds (Figure 23A). In these cells I recorded how many times KTs co-localised with the lattice of spindle-pole MTs and were captured, or co-localised but were not captured. In *STU1+* wild-type cells the majority of KTs that co-localised for at least two consecutive time-points with MT lattice, were efficiently captured and did not seem to be displaced away once a contact was established (Figure 23A, *STU1+*). However, after Stu1 depletion in *stu1-frb* cells KTs moved away more often from spindle-pole MTs following KT co-localisation with MT lattice; these KTs "bounced" on MT lattice and moved away after seemingly making a contact with the MT (Figure 23A, *stu1-frb*). I further quantified these events in Figure

23B. In *STU1+* cells only one in three trials for KT–MT interaction was unsuccessful, while in the mutant *stu1-frb* every one in three trials was successful (Figure 23B).

This analysis gives evidence that the efficiency of KT lateral interaction with a spindle-pole MT is compromised after Stu1 depletion. A plausible explanation of this difference is that KT-derived MTs support the initial contact between KTs and lateral surface of spindle-pole MTs, thus facilitating robust and continuous KT–MT interaction.

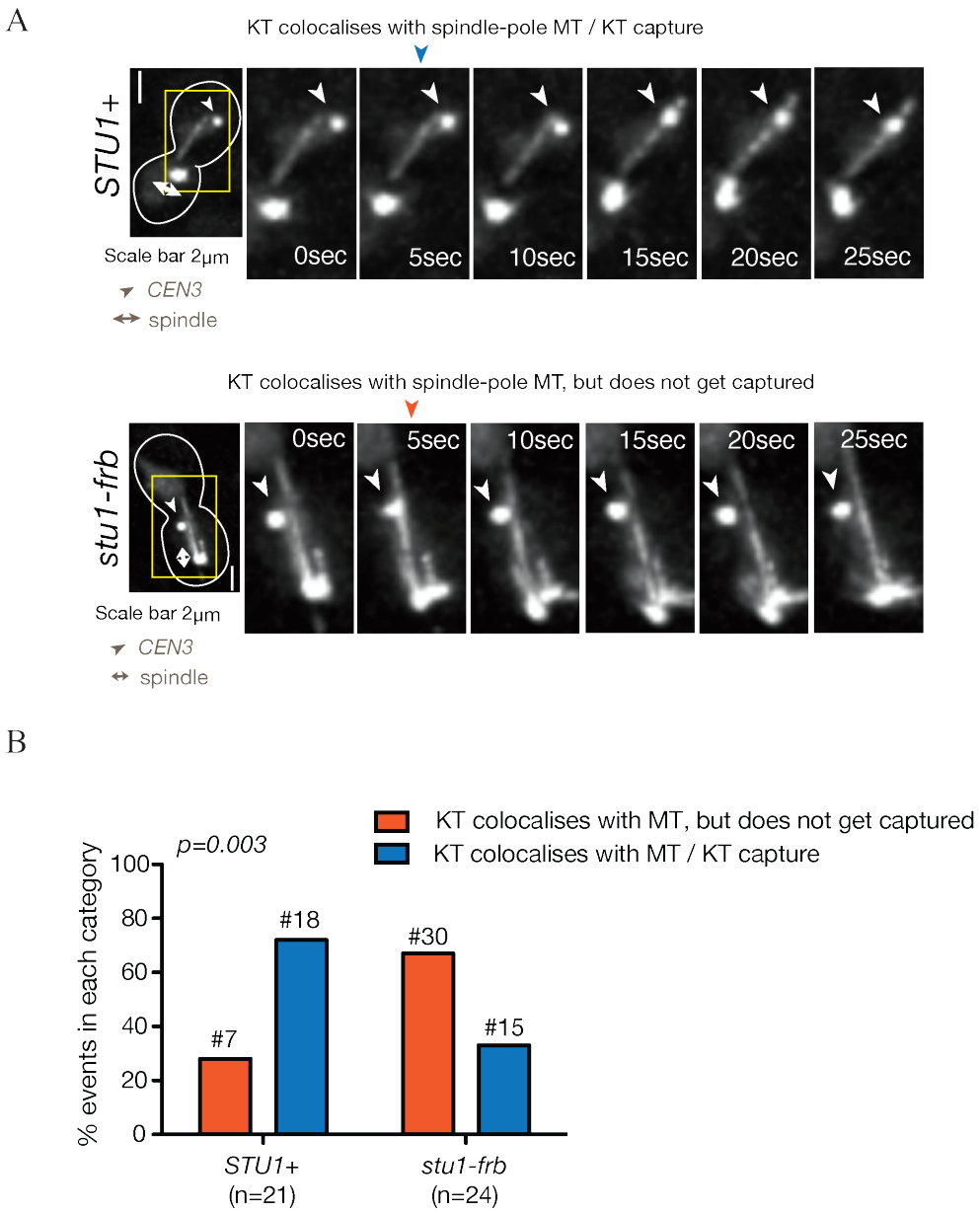

Figure 23. Kinetochores "bounce" on the lattice of spindle-pole microtubules after Stu1-frb depletion.

(A) Representative examples of KT–MT interaction leading to KT capture in *STU1+* cells and KT "bounces" on the spindle-pole MT lattice in *stu1-frb* cells. *STU1+* and *stu1-frb GFP-TUB1* P_{GAL}*-CEN3-tetO*$_{2x212}$ *terR-GFP tor1-1 fpr1*Δ *RPL13A* P_{MET3}*-CDC20* cells were treated as in Figure 5C. 3 hrs after the release into YPARG media, 10 µM rapamycin was added to the media for additional 30 min. Then cells were re-suspended in SC media supplemented with 2% glucose and incubated for 4 min to allow centromere reactivation. Images were acquired every 5 sec for the period of 20 min. (B) In *STU1+* wild-type control and *stu1-frb* (Stu1 depletion) cells, the percentage of co-localisations that did and did not lead to KT capture was counted. I counted all events, in which KT colocalised with the MT lattice for at least two consecutive time-points.

III. After kinetochore capture Stu1 is required for kinetochore-dependent microtubule rescue

After KT capture, KTs on the lateral surface of spindle-pole MTs are transported towards the spindle pole. During this transport, KTs often undergo the conversion from lateral to end-on attachment when depolymerizing MT plus end reaches the KT (Rieder and Alexander 1990; Tanaka et al. 2007; Tanaka 2010). However, this conversion from lateral to end-on may not always be successful. Upon failure in the establishment of end-on attachment, the KT is at increased risk to detach (drops-off) from spindle-pole MT plus end. In case KT detaches from MT end, it has to wait to be re-captured, which would cause a further delay in the establishment of *de novo* KT–MT interaction, KT transport and bi-orientation. To ensure sustained KT–MT interaction upon failure in the establishment of end-on attachment, KTs can change the dynamics of their associated MTs from shrinkage to growth, i.e. convert tubulin depolymerisation to polymerisation at the MT plus end (MT rescue) (Gandhi et al. 2011). Such KT-dependent MT rescue can be considered as a fail-safe mechanism, which ensures that KT does not detach from MT plus end, allowing the KT to wait for next trial of lateral to end-on conversion without losing MT interaction (Gandhi et al. 2011). It was previously shown that Stu2 is a central player in KT-dependent MT rescue (Gandhi et al. 2011). For example, a partial defect in Stu2 function led to less frequent MT rescue. It was proposed that, when the conversion from the lateral to end-on attachment fails, Stu2 at the KT is transferred to the MT end, promoting MT rescue (Gandhi et al. 2011). However, Stu2 also localizes at the MT end, irrespective of the KT-dependent MT rescue. Thus, it remained unclear whether KT-dependent MT rescue requires KT-associated Stu2 or MT-plus end-associated Stu2.

1. When Stu1 is depleted, KT-dependent MT rescue is compromised

Before the discovery that Stu1 was required for Stu2 recruitment at KTs, we did not have methods to remove Stu2 specifically from KTs without affecting its recruitment or function on MT plus ends (See Section I/2/2.1). In this respect Stu1 depletion provided us with a good molecular tool to study KT-dependent MT rescue in the absence of KT-associated Stu2. With Stu1 depletion we were able to specifically remove Stu2 from KTs without affecting Stu2 recruitment and function at MT plus ends (See Section I/2/2.1). Removal of Stu2 from KTs in *stu1-frb* mutant allowed us to switch off KT-dependent MT rescue (Figure 24A). While in *STU1+* cells KT-dependent MT rescue (Figure 24B, top example) and end-on pulling (Figure 24B, bottom example) happened with equal frequencies (Figure 24C), in *stu1-frb* cells KT-dependent MT rescue was nearly completely abolished (Figure 24C). The majority of the KTs underwent end-on pulling after a pause at the MT plus end (Figure 24C), as observed when Stu2 was partially defective with *stu2ΔTOG1* mutant (Gandhi et al. 2011).

The result suggests that Stu2 at the KT is important for KT-dependent MT rescue when the lateral attachment was not converted to the end-on attachment.

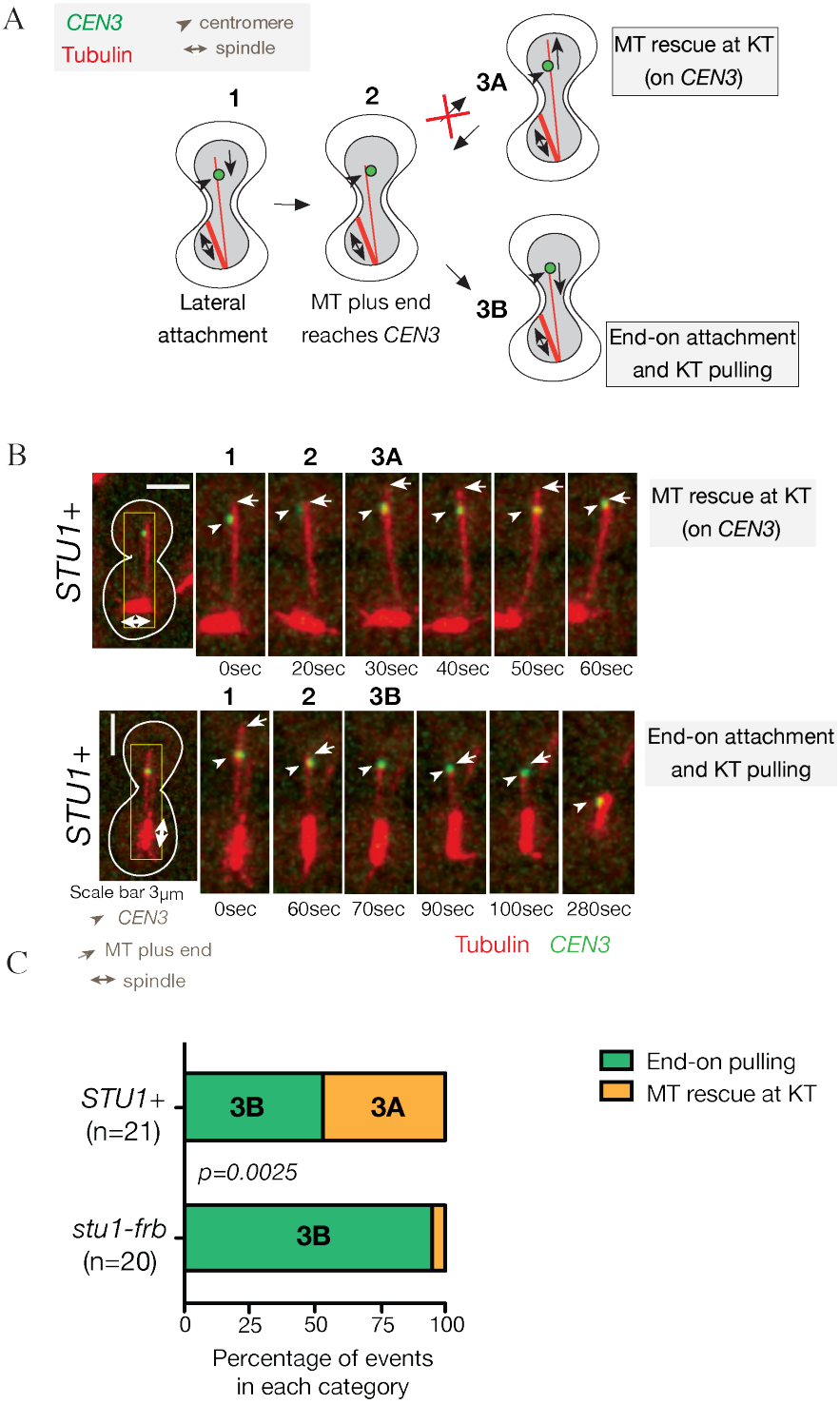

Figure 24. Kinetochore-dependent microtubule rescue is compromised after Stu1 depletion.

(A) Schematic representation of the two mechanisms responsible for sustained KT–MT interaction upon lateral to end-on conversion. (B) Representative examples for KT-dependent MT rescue and end-on pulling. *STU1+ GFP-TUB1* P_{GAL}*-CEN3-tetO*$_{2x212}$ *terR-3xCFP tor1-1 fpr1Δ RPL13A* P_{MET3}*-CDC20* cells were treated as in Figure 23C. (C) After Stu1-frb depletion the frequency of KT-dependent MT rescue is nearly completely reduced, while end-on pulling is increased.

2. When both KT-dependent MT rescue and end-on attachment are compromised, KT detaches from MT plus end upon lateral to end-on conversion

As discussed above, when the MT shrinks and its plus end catches up with the KT on its lateral surface, KT end-on attachment (and subsequent pulling) and KT-dependent MT rescue are alternate options. Given this, what happens if both options are compromised (Figure 25A)?

If efficiency of KT end-on attachment is further compromised and MT rescue at KT cannot compensate for it, then one would expect KTs may drop-off from MT plus end (Figure 25AB). The Ndc80 loop region is required for efficient lateral to end-on conversion (Maure et al. 2011). When this region was deleted (*ndc80*Δ*490–510* mutant), the frequency of end-on pulling was decreased to about 18%, while rescue was slightly increased to 65% when in 18% of cases KTs dropped-off from MT plus end; in reasonable agreement with previous observations (Figure 25C) (Maure et al. 2011). This result suggested that an increase in MT-rescue at KT is able to partially compensate, but not entirely for the defect in end-on attachment, further supporting the notion that MT-rescue at KT works as a fail-safe mechanism to prevent KT detachment.

Next we combined *stu1-frb* and *ndc80*Δ*490–510* (Figure 25C). In this double mutant we expect that both MT-rescue at the KT and the lateral to end-on conversion be compromised. In the double mutant, the frequency of KT drop-off increased from 18% to nearly 45% (Figure 25C). This suggests that MT-rescue at the KT is crucial to ensure sustained KT–MT interaction when lateral to end-on conversion is compromised.

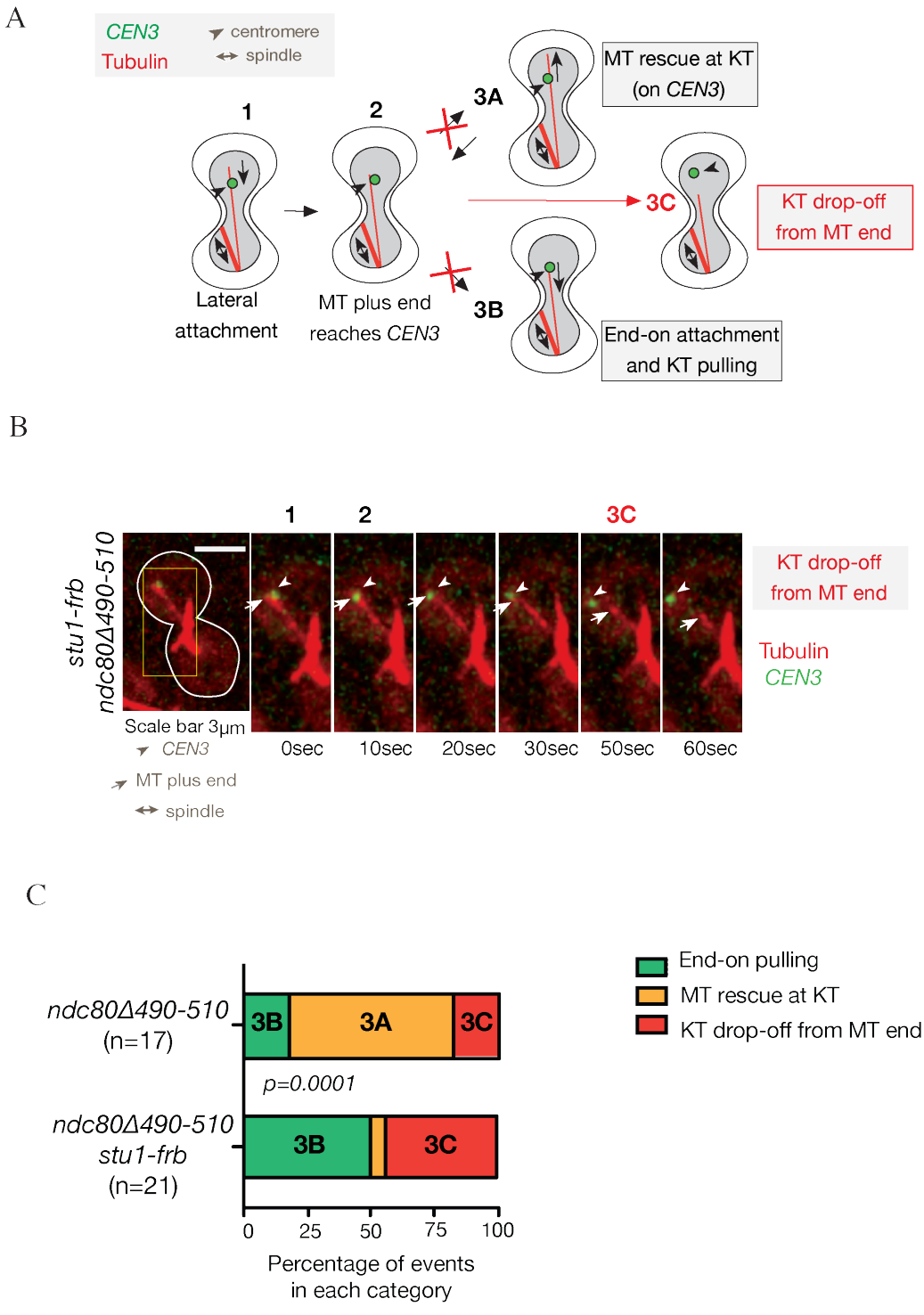

Figure 25. When both kinetochore-dependent microtubule rescue and end-on pulling are switched off, kinetochore drops off from microtubule plus end.

(A) Schematic representation of the two mechanisms in respect to their failure and KT detachment from MT plus ends (drop-off phenotype). (B) Representative example of KT drop-off from MT plus end in *stu1-frb ndc80Δ490-510* double mutant. *stu1-frb ndc80Δ490-510 GFP-TUB1* P_{GAL}*-CEN3-tetO*$_{2x212}$ *terR-3xCFP tor1-1 fpr1Δ RPL13A* P_{MET3}*-CDC20* cells were treated as in Figure 23C. (C) When both KT-dependent MT rescue and end-on pulling are compromised in *stu1-frb ndc80Δ490-510* double mutant, KTs drops off from MT plus end in 44% of cases.

DISCUSSION

I. Molecular regulation of kinetochore-derived microtubules

1. A platform for microtubule nucleation at kinetochores

From yeast to human cells, MTs are generated at KTs prior to their interaction with spindle-pole MTs (Kitamura et al. 2010; Tulu et al. 2006). Key components in the nucleation and extension of these KT-derived MTs are members of the Dis1/TOG family of MT polymerases (also known as the XMAP215 family) (Kitamura et al. 2010; Bucciarelli et al. 2009; Cassimeris et al. 2009). Nevertheless, their recruitment at KTs is not well understood.

In this study, using budding yeast as a model organism, we showed that Stu1, a member of CLASPs (cytoplasmic linker-associated proteins) family, is required for Stu2 recruitment specifically at KTs, but not at the spindle or at spindle poles. The family of CLASP proteins (*S. cerevisiae* Stu1, *S. pombe* Cls1, *C. elegans* Cls-2, *D. melanogaster* MAST/Orbit, *X. laevis* CLASP1, *H. sapiens* CLASP1/2) represents a class of large, multi-functional proteins that localize to a variety of cellular structures (such as KTs, spindle, Golgi apparatus), where they are involved in conserved functions; reviewed in (Al-Bassam and Chang 2011). Recent studies suggest that kinetochore recruitment of Cls-2^{CLASP} – a Stu1 orthologue in *C. elegans* – is dependent on the scaffold KNL-1 protein (Spc105 in *S. cerevisiae*) and on the checkpoint kinase Bub1 (Maton et al. 2015). Consistent with this notion, both published and unpublished observations in *S. cerevisiae* suggest that Spc105 and Bub1 are required for Stu1 and Stu2 localization at KTs (Funk et al. 2014) (Nori Kobayashi, unpublished). Thus, it is likely that Spc105 scaffold protein and Bub1 play conserved roles at kinetochores, throughout species, in providing a platform for assembling Stu1^{CLASP} and Stu2^{XMAP215} proteins.

Intriguingly, Spc105 is also required for kinetochore localization of Slk19 (TACC3 in metazoans; Nori Kobayashi, unpublished). In this study we showed that Slk19 facilitates loading of both Stu1 and Stu2 at KTs. Two-hybrid studies suggest that Stu1 may directly interact with Bub1 (Wong et al. 2007), while Slk19 may directly interact with Spc105 (Newman et al. 2000; Wong et al. 2007). Thus it is possible that Slk19 and Bub1 work together on the Spc105 scaffold protein to recruit Stu1 and Stu2. Nevertheless, how these proteins cooperate to set up a platform for MT generation at KTs remains unclear.

In addition to Spc105, the Ndc80 complex is required for Stu1 and Stu2 localization at KTs (Ortiz et al. 2009; Kitamura et al. 2010). Recent FRET studies suggest that Stu2 occupies a narrow area at the KT and is closely associated with the Ndc80 and Nuf2 C-termini (Aravamudhan et al. 2014). Our studies show no evidence that Ndc80 loop region is involved in Stu2 recruitment at KTs (this study) (Maure et al. 2011) in contrast to studies in *S. pombe* (Tang 2013). The discrepancy between the two studies may be due to use of deletion of different Ndc80 loop regions. In any case, functionally intact Ndc80 complex is still required for both Stu1 and Stu2 recruitment at KTs (Ortiz et al. 2009; Kitamura et al. 2010). In agreement with this, studies in *Drosophila* reveal that both Ndc80 and $Msps^{XMAP215}$ are involved in KT-driven MT formation (Bucciarelli et al. 2009).

In *S. cerevisiae*, Stu1 interacts with Nuf2 in a protein fragment complementation assay (Tarassov et al. 2008). Thus it is tempting to speculate that Stu1 may provide a link between the Spc105 and Ndc80 complexes, and this, in turn, may be important for the recruitment of Stu2. This would explain why interfering with either Ndc80 or Spc105 complexes compromises both Stu1 and Stu2 recruitment to KTs. Our studies suggest

that Stu1 is insufficient to recruit Stu2 when tethered at an engineered site on the chromosome arm. Thus it is possible that Stu1 requires both Ndc80 and Spc105 complexes to do that.

We could not detect any direct physical interaction between Stu1 and Stu2 by Y2H assay (Nori Kobayashi, unpublished), however BiFC assays (Hu et al. 2002) showed that Stu1 and Stu2 became closely associated at the spindle (within a distance of 10–15 nm). Nevertheless no such association could be detected at KTs. There are two possible explanations why we cannot detect this association. First, C-terminal tagging of Stu1 and Stu2 with VN and VC fragments may not be suitable for the detection, and we plan to use N-terminally tagged versions to test this. Recent studies suggest that the Stu1 N-terminal TOG1-like domain drives Stu1 recruitment at KTs (Funk et al. 2014). This TOG1-like domain contains HEAT repeats, which are involved in protein–protein interactions (Neuwald and Hirano 2000). Second, according to recent studies, Stu1 is the least abundant MAP, and is expressed at very low levels within the cell (Aravamudhan et al. 2014), thus it may be difficult to detect VN–VC association signals from such a low amount of proteins.

Thus it remains unclear whether Stu1 and Stu2 directly associate at KTs or whether their interaction is mediated by another protein, for example Slk19. In higher eukaryotes, *X. laevis* TACC3 (potential orthologue of Slk19) (Tang and Toda 2015) and XMAP215 (orthologue of Stu2) are associated via coiled-coil interactions and work together to promote MT generation (Mortuza et al. 2014). Nevertheless, a close association between Stu1 and Stu2 may have a conserved role throughout species, because physical and genetic interactions were also observed in *Drosophila* (Lowery et al. 2010; Long et al. 2013).

2. Mechanism for generation of kinetochore-derived microtubules

Both Stu1 and Stu2 are MAP proteins, which contain two TOG (tumour overexpressed gene) domains responsible for tubulin binding (Al-Bassam and Chang 2011). In yeast cells, both Stu1 and Stu2 operate as homo dimers (Al-Bassam and Chang 2011). Their vertebrate orthologues XMAP215/ch-TOG and CLASP are larger and contain more TOG domains, but generally operate as monomers (Al-Bassam and Chang 2011). Thus the number of TOG domains may play a conserved role throughout species.

Although both Stu1 and Stu2 have TOG domains, their TOG domains may be involved in different functions by recognising different conformations of tubulin dimers and/or different MT structures (Leano et al. 2013). For example, Stu2 TOG domains are involved in binding to free tubulin dimers in solution (Al-Bassam et al. 2006). Stu2 is proposed to work as a MT polymerase by facilitating the incorporation of these tubulin dimers into growing MT plus ends (Al-Bassam et al. 2006). Stu2 TOG1 interacts strongly with tubulin dimers, while Stu2 TOG2 alone does not (Al-Bassam et al. 2006). A recent model proposes that Stu2 binds to tubulin dimers exclusively via TOG1 domain, while TOG2 and the Stu2 C-terminus facilitate Stu2 binding to MT plus ends (Ayaz et al. 2012).

In contrast, studies on CLASP TOG-like (TOGL) domains provide experimental evidence that N-terminal TOGL1 domain alone is insufficient to support the binding of MTs, and that it does not bind to αβ-tubulin (Yin et al. 2002; De la Mora-Rey et al. 2013). At the same time, the structure of a second, TOGL2, domain, which is involved in MT binding (Yin et al. 2002), suggests that it is an unusual TOG domain that may recognise tubulin dimers in curved protofilament structures (Leano et al. 2013).

Structural analyses of CLASP and XMAP215 show that they are thin, elongated molecules (Patel et al. 2012; Cassimeris et al. 2001). XMAP215 can span up to eight tubulin dimers along a protofilament (Cassimeris et al. 2001). In this respect XMAP215 ch-TOG is thought to bind along the length of individual protofilaments and is proposed to promote MT growth through both stabilization of nascent protofilaments and addition of tubulin dimers at MT plus ends (Spittle et al. 2000). Thus, it is possible that Stu2 and its orthologues in other species promote MT generation via a protofilament model, in which they first stabilise nascent MT protofilaments, which are then subsequently extended by incorporation of αβ-tubulin dimers. Our studies suggest that linear organisation of Stu2 molecules at the engineered site on the chromosome arm (i.e. Stu2-LacI molecules interacting along the length of chromosome with *LacO* sites) is sufficient for MT generation, independently of Stu1. Thus, it is possible that at KTs also, the unique prerequisite for MT nucleation is the recruitment of multiple linear molecules of Stu2 that can stabilise nascent MT protofilaments. However, the role of Stu1 TOG domains in MT nucleation at KTs remains unclear.

Although we could not detect any direct interaction between Stu1 and Stu2, it may be the case that Stu1 provides direct binding sites for Stu2. Another possibility is that Stu1 may promote stabilisation of nascent MT protofilaments by changing their conformation so they can be more easily recognised by Stu2 molecules. In this regard, I tried to study MT generation at KTs in the absence of Stu1, but attempts to rescue MT generation at KTs by artificially tethering Stu2 to various KT components were unsuccessful (data not shown). At an engineered site on the chromosome arm, linear organisation of Stu2 is sufficient to promote MT generation in the absence of Stu1. Thus, Stu1 seems dispensable for MT generation when multiple Stu2 molecules are organised correctly. It is possible that the major role of Stu1 in MT nucleation at KTs is

to facilitate recruitment and organise Stu2 molecules, which then promotes stabilisation of nascent MT protofilaments and MT nucleation.

In contrast to Stu2, Stu1 does not localise to MT plus ends. Thus it is unlikely that Stu1 regulates MT dynamics at MT plus ends. This notion was also supported by our studies showing that depletion of Stu1 does not alter the dynamics of spindle-pole MTs. In this respect Stu1 depletion was a useful tool to study the roles of KT-derived MTs in KT capture, because it allowed us to specifically remove Stu2 from KTs and abolish KT-associated MT generation without compromising Stu2 function at the spindle poles and MT plus ends, i.e. extension of spindle-pole MTs.

Nevertheless, Stu1 is not only important at KTs, but also at the spindle mid-zone, where is required to maintain a bipolar spindle after KTs are being loaded on the spindle (Pasqualone and Huffaker 1994; Yin et al. 2002; Funk et al. 2014). Thus, based on the previous report that Stu1 C-terminus is required for its KT targeting (Ortiz et al. 2009) I tried to remove Stu1 specifically from KTs by deleting its C-terminus. My results suggested that the Stu1 C-terminus is not essential for its function at KTs. Although tubulin accumulation at KTs was reduced in a small subset of cells upon removal of Stu1 C-terminus, in many cells MTs were still generated at KTs and Stu2 co-localised with them. This suggests that Stu1 recruitment at KTs is not exclusively mediated by its C-terminus. Moreover, it suggests that the Stu1 C-terminus does not mediate its interaction with Stu2. More recent studies propose that not only the C-terminal part of the protein, but also TOGL1, is required for Stu1 localisation to KTs (Funk et al. 2014). It is an interesting prospect that Stu1 TOGL1 domain, which is not involved in tubulin binding, may be important for recruitment of Stu1 to KTs and at the same time mediate an interaction with Stu2.

II. Role of kinetochore-derived microtubules in facilitating kinetochore capture

KT capture is a stochastic process, in which spindle-pole MTs switch rapidly between MT growth and shrinkage to probe the cellular space for target KTs (Mitchison and Kirschner 1985c; Hill 1985; Holy and Leibler 1994). Nevertheless, the random search and capture model does not explain completely efficient KT capture within characteristic mitotic timescales (Wollman et al. 2005). The efficiency of random search and capture can be improved by different strategies such as 1) bias of MT growth towards KTs (Carazo-Salais et al. 1999; Wollman et al. 2005), 2) pivoting of MTs around the spindle pole (Kalinina et al. 2013), 3) kinetochore movements (Paul et al. 2009), and 4) MT nucleation from pre-existing spindle-pole MTs (Burbank et al. 2006; Mahoney et al. 2006) or from KTs (Witt et al. 1980; Kitamura et al. 2010; Paul et al. 2009), or by a combination of any of these mechanisms (Mogilner and Craig 2010; O'Connell and Khodjakov 2007; Duncan and Wakefield 2011) (see Introduction).

In this study we investigated the relative contribution of MTs originated at KTs in promoting efficient KT capture in mitosis. In physiological conditions these KT-derived MTs appear and have different duration in time prior to KT capture (Kitamura et al. 2010). Moreover, there seemed to be a clear correlation between the appearance of tubulin/MT signals at KTs and increased rate of KT capture, which is in reasonable agreement with previous observations (Kitamura et al. 2010). To investigate this correlation further, and to establish a causative relationship between the two, I studied how abolishing MT-generation at KTs affected KT capture. When the generation of KT-derived MTs was abolished in *stu1-frb* mutant, each KT took, on average, 16 sec longer to be captured. Such a delay in KT capture would mean slower KT collection, leading to a higher percentage of uncaptured KTs upon establishment of a bipolar spindle. Our experimental results suggest that, after KT assembly, spindle-pole MTs

will take up to 300 sec to collect all KTs. If each KT takes on average 16 sec longer to become captured, this would result in a 7-fold higher percentage of uncaptured KTs at 300 sec in *stu1-frb* compared to *STU1+* cells. This difference increases over time to 50 fold at 600 sec after KT assembly and goes up to 400 fold at 900 sec. This result is in agreement with the previous observation that removal of Stu1 from uncaptured KTs increases chromosome loss rates up to 400 fold (Funk et al. 2014).

Nevertheless not all KT-derived MTs seem to function in KT capture. In physiological conditions I quantified the rate of success in KT capture by counting successful KT-derived-MTs, which appear prior to KT capture, versus unsuccessful MTs, which appear at earlier time-points. On average, one out of every two KT-derived MTs may be successful. Our mathematical modelling, in which we apply the properties of KT-derived MTs such as their success rate in capture, random appearance and different duration, suggests that delay in KT capture in the *stu1-frb* mutant is mainly due to lack of KT-derived MTs. If KT-derived MTs are applied randomly throughout the *stu1-frb* mutant cell time-lines with the same duration and success in capture, they can recapitulate the advanced KT capture that is observed in *STU1+* wild-type cells. Our observation in physiological conditions, and studies in the centromere reactivation system, suggest that upon depletion of Stu1, lateral interaction between KT and spindle-pole MTs is compromised, which causes KT "bounces" on MT lattice. Similarly, in metazoans, MAST/Orbit ^{CLASP} is proposed to play a role in KT–MT interaction by holding KTs onto dynamic MTs (Maiato et al. 2002). An inefficient lateral interaction in *stu1-frb* cells may explain the observed delay in KT capture.

CLASPs are MAPs that localise to the outer periphery of KTs (Al-Bassam and Chang 2011). Thus it is not likely that depletion of Stu1^{CLASP} compromises the assembly and

function of KTs. Our studies confirmed this notion. In physiological conditions KTs were first assembled within normal distances from the spindle pole after Stu1 depletion. If KT assemblies were delayed after centromere replication, one would expect these KTs to become further displaced away from the spindle by diffusion. In addition, our measurements of the fluorescence intensity of KT signals show that KT assembly was not compromised in the absence of Stu1.

Surprisingly, in both *STU1+* and *stu1-frb* cells, KTs are captured within similar distances from the spindle-pole. Nevertheless, in *stu1-frb* cells, KT capture is delayed. This delay can be explained in at least two different ways: Accumulation of KT-derived MTs may increase an effective size of KTs for capture, and this would reduce the time required for KT capture (Wollman et al. 2005). In this model, in the absence of KT-derived MTs in *stu1-frb* cells, KTs would take longer to be captured. KT capture would be delayed until random KT motions bring them closer to the spindle-pole where they are more likely to be captured. Alternatively, our studies suggest that lateral interaction of KTs with spindle-pole MTs is defective upon removal of Stu1 and KT-derived MTs. This defect with Stu1 depletion is explained if KT-derived MTs stabilize the initial encounter between KTs and spindle-pole MTs, making it into sustained interaction between the two. In this situation, KT would need to make an initial encounter with spindle-pole MTs all over again through lateral interactions. This will slow down KT capture.

A model of KT capture in *S. pombe* suggests that the capture process depends mainly on MT pivoting and MT length, whereas KT size and KT motions appear to have a smaller effect on KT capture (Kalinina et al. 2013). The fact that in *S. cerevisiae* KTs are all captured within similar distances from the spindle pole suggests that there may be an

average optimal MT length that cells need to maintain for KT capture. We show that reduction of KT-derived MTs leads to delay in KT capture. Thus, none of the previously mechanisms proposed to facilitate KT capture may compensate for the loss of KT-derived MTs. Nevertheless, further studies are necessary to reveal which mechanisms are redundant and which are independently required, for efficient KT capture. Mathematical modelling can be instrumental in attempting to study this issue.

Intriguingly, recent studies show that assembly of acentrosomal TACC3–MT asters at KTs facilitate KT capture in HeLa cells (Fu et al. 2013). Thus, KT-driven MT formation may be a conserved mechanism that facilitates KT capture.

III. Molecular regulation and role of kinetochore-dependent microtubule rescue in maintenance of kinetochore–microtubule interactions

After initial KT capture, KTs need to regulate the dynamics of their associated spindle-pole MTs to ensure a sustained KT–MT interaction, i.e. KTs do not detach from spindle-pole MTs and are efficiently transported towards the spindle. How this regulation occurs remains unknown. Our studies show that KT-associated Stu1^{CLASP} is required for KT-dependent switching from MT depolymerisation to growth (MT rescue). *In vitro* studies demonstrate that the Stu1 orthologue in *S. pombe,* Cls1^{CLASP,} promotes MT rescue and suppresses MT disassembly and catastrophe at sites of high local concentration (Al-Bassam et al. 2010). Based on the unique architecture of CLASP TOGL2 domain, a model was proposed in which TOGL2 can promote MT rescue by recognising and stabilising curved depolymerising MT protofilaments (Leano et al. 2013; Wilbur and Heald 2013). As a result of such stabilisation, MT shrinkage would be inhibited, leading to pausing and, potentially, rescue if the MT could regain a conformation compatible with polymerisation (Wilbur and Heald 2013). Our discoveries support such a model, because in the absence of KT-associated Stu1, I did

not observe KT-dependent MT rescue. Nevertheless, it remains unclear whether Stu1^{CLASP} and not Stu2$^{XMAP215/TOG}$ directly promote MT rescue, because Stu1 removal from KTs leads also to removal of Stu2. Partial reduction of Stu2 function leads to reduction of KT-dependent MT rescue (Gandhi et al. 2011). Moreover, after Stu2 is transported from KT along the length of spindle-pole MT towards MT plus end, MT rescue is induced although Stu1 is not at the tip of the MT (Gandhi et al. 2011). This result suggests that Stu2 can promote MT rescue independently of Stu1. Nevertheless, Stu1 may play an additional role in KT-dependent MT rescue in stabilising depolymerising curved protofilaments and promoting a shorter MT "pause" prior to rescue. Our studies show that in the absence of Stu1^{CLASP} and Stu2^{XMAP215}, the MT plus end pauses at KTs for a longer time. Thus, Stu1 may be important in shortening the period of MT pause, by quickly changing conformation of depolymerising MT plus end to a conformation compatible with MT growth, which is then more easily recognised by Stu2.

By switching between MT depolymerisation and growth (MT rescue), KTs may ensure their sustained interaction with their associated spindle-pole MTs. KT-dependent MT rescue may be important when a depolymerising MT plus end reaches the KT and fails to establish a robust end-on attachment. If KTs fail to attach to the depolymerising MT plus end, there are two consequences: either they detach from MT plus end, or they promote MT rescue. Our studies support such a model, because when both end-on attachment and MT rescue are compromised in the double *ndc80Δ490-510 stu1-frb* mutant, I observed a high rate of KT detachment from the MT plus end. In addition, KT-dependent MT rescue may be required not only for sustained interaction of KT with its associated spindle-pole MT. Indeed, mathematical simulation suggests that KT-dependent MT rescue may play a role in promoting spindle-pole MT interaction with

more than one KT, facilitating the collection of widely scattered KTs (Gandhi et al. 2011).

IV. At the (kineto)chore yeast are really like people (Jason Swedlow)

Molecular regulation of KT-driven MT formation in metazoans has been intensively studied (Tulu et al. 2006; Suzuki et al. 2006; Torosantucci et al. 2008; Bucciarelli et al. 2009; Mishra et al. 2010; Fu et al. 2013). Some of the proteins involved were also found to be implicated in cancer (Suzuki et al. 2006; Torosantucci et al. 2008).

In this study we propose a novel role for CLASP in promoting MT generation at KTs. In metazoans, CLASP is important for asymmetric nucleation of non-centrosomal MTs at the Golgi network (Efimov et al. 2007). In addition, *Dm* MAST/Orbit ^{CLASP} has been proposed to regulate dynamics of KT-associated MTs by promoting MT turnover and poleward flux (Maiato et al. 2005; Maffini et al. 2009). Intriguingly, mammalian cells lacking one of the CLASP paralogues, *CLASP2*, progress normally through mitosis, but are prone to generate aneuploidy (Pereira et al. 2006). This result provided evidence for a role of *CLASP2* in chromosome segregation and mitotic fidelity (Pereira et al. 2006). Nevertheless whether this phenotype was due to defects in MT poleward flux, defects at the KT–MT interface or in spindle function remains unclear (see CLASPs, mitotic fidelity, and cancers) (Pereira et al. 2006). Furthermore, CLASPs may play an important role at the KT–MT interface, as *in vitro* studies propose that *Xl* Xorbit ^{CLASP} is required for chromatin-induced MT formation (Hannak and Heald 2006).

We propose that CLASPs play a role in promoting KT-driven MT formation via recruitment of XMAP215/ch-TOG polymerases. KT-associated MT formation may increase the effective KT size for MT capture, facilitating their “location” and interaction with spindle-pole MTs. In addition, KT-derived MTs and their associated

CLASP and XMAP215 MAPs may be required for efficient lateral interaction of KTs with spindle-pole MTs by serving as a bridge between KTs and spindle-pole MTs. After KT capture, CLASP and XMAP215/ch-TOG may be required to regulate the dynamics of their associated spindle-pole MTs to ensure that KTs do not detach, and are thus efficiently transported towards the spindle.

Intriguingly loss of heterozygosity in a region of chromosome 3p, where the CLASP2 locus is situated, is a hallmark of mammary carcinoma and non-small cell lung cancer (Tai et al. 2006; Maitra et al. 2001). Thus, loss of CLASP2 may lead to genetic instability and development of cancer (Tai et al. 2006). Investigating the role of CLASP2 in KT capture and mitosis may provide a key to understanding the molecular mechanisms, whose failure leads to cancer, and for development of better therapeutic strategies.

Summary and Future Directions

Molecular regulation of KT-derived MTs has been a topic of research over the last four decades. We propose a novel role of KT-associated Stu1^{CLASP} MAP in promoting KT-driven MT formation via recruitment of Stu2^{XMAP215} MT polymerase. Our studies show that Stu1^{CLASP} MAP is required for recruitment Stu2^{XMAP215} and, once recruited at KTs, Stu2^{XMAP215} polymerase may promote nucleation and extension of KT-derived MTs independently of Stu1^{CLASP}. Although we could not detect a direct association between Stu1^{CLASP} and Stu2^{XMAP215}, we detected close associations between them *in vivo*, at least on the spindle. Nevertheless, it remains unclear whether these MAPs directly interact at KTs to promote generation of KT-derived MTs, or if other proteins mediate their interactions. Intriguingly the recruitment of both Stu1^{CLASP} and Stu2^{XMAP215} at KTs is dependent on Spc105 (KNL-1 in metazoans) and Ndc80 protein scaffolds (Ortiz et al. 2009; Funk et al. 2014) (Nori Kobayashi, unpublished). It would be interesting to further explore the platform for KT-associated MT formation by investigating how Spc105 and Ndc80 complexes facilitate their recruitment to KTs.

Our studies also show that KT-derived MTs are important for efficient KT capture. In the absence of KT-derived MTs, KT capture is delayed. Thus none of the previously proposed mechanisms can compensate for this delay (See Discussion). KT-derived MTs may increase the effective KT size for MT capture so that they can be more efficiently located by spindle-pole MTs. In addition, our studies show evidence that KT-derived MTs and their associated Stu1^{CLASP} and Stu2^{XMAP215} MAPS may be important to hold KTs onto spindle-pole MTs so that KTs would avoid having to make repetitive lateral interactions until more robust end-on attachment is achieved. Mathematical modelling demonstrates that applying the properties of KT-derived MTs, such as random appearance, duration in time and success in capture, could recapitulate the advanced KT

capture. Nevertheless, it is an open question how multiple mechanisms such as biased MT towards KTs, MT pivoting around the spindle poles, KT movements or various MT nucleation pathways, including KT-derived MTs, contribute together to efficient KT interaction with spindle-pole MTs. To address this, we plan to develop a spatial–temporal model based on our live-cell imaging analyses.

Furthermore, KT-derived MTs and their associated Stu1^{CLASP} and Stu2^{XMAP215} MAPs may be not only important in facilitating initial KT capture. After establishment of KT-MT interaction, they may be important in sustaining the interaction of KTs with spindle-pole MTs. KT-derived MTs may serve as a reservoir for Stu2^{XMAP215} MAPs. Unlike other KT components, the localisation of Stu2 at KTs seems to be highly dynamic (Aravamudhan et al. 2014). Thus, this turnover of the protein may be regulated by highly dynamic MTs at KTs. Once the interaction of KT-derived MTs with spindle-pole MTs is established, generation of KT-derived MTs is suppressed (Kitamura et al. 2010), which may lead to a release of the pool of Stu2 molecules from KTs towards spindle-pole MTs, which will induce KT-dependent MT rescue. This would ensure that KT stays does not detach from its associated spindle-pole MT.

Both of these steps, i.e. initial encounter of KTs and sustained KT interaction with spindle-pole MTs, are critical to ensure that chromosome segregation occurs within characteristic mitotic timescales and no chromosomes are lost.

REFERENCES

Al-Bassam J, Chang F (2011) Regulation of microtubule dynamics by TOG-domain proteins XMAP215/Dis1 and CLASP. Trends Cell Biol 21 (10):604-614.

Al-Bassam J, Kim H, Brouhard G, van Oijen A, Harrison SC, Chang F (2010) CLASP promotes microtubule rescue by recruiting tubulin dimers to the microtubule. Dev Cell 19 (2):245-258.

Al-Bassam J, van Breugel M, Harrison SC, Hyman A (2006) Stu2p binds tubulin and undergoes an open-to-closed conformational change. J Cell Biol 172 (7):1009-1022

Amberg DC, Burke DJ, Strathern JN (2005) Methods in yeast genetics.

Akiyoshi B, Sarangapani KK, Powers AF, Nelson CR, Reichow SL, Arellano-Santoyo H, Gonen T, Ranish JA, Asbury CL, Biggins S (2010) Tension directly stabilizes reconstituted kinetochore-microtubule attachments. Nature 468 (7323):576-579

Aravamudhan P, Felzer-Kim I, Gurunathan K, Joglekar AP (2014) Assembling the protein architecture of the budding yeast kinetochore-microtubule attachment using FRET. Curr Biol 24 (13):1437-1446.

Athale CA, Dinarina A, Mora-Coral M, Pugieux C, Nedelec F, Karsenti E (2008) Regulation of microtubule dynamics by reaction cascades around chromosomes. Science 322 (5905):1243-1247.

Ayaz P, Xuecheng Y, Huddleston P, Brautigam C, Rice L (2012) A TOG:alpha beta-tubulin complex structure reveals conformation-based mechanisms for a microtubule polymerase. Science 337:857-860

Bergen LG, Kuriyama R, Borisy GG (1980) Polarity of microtubules nucleated by centrosomes and chromosomes of Chinese hamster ovary cells in vitro. J Cell Biol 84 (1):151-159

Biggins S (2013) The composition, functions, and regulation of the budding yeast kinetochore. Genetics 194 (4):817-846.

Bressan DA, Vazquez J, Haber JE (2004) Mating type-dependent constraints on the mobility of the left arm of yeast chromosome III. J Cell Biol 164 (3):361-371.

Brouhard GJ (2015) Dynamic instability 30 years later: complexities in microtubule growth and catastrophe. Mol Biol Cell 26 (7):1207-1210.

Bucciarelli E, Pellacani C, Naim V, Palena A, Gatti M, Somma MP (2009) Drosophila Dgt6 interacts with Ndc80, Msps/XMAP215, and gamma-tubulin to promote kinetochore-driven MT formation. Curr Biol 19 (21):1839-1845.

Burbank KS, Groen AC, Perlman ZE, Fisher DS, Mitchison TJ (2006) A new method reveals microtubule minus ends throughout the meiotic spindle. J Cell Biol 175 (3):369-375.

Buster DW, Zhang D, Sharp DJ (2007) Poleward tubulin flux in spindles: regulation and function in mitotic cells. Mol Biol Cell 18 (8):3094-3104.

Carazo-Salais R, Guarguaglini G, Gruss O, Segref A, Karsenti E, Mattaj I (1999) Generation of GTP-bound ran by RCC1 is required for chromatin-induced mitotic spindle formation. Nature 400:178-181

Carazo-Salas RE, Karsenti E (2003) Long-range communication between chromatin and microtubules in Xenopus egg extracts. Curr Biol 13 (19):1728-1733

Cassimeris L, Becker B, Carney B (2009) TOGp regulates microtubule assembly and density during mitosis and contributes to chromosome directional instability. Cell Motil Cytoskeleton 66 (8):535-545.

Cassimeris L, Gard D, Tran P, Erickson H (2001) XMAP215 is a long thin molecule that does not increase mirotubule stiffness. Journal of Cell Science 114 (15):3025-3033

Caudron M, Bunt G, Bastiaens P, Karsenti E (2005) Spatial coordination of spindle assembly by chromosome-mediated signaling gradients. Science 309 (5739):1373-1376

Chandhok NS, Pellman D (2009) A little CIN may cost a lot: revisiting aneuploidy and cancer. Curr Opin Genet Dev 19 (1):74-81.

Cheeseman IM, Chappie JS, Wilson-Kubalek EM, Desai A (2006) The conserved KMN network constitutes the core microtubule-binding site of the kinetochore. Cell 127 (5):983-997

Cheeseman IM, Desai A (2008) Molecular architecture of the kinetochore-microtubule interface. Nat Rev Mol Cell Biol 9 (1):33-46

Ciferri C, Pasqualato S, Screpanti E, Varetti G, Santaguida S, Dos Reis G, Maiolica A, Polka J, De Luca JG, De Wulf P, Salek M, Rappsilber J, Moores CA, Salmon ED, Musacchio A (2008) Implications for kinetochore-microtubule attachment from the structure of an engineered Ndc80 complex. Cell 133 (3):427-439

Courtwright AM, He X (2002) Dam1 is the right one: phosphoregulation of kinetochore biorientation. Dev Cell 3 (5):610-611.

Cuff J, Clamp M, Siddiqui A, Finlay M, Barton G (1998) JPred: a consensus secondary structure prediction server. Bioinformatics 14 892-893

De la Mora-Rey T, Guenther BD, Finzel BC (2013) The structure of the TOG-like domain of Drosophila melanogaster Mast/Orbit. Acta Crystallogr Sect F Struct Biol Cryst Commun 69 (Pt 7):723-729.

DeLuca JG, Musacchio A (2012) Structural organization of the kinetochore-microtubule interface. Curr Opin Cell Biol 24 (1):48-56.

Desai A, Mitchison T (1997a) Microtubule polymerization dynamics. Annu Rev Cell Dev Biol 13:83-117

Desai A, Mitchison TJ (1997c) Microtubule polymerization dynamics. Annu Rev Cell Dev Biol 13:83-117

Duncan T, Wakefield JG (2011) 50 ways to build a spindle: the complexity of microtubule generation during mitosis. Chromosome Res 19 (3):321-333.

Efimov A, Kharitonov A, Efimova N, Loncarek J, Miller PM, Andreyeva N, Gleeson P, Galjart N, Maia AR, McLeod IX, Yates JR, 3rd, Maiato H, Khodjakov A, Akhmanova A, Kaverina I (2007) Asymmetric CLASP-dependent nucleation of noncentrosomal microtubules at the trans-Golgi network. Dev Cell 12 (6):917-930.

Erlemann S, Neuner A, Gombos L, Gibeaux R, Antony C, Schiebel E (2012) An extended gamma-tubulin ring functions as a stable platform in microtubule nucleation. J Cell Biol 197 (1):59-74.

Euteneuer U, McIntosh J (1981) Structural polarity of kinetochore microtubules in PtK1 cells. The Journal of Cell Biology 89 (May):338-345

Euteneuer U, Ris H, Borisy G (1983) Polarity of kinetochore microtubules in chinese hamster ovary cells after recovery from a colcemid block. The Journal of Cell Biology 97 (July):202-208

Faust AME (2011) Regulation of mitotic progression in Saccharomyces cerevisiae by the microtubule-associated proteins Slk19 and Stu1. UC Berkeley, UC Berkeley Eletronic Theses and Dissertations

Fu W, Chen H, Wang G, Luo J, Deng Z, Xin G, Xu N, Guo X, Lei J, Jiang Q, Zhang C (2013) Self-assembly and sorting of acentrosomal microtubules by TACC3 facilitate kinetochore capture during the mitotic spindle assembly. Proc Natl Acad Sci U S A 110 (38):15295-15300.

Funk C, Schmeiser V, Ortiz J, Lechner J (2014) A TOGL domain specifically targets yeast CLASP to kinetochores to stabilize kinetochore microtubules. J Cell Biol 205 (4):555-571.

Gandhi SR, Gierlinski M, Mino A, Tanaka K, Kitamura E, Clayton L, Tanaka TU (2011) Kinetochore-dependent microtubule rescue ensures their efficient and sustained interaction in early mitosis. . Dev Cell 21:920-933

Garcia M, Vardy L, Koonrugsa N, Toda T (2001) Fission yeast ch-TOG/XMAP215 homologue Alp14 connects mitotic spindles with the kinetochore and is a component of the Mad2-dependent spindle checkpoint. The EMBO Journal 20 (13):3389-3401

Hannak E, Heald R (2006) Xorbit/CLASP links dynamic microtubules to chromosomes in the Xenopus meiotic spindle. J Cell Biol 172 (1):19-25.

Haruki H, Nishikawa J, Laemmli UK (2008) The anchor-away technique: rapid, conditional establishment of yeast mutant phenotypes. Mol Cell 31 (6):925-932.

He X, Rines DR, Espelin CW, Sorger PK (2001) Molecular analysis of kinetochore-microtubule attachment in budding yeast. Cell 106 (2):195-206.

Hill T (1985) Theoretical problems related to the attacment of microtubules to kinetochores. PNAS 82:4404-4408

Holland AJ, Cleveland DW (2009) Boveri revisited: chromosomal instability, aneuploidy and tumorigenesis. Nat Rev Mol Cell Biol 10 (7):478-487.

Holy TE, Leibler S (1994) Dynamic instability of microtubules as an efficient way to search in space. Proc Natl Acad Sci U S A 91 (12):5682-5685

Hsu K-S, Toda T (2011) Ndc80 internal loop interacts with Dis1/TOG to ensure proper kinetochore-spindle attachment in fission yeast. Curr Biol 21:214-220

Hu C, Chinenov Y, Kerppola T (2002) Visualisation of interactions among bZIP and rel family proteins in living cells using bimolecular fluorescence complementation. Molecular Cell 9 (April):789-798

Janke C, Ortiz J, Tanaka TU, Lechner J, Schiebel E (2002) Four new subunits of the Dam1-Duo1 complex reveal novel functions in sister kinetochore biorientation. Embo J 21 (1-2):181-193.

Kakui Y, Sato M, Okada N, Toda T, Yamamoto M (2013) Microtubules and Alp7-Alp14 (TACC-TOG) reposition chromosomes before meiotic segregation. Nat Cell Biol 15 (7):786-796.

Kalantzaki M, Kitamura E, Zhang T, Mino A, Novak B, Tanaka TU (2015) Kinetochore-microtubule error correction is driven by differentially regulated interaction modes. Nat Cell Biol 17 (4):421-433.

Kalinina I, Nandi A, Delivani P, Chacon MR, Klemm AH, Ramunno-Johnson D, Krull A, Lindner B, Pavin N, Tolic-Norrelykke IM (2013) Pivoting of microtubules around the spindle pole accelerates kinetochore capture. Nat Cell Biol 15 (1):82-87.

Khodjakov A, Cole R, Oakley B, Rieder C (2000) Centrosome-indipendent mitotic spindle formation in vertebrates. Current Biology (10):59-67

Khodjakov A, Copenagle L, Gordon MB, Compton DA, Kapoor TM (2003) Minus-end capture of preformed kinetochore fibers contributes to spindle morphogenesis. J Cell Biol 160 (5):671-683

Kirschner M, Mitchison T (1986) Beyond self-assembly: from microtubules to morphogenesis. Cell 45 (3):329-342

Kitamura E, Tanaka K, Kitamura Y, Tanaka TU (2007) Kinetochore microtubule interaction during S phase in Saccharomyces cerevisiae. Genes Dev 21 (24):3319-3330.

Kitamura E, Tanaka K, Komoto S, Kitamura Y, Antony C, Tanaka TU (2010) Kinetochores generate microtubules with distal plus ends: their roles and limited lifetime in mitosis. Dev Cell 18 (2):248-259.

Knop M, Siegers K, Pereira G, Zachariae W, Winsor B, Nasmyth K, Schiebel E (1999) Epitope tagging of yeast genes using a PCR-based strategy: more tags and improved practical routines. Yeast 15 (10B):963-972.

Kollman JM, Merdes A, Mourey L, Agard DA (2011) Microtubule nucleation by gamma-tubulin complexes. Nat Rev Mol Cell Biol 12 (11):709-721.

Lampert F, Mieck C, Alushin GM, Nogales E, Westermann S (2013) Molecular requirements for the formation of a kinetochore-microtubule interface by Dam1 and Ndc80 complexes. J Cell Biol 200 (1):21-30.

Leano JB, Rogers SL, Slep KC (2013) A cryptic TOG domain with a distinct architecture underlies CLASP-dependent bipolar spindle formation. Structure 21 (6):939-950.

Levenberg K (1944) A Method for the Solution of Certain Problems in Least Squares. Quart Appl Math 2:164-168

Levesque AA, Compton DA (2001) The chromokinesin Kid is necessary for chromosome arm orientation and oscillation, but not congression, on mitotic spindles. J Cell Biol 154 (6):1135-1146.

Lim HH, Goh PY, Surana U (1996) Spindle pole body separation in Saccharomyces cerevisiae requires dephosphorylation of the tyrosine 19 residue of Cdc28. Mol Cell Biol 16 (11):6385-6397

Long J, Bagonis M, Lowery L, Lee H, Danuser G, Van Vactor D (2013) Multiparametric analysis of CLASP-interacting protein functions during interphase microtubule dynamics. Molecular and Cellular Biology 33 (8):1528-1545

Lowery LA, Lee H, Lu C, Murphy R, Obar RA, Zhai B, Schedl M, Van Vactor D, Zhan Y (2010) Parallel genetic and proteomic screens identify Msps as a CLASP-Abl pathway interactor in Drosophila. Genetics 185 (4):1311-1325.

Ma L, McQuenn J, Cuchieri L, Vegel J, Measday V (2007) Spc24 and Stu2 promote spindle integrity when DNA replication is stalled. Molecular Biology of the Cell 18 (August).

Maekawa H, Usui T, Knop M, Schiebel E (2003) Yeast Cdk1 translocates to the plus end of cytoplasmic microtubules to regulate bud cortex interactions. EMBO J 22 (3):438-449.

Maffini S, Maia AR, Manning AL, Maliga Z, Pereira AL, Junqueira M, Shevchenko A, Hyman A, Yates JR, 3rd, Galjart N, Compton DA, Maiato H (2009) Motor-independent targeting of CLASPs to kinetochores by CENP-E promotes microtubule turnover and poleward flux. Curr Biol 19 (18):1566-1572.

Mahoney NM, Goshima G, Douglass AD, Vale RD (2006) Making microtubules and mitotic spindles in cells without functional centrosomes. Curr Biol 16 (6):564-569.

Maiato H, Deluca J, Salmon ED, Earnshaw WC (2004a) The dynamic kinetochore-microtubule interface. J Cell Sci 117 (Pt 23):5461-5477

Maiato H, Khodjakov A, Rieder CL (2005) Drosophila CLASP is required for the incorporation of microtubule subunits into fluxing kinetochore fibres. Nat Cell Biol 7 (1):42-47

Maiato H, Rieder CL, Khodjakov A (2004b) Kinetochore-driven formation of kinetochore fibers contributes to spindle assembly during animal mitosis. J Cell Biol 167 (5):831-840

Maiato H, Sampaio P, Lemos CL, Findlay J, Carmena M, Earnshaw WC, Sunkel CE (2002) MAST/Orbit has a role in microtubule-kinetochore attachment and is essential for chromosome alignment and maintenance of spindle bipolarity. J Cell Biol 157 (5):749-760

Maiato H, Sampaio P, Sunkel C (2004e) Microtubule-associated proteins and their essential roles during mitosis. International Review of Cytology 2 (241):53-153

Maitra A, Wistuba I, Washington C, Virmani A, Ashfaq R, Milchgrub S, Gazdar A, Minna J (2001) High-Resolution chromosome 3p allelotyping of breast carcinomas and precursor lesions demonstrates frequent loss of heterozybosity and discontinuous pattern of allele loss. American Journal of Pathology 159 (1):119-130.

Malvezzi F, Litos G, Schleiffer A, Heuck A, Mechtler K, Clausen T, Westermann S (2013) A structural basis for kinetochore recruitment of the Ndc80 complex via two distinct centromere receptors. EMBO J 32 (3):409-423.

Malvezzi F, Westermann S (2014) "Uno, nessuno e centomila": the different faces of the budding yeast kinetochore. Chromosoma 123 (5):447-457.

Marquardt D (1963) An algorithm for least-squares estimation of nonlinear parameters. SIAM J Appl Math 11 (2):431-441

Maton G, Edwards F, Lacroix B, Stefanutti M, Laband K, Lieury T, Kim T, Espeut J, Canman JC, Dumont J (2015) Kinetochore components are required for central spindle assembly. Nat Cell Biol 17 (5):697-705.

Maure J-F, Komoto S, Oku Y, Mino A, Pasqualato S, Natsume K, Clayton L, Musacchio A, Tanaka TU (2011) The Ndc80 loop region facilitates formation of kinetochore attachment to the dynamic microtubule plus end. Curr Biol 21:207-213

McCarroll RM, Fangman WL (1988) Time of replication of yeast centromeres and telomeres. Cell 54 (4):505-513.

McNally F (2003) Microtubule dynamics: new surprises from an old MAP. Current Biology 13:R597-R599.

Michaelis C, Ciosk R, Nasmyth K (1997) Cohesins: chromosomal proteins that prevent premature separation of sister chromatids. Cell 91 (1):35-45

Mishra RK, Chakraborty P, Arnaoutov A, Fontoura BM, Dasso M (2010) The Nup107-160 complex and gamma-TuRC regulate microtubule polymerization at kinetochores. Nat Cell Biol 12 (2):164-169.

Mitchison TJ, Kirschner MW (1985a) Properties of the kinetochore in vitro. I. Microtubule nucleation and tubulin binding. J Cell Biol 101 (3):755-765

Mitchison TJ, Kirschner MW (1985c) Properties of the kinetochore in vitro. II. Microtubule capture and ATP-dependent translocation. J Cell Biol 101 (3):766-777

Mogilner A, Craig E (2010) Towards a quantitative understanding of mitotic spindle assembly and mechanics. J Cell Sci 123 (Pt 20):3435-3445.

Morgan D (2007) The cell cycle principles of control. Oxford University Press.

Mortuza GB, Cavazza T, Garcia-Mayoral MF, Hermida D, Peset I, Pedrero JG, Merino N, Blanco FJ, Lyngso J, Bruix M, Pedersen JS, Vernos I, Montoya G (2014) XTACC3-XMAP215 association reveals an asymmetric interaction promoting microtubule elongation. Nat Commun 5:5072.

Murata-Hori M, Wang YL (2002) The kinase activity of aurora B is required for kinetochore-microtubule interactions during mitosis. Curr Biol 12 (11):894-899.

Nakaseko Y, Goshima G, Morishita J, Yanagida M (2001) M-phase-specific kinetochore proteins in fission yeast: microtubule-associating Dis1 and Mtc1 display rapid separation and segregation during anaphase. Current Biology 11:537-549

Natsume T, Muller CA, Katou Y, Retkute R, Gierlinski M, Araki H, Blow JJ, Shirahige K, Nieduszynski CA, Tanaka TU (2013) Kinetochores coordinate pericentromeric cohesion and early DNA replication by cdc7-dbf4 kinase recruitment. Mol Cell 50 (5):661-674.

Neuwald A, Hirano T (2000) HEAT repeats associated with condensins, cohesins, and other complexes involved in chromosome-related functions. Genome Res 10:1445-1452.

Newman J, Wolf E, Kim P (2000) A computationally directed screen identifying interacting coiled coils from Saccharomyces cerevisiar. PNAS 97 (24):13203-13208

Nishimura K, Fukagawa T, Takisawa H, Kakimoto T, Kanemaki M (2009) An auxin-based degron system for the rapid depletion of proteins in nonplant cells. Nat Methods 6 (12):917-922.

Nogales E (2001) Structural insights into microtubule function. Annu Rev Biophys Biomol Struct 30:397-420

O'Connell CB, Khodjakov AL (2007) Cooperative mechanisms of mitotic spindle formation. J Cell Sci 120 (Pt 10):1717-1722.

O'Reilly N, Charbin A, Lopez-Serra L, Uhlmann F (2012) Facile synthesis of budding yeast a-factor and its use to synchronize cells of alpha mating type. Yeast 29 (6):233-240.

Ohkura H, Garcia MA, Toda T (2001) Dis1/TOG universal microtubule adaptors - one MAP for all? J Cell Sci 114 (Pt 21):3805-3812

Ortiz J, Funk C, Schafer A, Lechner J (2009) Stu1 inversely regulates kinetochore capture and spindle stability. Genes Dev 23 (23):2778-2791.

Ostergren G, Mole-Bajer J, Bajer A (1960) An interpretation of transport phenomena at mitosis. Ann NY Acad Sci 90:381–408

Pasqualone D, Huffaker TC (1994) STU1, a suppressor of a beta-tubulin mutation, encodes a novel and essential component of the yeast mitotic spindle. J Cell Biol 127 (6 Pt 2):1973-1984

Patel K, Nogales E, Heald R (2012) Multiple domains of human CLASP contribute to microtubule dynamics and organization in vitro and in Xenopus egg extracts. Cytoskeleton (Hoboken) 69 (3):155-165.

Paul R, Wollman R, Silkworth WT, Nardi IK, Cimini D, Mogilner A (2009) Computer simulations predict that chromosome movements and rotations accelerate mitotic spindle assembly without compromising accuracy. Proc Natl Acad Sci U S A 106 (37):15708-15713.

Pereira A, Pereira A, Maia A, Drabek K, Sayas C, Hergert P, Lince-Faria M, Matos I, Duque C, Stepanova T, Rieder C, Earnshaw W, Galjart N, Maiato H (2006) Mammalian CLAS1 and CLASP2 cooperate to ensure mitotic fidelity by regulating spindle and kinetochore function. Molecular Biology of the Cell 17 (October):4526-4542.

Pluta AF, Mackay AM, Ainsztein AM, Goldberg IG, Earnshaw WC (1995) The centromere: hub of chromosomal activities. Science 270 (5242):1591-1594.

Rieder CL, Alexander SP (1990) Kinetochores are transported poleward along a single astral microtubule during chromosome attachment to the spindle in newt lung cells. J Cell Biol 110 (1):81-95.

Rogers GC, Rogers SL, Sharp DJ (2005) Spindle microtubules in flux. J Cell Sci 118 (Pt 6):1105-1116

Sagolla MJ, Uzawa S, Cande WZ (2003) Individual microtubule dynamics contribute to the function of mitotic and cytoplasmic arrays in fission yeast. J Cell Sci 116 (Pt 24):4891-4903

Sambrook J, Russell D (2001) Molecular Cloning: A laboratory Manual. Cold Spring Harbor Laboratory Press.

Schneiter R (2004) Genetics, Molecular and Cell Biology of yeast. Universitat Freiburg Schweiz, Spittle C, Charrasse S, Larroque C, Cassimeris L (2000) The interaction of TOGp with microtubules and tubulin. J Biol Chem 275 (27):20748-20753.

Sullivan M, Higuchi T, Katis VL, Uhlmann F (2004) Cdc14 phosphatase induces rDNA condensation and resolves cohesin-independent cohesion during budding yeast anaphase. Cell 117 (4):471-482

Summers K, Kirschner MW (1979) Characteristics of the polar assembly and disassembly of microtubules observed in vitro by darkfield light microscopy. J Cell Biol 83 (1):205-217

Sung MK, Huh WK (2007) Bimolecular fluorescence complementation analysis system for in vivo detection of protein-protein interaction in Saccharomyces cerevisiae. Yeast 24 (9):767-775.

Suzuki H, Akiyama N, Tsuji M, Ohashi T, Saito S, Eto Y (2006) Human Shugoshin mediates kinetochore-driven formation of kinetochore microtubules. Cell Cycle 5:10 (15 May):1094-1101

Tai AL, Mak W, Ng PK, Chua DT, Ng MY, Fu L, Chu KK, Fang Y, Qiang Song Y, Chen M, Zhang M, Sham PC, Guan XY (2006) High-throughput loss-of-heterozygosity study of chromosome 3p in lung cancer using single-nucleotide polymorphism markers. Cancer Res 66 (8):4133-4138.

Tanaka K, Kitamura E, Kitamura Y, Tanaka TU (2007) Molecular mechanisms of microtubule-dependent kinetochore transport toward spindle poles. J Cell Biol 178 (2):269-281.

Tanaka K, Kitamura E, Tanaka TU (2005a) Live-cell analysis of kinetochore-microtubule interaction in budding yeast. Methods 51 (2):206-213.

Tanaka K, Kitamura E, Tanaka TU (2010) Live-cell analysis of kinetochore-microtubule interaction in budding yeast. Methods 51 (2):206-213.

Tanaka K, Mukae N, Dewar H, van Breugel M, James EK, Prescott AR, Antony C, Tanaka TU (2005d) Molecular mechanisms of kinetochore capture by spindle microtubules. Nature 434 (7036):987-994

Tanaka TU (2010) Kinetochore-microtubule interactions: steps towards bi-orientation. EMBO J 29:4070-4082

Tanaka TU, Rachidi N, Janke C, Pereira G, Galova M, Schiebel E, Stark MJ, Nasmyth K (2002) Evidence that the Ipl1-Sli15 (Aurora kinase-INCENP) complex promotes chromosome bi-orientation by altering kinetochore-spindle pole connections. Cell 108 (3):317-329.

Tang NH, Toda T (2015) MAPping the Ndc80 loop in cancer: A possible link between Ndc80/Hec1 overproduction and cancer formation. Bioessays 37 (3):248-256.

Tang NHaT, T. (2013) Ndc80 Loop as a protein-protein interaction motif. Cell Division 2013 (8:2)

Tarassov K, Messier V, Landry C, Radinovic S, Serna Molina M, Shames I, Malitskaya Y, Vogel J, Bussey H, Michnick S (2008) An in vivo map of the yeast protein interactome. Science 320 (13 June):1465-1470

Telzer BR, Moses MJ, Rosenbaum JL (1975) Assembly of microtubules onto kinetochores of isolated mitotic chromosomes of HeLa cells. Proc Natl Acad Sci U S A 72 (10):4023-4027

Thompson SL, Bakhoum SF, Compton DA (2010) Mechanisms of chromosomal instability. Curr Biol 20 (6):R285-295.

Torosantucci L, De Luca M, Guarguaglini G, Lavia P, Degrassi F (2008) Localized RanGTP accumulation promotes microtubule nucleation at kinetochores in somatic mammalian cells. Molecular Biology of the Cell 19 (May):1873-1882.

Tulu U, Fagerstorm C, Ferenz N, Wadsworth P (2006) Molecular requirements for kinetochore-associated microtubule formation in mammalian cells. Current Biology 16 (5):536-541

Uhlmann F, Wernic D, Poupart MA, Koonin EV, Nasmyth K (2000) Cleavage of cohesin by the CD clan protease separin triggers anaphase in yeast. Cell 103 (3):375-386

Wang HW, Long S, Ciferri C, Westermann S, Drubin D, Barnes G, Nogales E (2008) Architecture and flexibility of the yeast Ndc80 kinetochore complex. J Mol Biol 383 (4):894-903.

Waterhouse AM, Procter JB, Martin DM, Clamp M, Barton GJ (2009) Jalview Version 2--a multiple sequence alignment editor and analysis workbench. Bioinformatics 25 (9):1189-1191.

Webster T, Dickson R (1983) Direct selection of Saccharomyces cerevisiae resistant to the antibiotic G418 following transformation with a DNA vector carrying kanamycin-resistance gene of Tn903. Gene 26 (2-3):243-252.

Wei RR, Sorger PK, Harrison SC (2005) Molecular organization of the Ndc80 complex, an essential kinetochore component. Proc Natl Acad Sci U S A 102 (15):5363-5367

Wilbur JD, Heald R (2013) Cryptic no longer: arrays of CLASP1 TOG domains. Structure 21 (6):869-870.

Winey M, Bloom K (2012) Mitotic spindle form and function. Genetics 190 (4):1197-1224.

Winey M, O'Toole ET (2001) The spindle cycle in budding yeast. Nat Cell Biol 3 (1):E23-27.

Witt PL, Ris H, Borisy GG (1980) Origin of kinetochore microtubules in Chinese hamster ovary cells. Chromosoma 81 (3):483-505

Wollman R, Cytrynbaum EN, Jones JT, Meyer T, Scholey JM, Mogilner A (2005) Efficient Chromosome Capture Requires a Bias in the 'Search-and-Capture' Process during Mitotic-Spindle Assembly. Curr Biol 15 (9):828-832

Wolyniak MJ, Blake-Hodek K, Kosco K, Hwang E, You L, Huffaker TC (2006) The regulation of microtubule dynamics in Saccharomyces cerevisiae by three interacting plus-end tracking proteins. Mol Biol Cell 17 (6):2789-2798

Wong J, Nakajima Y, Westermann S, Shang C, Kang JS, Goodner C, Houshmand P, Fields S, Chan CS, Drubin D, Barnes G, Hazbun T (2007) A Protein Interaction Map of the Mitotic Spindle. Mol Biol Cell 18 (10):3800-3809

Yamagishi Y, Sakuno T, Shimura M, Watanabe Y (2008) Heterochromatin links to centromeric protection by recruiting shugoshin. Nature 455 (7210):251-255.

Yin H, You L, Pasqualone D, Kopski KM, Huffaker TC (2002) Stu1p is physically associated with beta-tubulin and is required for structural integrity of the mitotic spindle. Mol Biol Cell 13 (6):1881-1892

Zeng X, Kahana JA, Silver PA, Morphew MK, McIntosh JR, Fitch IT, Carbon J, Saunders WS (1999) Slk19p is a centromere protein that functions to stabilize mitotic spindles. J Cell Biol 146 (2):415-425